FINITE STATE MACHINE AND EOG ARTIFACTS IN EEG SIGNALS FOR WHEELCHAIR NAVIGATION

ROZIANA BINTI RAMLI

FACULTY OF ENGINEERING
UNIVERSITY OF MALAYA
KUALA LUMPUR

2014

FINITE STATE MACHINE AND EOG ARTIFACTS IN EEG SIGNALS FOR WHEELCHAIR NAVIGATION

ROZIANA BINTI RAMLI

DISSERTATION SUBMITTED IN FULFILLMENT OF THE REQUIREMENTS FOR THE DEGREE OF MASTER OF ENGINEERING SCIENCE

FACULTY OF ENGINEERING
UNIVERSITY OF MALAYA
KUALA LUMPUR

2014

Abstract

Supporting physically disabled society with severe motor disabilities is very challenging as their needs differ depending on the severity of the impairment incurred. As an attempt to support them, a BCI for wheelchair navigation is developed to help them regain some mobility. In this study, a hybrid BCI that combine inputs from EEG and EOG signals for a more effective interface is proposed. Specifically, one EEG signal at O2 and two EOG artifacts embedded in EEG signals at C3 and C4 are used as inputs to an asynchronous wheelchair navigation system. Cz is taken as reference and the signals are all recorded using g.mobilab amplifier from 20 participants. The alpha rhythm extracted from O2 signal is related to eyelid position that determines whether the eyes are closed or open, while the delta rhythms extracted from C3 and C4 signals are related to horizontal eyeball movement used to infer the gaze direction. A sliding window is utilized to position important cues in the EEG signals at the center of the window to extract consistent features for accurate classification. The features from the O2 signal are variance, 2nd order difference plot and area. They are classified by thresholding and CTM. The delta rhythm data can be used directly as inputs to an LDA or K-Means classifier. Otherwise, a feature like area can be extracted from the delta signal and classified by thresholding. The system is modeled as a finite state machine with two modes, each containing three states. The transition between states is determined by fuzzy logic. This is to allow the wheelchair to move FORWARD and BACKWARD in six different directions with minimum error. In Online Session, the performance of various features and classifiers used are recorded and compared. A combination of features and classifier that achieve the highest accuracy is then implemented in the Navigation Session which are variance (98%) in alpha rhythm and K-Means (98%) in delta rhythms. Then, performance of the system is tested in

Navigation Session. Only five participants who obtained the score higher than 98% in the Online Session were invited to perform the actual navigation tasks by maneuvering the wheelchair along two designated routes. High average performance rates of 98% for Route 1 and 96% for Route 2 were recorded and the participants managed to complete the tasks without collisions. This experiment also tested the usability of the BACKWARD movement when the wheelchair was trapped at tight dead ends with no space to make u-turn. The main contribution of this research work is in the right selection of the EOG artifacts and EEG signals used, the choice of the model that allows FORWARD and BACKWARD wheelchair movement and the fast execution time. Finally, the implementation of sliding window helps increase the performance rate.

Abstrak

Sebagai usaha untuk membantu masyarakat kurang upaya yang hilang keupayaan fisikal, pacuan kerusi roda melalui BCI dibina bagi membantu mereka untuk bergerak. Tesis ini mencadangkan gabungan isyarat EEG dan EOG sebagai masukkan untuk antara muka yang lebih berkesan. Secara khususnya, satu isyarat EEG di O2 dan dua artifak EOG yang tertanam dalam isyarat EEG di C3 dan C4 digunakan sebagai masukkan kepada sistem navigasi kerusi roda tak segerak. Cz diambil sebagai rujukan dan isyarat semuanya dirakam menggunakan penguat g.mobilab daripada 20 peserta. . Isyarat alpha dari O2 yang digunakan untuk menentukan sama ada mata ditutup atau dibuka manakala isyarat delta dari C3 dan diperiksa untuk menetukan arah pandangan mendatar. Tetingkap gelongsor digunakan di dalam analisis supaya isyarat penting dalam EEG dapat diambil bagi pengelasan yang berkesan. Ciri-ciri dari isyarat O2 adalah varians, *2nd order difference plot* dan keluasan isyarat dan dikelaskan oleh pengambangan dan CTM. Data isyarat delta boleh digunakan secara langsung sebagai masukkan pada pengelas LDA atau K-Means. Jika tidak, satu ciri seperti keluasan boleh diekstrak daripada isyarat delta dan dikelaskan oleh pengambangan. Sistem ini dimodelkan sebagai mesin keadaan terhingga dengan sebagai peralihan dengan dua mod, masing-masing mengandungi tiga keadaan. Peralihan antara keadaan ditentukan oleh logik kabur. Ini bagi membolehkan kerusi roda untuk bergerak hadapan dan ke belakang dalam enam arah yang berbeza dengan ralat yang minimum. Dalam Sesi Online, prestasi pelbagai ciri-ciri dan pengelas direkodkan dan dibandingkan. Gabungan ciri-ciri dan pengelas yang mencapai ketepatan tertinggi kemudiannya dilaksanakan dalam Sesi Navigasi iaitu varians (98%) dalam isyarat alpha dan K-Means (98%) dalam isyarat delta. Kemudian, prestasi system ini yang diuji dalam Sesi Navigasi. Hanya lima peserta yang mendapat markah yang lebih tinggi daripada 98% dalam Sesi Online telah

dipilih untuk melaksanakan tugasan navigasi sebenar memacu kerusi roda di sepanjang dua laluan yang ditetapkan. Kadar prestasi purata yang tinggi iaitu 98% untuk Laluan 1 dan 96% untuk Laluan 2 telah direkodkan dan para peserta berjaya menyelesaikan tugasan tanpa perlanggaran. Eksperimen ini juga menguji kebolehgunaan pergerakan ke belakang apabila kerusi roda yang telah terperangkap di hujung mati ketat dengan tiada ruang untuk membuat u-turn. Sumbangan utama penyelidikan ini adalah dalam ketepatan pemilihan artifak EOG dan isyarat EEG yang digunakan, pemilihan model yang membolehkan pergerakan ke HADAPAN dan ke BELAKANG, dan masa pelaksanaan yang cepat. Akhir sekali, pelaksanaan gelongsor tetingkap membantu meningkatkan kadar prestasi pemprosesan isyarat.

Acknowledgement

Table of Content

List of Figures

List of Tables

List of Abbreviations

ADD	Attention Deficit Disorder
ALS	Amyotrophy Lateral Sclerosis
BCI	Brain Computer Interface
BLR NN	Bayesian Logistic Regression Neural Network
CCA	Canonical Correlation Analysis
CSP	Common Spatial Patterns
CTM	Central Tendency Measurement
EEG	Electroencephalogram
EMG	Electromyogram
EOG	Electrooculogram
ERD	Event Related Desynchronization
ERP	Event Related Potential
FFT	Fast Fourier Transform
FIRNN	Finite Impulse Response Neural Network
FLDA	Fisher's LDA
GDNN	Gamma Dynamic Neural Network
GUI	Graphical User Interface
HEOG	Horizontal EOG
HMI	Human Machine Interface
HMM	Hidden Markov Model
ICA	Independent Component Analysis
IOHMM	Input–output HMM
ITR	Information Transfer Rate

kNN	K Nearest Neighbors
LDA	Linear Discriminant Analysis
Linear-SVM	Linear-Support Vector Machine
MLD	Mahalanobis Linear Distance
MLP	Multi Layer Perceptron
PeGNC	Probability Estimating Guarded Neural Classifier
RBF-SVM	Radial Basis Function SVM
RFLDA	Regularized FLDA
SSVEP	Steady State Visually Evoked Potential
SVM	Support Vector Machine
SWLDA	Stepwise Linear Discriminant Analysis
TDNN	Time-Delay Neural Network
VEOG	Vertical EOG
VQ NN	Vector Quantization Neural Network

List of Appendices

CHAPTER 1

INTRODUCTION

1.1 Introduction

Supporting physically disabled society with severe motor disabilities is very challenging as their needs differ on the severity of the impairment incurred. Therefore, Human Machine Interface (HMI) has been introduced to help them improve their quality of life. Various electrophysiological signals such as electroencephalogram (EEG), electrooculogram (EOG) and electromyogram (EMG) have been used and tested as a control mechanism for HMI. Using these electrophysiological signals, variety of assistive applications have been proposed in many studies (Latif, Sherkat, & Lotfi, 2008; Nguyen & Jo, 2012; Thorsten O. Zander, Matti Gaertner et al., 2010).

1.2 Motivation and Problem Statement

Neurophysiological signals such as P300 wave, mu and beta rhythms and steady state visually evoked potential (SSVEP) can be recorded from the scalp using EEG. These signals have been utilized by researchers from diverse fields to develop a variety of HMI known as a brain computer interface (BCI). However, the presence of cognitive impairments in physically disabled can cause difficulties in operating BCI that requires a high degree of concentration.

Operating BCI can be more effective by reducing the cognitive load by combining EEG signals with other physiological signals known as hybrid BCI. Physiological signals such as EOG or EMG can provide an efficient channel of interaction for patients who are partially lost control over muscular activity. Recently, there have been many studies that proposed wheelchair navigation controllers based hybrid BCI (Cao, Li *et*

al., 2014; Long, Li *et al.*, 2012; Wang, Li *et al.*, 2014; Yuanqing, Jiahui *et al.*, 2013; Zhijun, Shuangshuang *et al.*, 2013). However, contamination of ocular and muscular activities remains a significant problem in the design of hybrid BCI systems (Fatourechi, Bashashati *et al.*, 2007; Yong, Fatourechi *et al.*, 2012). It is no surprise the hybrid BCI system that relies on eye movements as input is more contaminated with ocular artifacts compared to a pure BCI system.

Since EEG signals have always been contaminated by ocular artifacts, we employ these artifacts as inputs into our system. Therefore, in this study we utilized alpha rhythm and EOG artifacts in EEG as inputs to the hybrid BCI. Both inputs are fast, stable and easy to generate that are suitable for physically disabled with cognitive impairments. Due to constant eye movement, it is difficult to keep the EOG artifacts in idling state or to avoid the Midas touch problem (Baihan, Lo, & Shi, 2013). Furthermore, only a limited number of gaze directions can be realized from eye movement. Therefore, outputs from the hybrid BCI will be translated into commands to steer the wheelchair that is modeled as a finite state machine. Using finite state machine, the Midas touch problem can be avoided and the wheelchair can be commanded to move in a different direction from a limited number of gaze.

1.3   Objective

The primary objective of this work is to develop a navigation controller for a motorized wheelchair using a hybrid of EEG and EOG artifacts in EEG signals and finite state machine technique. The sub-objectives include:

1) Investigating the best techniques to process the signals and extract suitable features for detecting EOG artifacts in EEG signals.

2) Developing a finite state model with the correct modes and states.

1.4 Scope

This work focuses on developing the controller of an asynchronous wheelchair navigation that utilizes EEG and EOG artifacts embedded in EEG signals. The system should allow the wheelchair to move FORWARD and BACKWARD in three different directions namely LEFT, RIGHT and STRAIGHT. The wheelchair should also be able to STOP when instructed. In short, the system takes input signals from the user and transforms them into a command executed by the wheelchair. A graphical user interface (GUI) that provides system information like state, mode and remaining battery life must be provided. The proposed system must be tested in real-time experiments by healthy participants.

1.5 Thesis Organization

This thesis is organized as follows. In Chapter 2, the EEG acquisition system, the characteristics of main EEG rhythms and its artifacts are introduced. Then, existing works related to EEG and EOG based HMI are reviewed. Also, related works to wheelchair navigation and its current trend are discussed. Finally, the key techniques in signal processing for BCI controlled mobile robots are explained.

Chapter 3 describes the flow of the research process, the participants, the acquisition system and the protocols during the experimental sessions. Then, processing techniques for eyelid position and the horizontal gaze detection used in this study are described. Also, the implementation of sliding window is explained. Towards the end of this chapter, the proposed system that model as a finite state machine and fuzzy state transition are explained. This is followed by the hardware implementation in this study.

Subsequently, Chapter 4 discusses the findings obtained during experimental sessions and examples of signal analysis for each classification techniques will be

presented. The discussion will include the characteristics, property and uncontrolled factors contribute to performance in this study.

Finally, Chapter 5 concludes the study by presenting the contribution of this work, limitation and the implications of the work for future research.

CHAPTER 2

LITERATURE REVIEW

2.1 Introduction

In this chapter, a survey of the literature related to BCI is presented. First, a general overview of electrode placement, acquisition system, main frequency rhythms and artifacts in the EEG are defined. Then, the characteristics of EOG signals acquired from outer canthi will be described. Also, the existing studies that used EEG and EOG as a control input to HMI are reviewed. This is followed by the current trends of research in mobile robot application. Finally, the approaches in EEG signal processing are presented.

2.2 Electroencephalography

EEG signal is an electrical signal caused by the flow of the neurons during synaptic excitations in the brain. Acquiring a non-invasive EEG signal requires electrodes that placed on the scalp and acquisition system. The characteristics of the EEG signal can be defined according to their frequencies and position on the scalp.

2.2.1 Electrodes Placement

The electrode placement using International 10–20 system as shown in Figure 2.1 is the most common system used to acquire EEG signals. This system has two reference points at the middle in between two eyes (nasion) and at the base of the skull (inion).

The intervals of 10% and 20% are marked over the scalp based on these two reference points to determine the electrode positions.

A: Ear lobe

C: Central region

P_g: Nasopharyngeal

P: Parietal

F: Frontal

F_p: Frontal polar

O: Occipital area
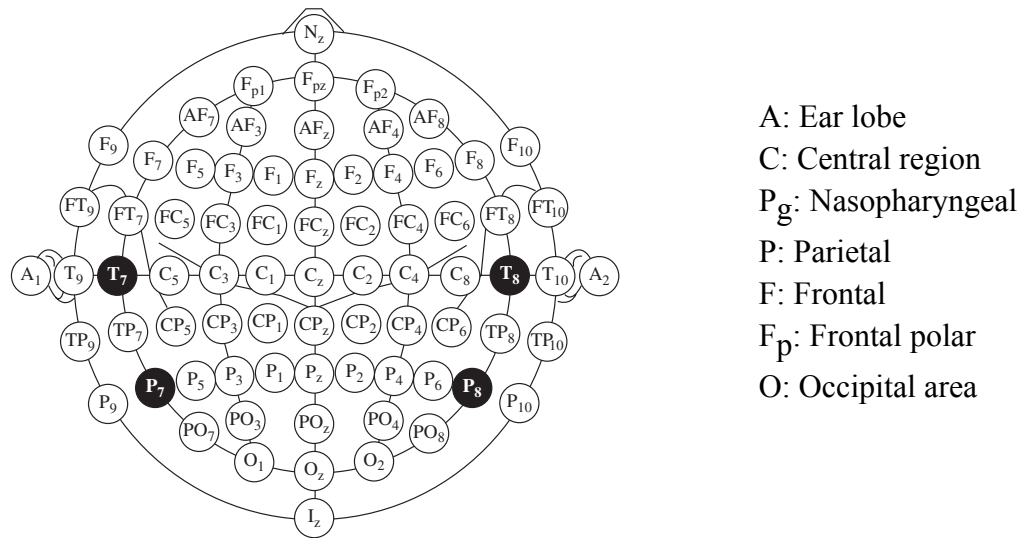
Figure 2.1: Electrodes placement based on the International 10–20 system for 75 electrodes (S. Sanei & Chambers, 2007). The letters that correspond to specific brain regions are described in the lower right of the figure.

In the EEG measurement, the signals can be recorded using two types of montage known as monopolar and bipolar (P. F. Diez, Mut *et al.*, 2010). The monopolar montage recorded the EEG signals by comparing it with a common reference as depicted in Figure 2.2 (a). Typically, the reference is placed at Cz or earlobe that has minimal cerebral activity. This montage allows a valid comparison of the EEG signals recorded from various electrode placements. In the bipolar montage, two interest channels are compared and their difference is recorded as shown in Figure 2.2 (b). Each of these montages has its own advantages and disadvantages as outlined in Table 2.1.
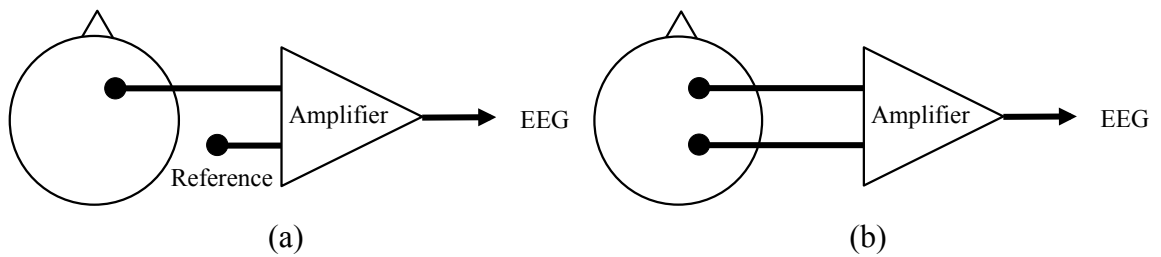
Figure 2.2: The EEG signals can be recorded using two types of montage known as (a) monopolar and (b) bipolar.

Table 2.1: The descriptions and comparison between monopolar and bipolar montage.

Montage	Advantage	Disadvantage
Monopolar	The EEG signal reflects the cerebral activity.	No ideal site for common reference.
• Cz reference	Equal distances between electrodes.	This channel contaminated with sleep potentials when the subject is asleep.
• Ear reference	A little cancelation and the signal appear higher in amplitude make it easier for detection.	Contaminate with ECG signals.
Bipolar	Typically use to record low to medium amplitude signals that are highly localized.	A flat line signal occurs due to equal potential between two channels.
• Longitudinal	Gold standard in EEG monitoring.	
• Transverse	Easy comparison of EEG signal between left and right, anterior and posterior head.	

2.2.2 EEG Acquisition System

The EEG acquisition system consists of an analog circuit and digital system to amplify the EEG signal in microvolt then transmit the data. For the past two decades, the advancement of the EEG acquisition system has improved the quality of signal recording and transmission mode. Basically, the system with a sampling rate up to 38.4kHz is available for consumer and research use from various manufacturers. The system with wired transmission mode offered higher signal quality compared to the wireless system. However, the wired systems are heavier with shorter operation time using batteries. The comparison of the acquisition system that powered from batteries is summarized in Table 2.2.

Table 2.2: Comparison of EEG acquisition system available for consumer and research usage that powered by batteries in Malaysia (Ramli, Mokhtar *et al.*, 2009).

Specifications	g.USBamp	g.Mobilab	Trackit	ActiveTwo
Manufacturer	g.tec	g.tec	Lifelines	Biosemi
Input channels	8 channels	4 channels	24 channels	16 channels.
Digitalization	24 bit	16 bit	16 bit	24 bit
Sampling rate	Up to 38.4kHz	256Hz	Up to 256Hz	Up to 16.384 kHz
Weight	1.55kg	360g	500g	1.1kg
Driver (LabVIEW)	Yes	Yes	No	Yes
PC transmission	Wired (USB)	Wired (USB) Bluetooth	Wired (USB) Bluetooth	Wired (USB)
Power source	Rechargeable battery pack	AA batteries	9V batteries	Rechargeable battery pack
Operation time	10 hours	100 hours	96 hours	>5 hours
Price rank	1st (Most expensive)	3rd	4th	2nd

In the research field, several scientific articles have been published in wireless EEG acquisition system for the last few years as listed in Table 2.3. The specifications of the proposed wireless systems are optimized to target their specific application such as workload observation, drowsiness detection and game control. In the listed studies, the highest sampling rate is offered by Brown *et al.* (Brown, van de Molengraft *et al.*, 2010) while Matthews *et al.* (Matthews, Turner *et al.*, 2008) recorded the longest operation time powered by batteries.

Table 2.3: Comparison of wireless EEG acquisition system in published papers (Lee, Shin *et al.*, 2013).
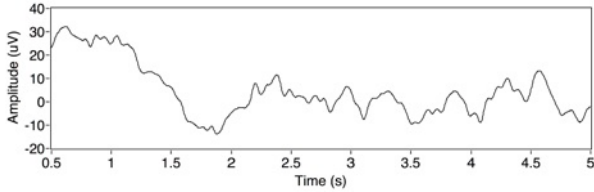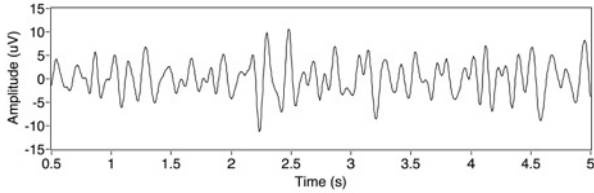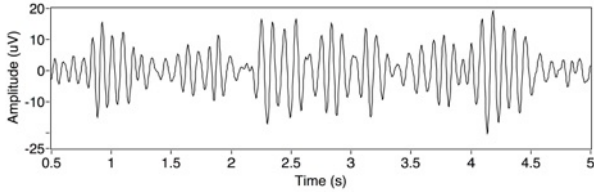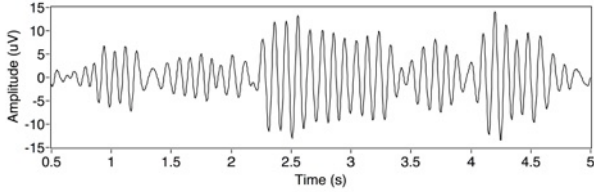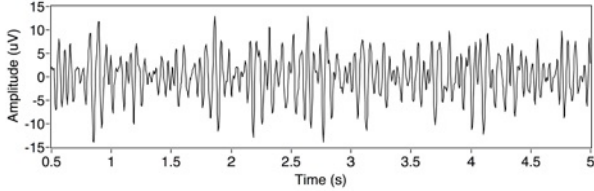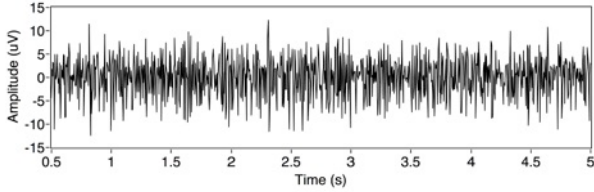
Specifications	(Matthews *et al.*, 2008)	(Brown *et al.*, 2010)	(Lin, Chang *et al.*, 2010)	(Liao, Chen *et al.*, 2012)	(Dias, Carmo *et al.*, 2012)
Input channels	7 channels	8 channels	3 channels	3 channels	5 channels
Digitalization	16 bit	11 bit	12 bit	12 bit	16 bit
Sampling rate	240Hz	256-1024Hz	512 Hz	256Hz	1kHz
Interface unit	PC	Not mentioned	Embedded processor	PC	PC
Power source	AAA batteries	3.7v 140mAh Li- Ion battery	3.7v 1.1Ah Li-Ion battery	3.7v 750mAh Li- ion battery	AA batteries
Operation time	80 hours	30 hours	33 hours	23 hours	25 hours
Design	Helmet	Headset	Headband	Headset	Brain cap
Application	Workload observation	Not mentioned	Drowsiness detection	Game control	Not mentioned

2.2.3 EEG Rhythms

The EEG signal consists of five main frequency rhythms known as Delta (θ), Theta (θ), Alpha (α), Beta (β) and Gamma (γ). These frequencies can be defined according to their placement over the scalp or biological significance. The examples of

the signals are shown in Table 2.4. The relevant characteristics of these frequencies are described as follows.

Table 2.4: Comparison of signal pattern in five main EEG rhythms.

Rhythm	Frequency	Signal Pattern
Delta	0.5 - 4Hz	
Theta	4 - 8Hz	
Alpha	8 - 14Hz	
Mu	8-13Hz	
Beta	14 - 30Hz	
Gamma	30-100Hz	

a) *Delta rhythm*

The frequency range of delta rhythm is below 4Hz. It can be observed during slow wave sleep in adult and normally seen in babies. The signal appears to be the slowest but highest in amplitude. It occurs most prominently in the frontal region for adults and the posterior region for babies. Individuals that suffer from neurological diseases show a large amount of delta activity during awake (Kübler, Kotchoubey *et al.*, 2001).

b) *Theta rhythm*

The frequency of the theta rhythm range between 4Hz to 7Hz and normally found in young children, during drowsiness or arousal and meditation in adults (Aftanas & Golocheikine, 2001). This rhythm is generally associated with creativity and intuition. The lower range of this rhythm presents during the states of calm, composed and drift between waking and sleep, while the higher range presents when the brain engaging with a complex and focused on problem solving (Fernández, Harmony *et al.*, 1995). Excessive theta rhythm during awake indicates problems with attention, head injuries, and learning disorders.

c) *Alpha rhythm*

Alpha rhythm occurs in the frequency range between 7Hz to 14Hz during relaxation or idle state. The signal is dominant in the posterior region (Pineda, 2005) when the eyes are closed and attenuates when the eyes are open. However, if excessive alpha activity is found in the frontal region, it is linked to depression and attention deficit disorder (ADD) in adults.

In addition, there is mu rhythm (8-13Hz) that partly overlaps to the normal alpha rhythm. It reflects the activity of motor neurons and dominant in the sensory and motor cortex area (G Pfurtscheller, Brunner *et al.*, 2006).

d) Beta rhythm

Beta rhythm is most evident in the frontal region and ranges between 15Hz to 30Hz. Generally, this rhythm is associated with intellectual activity and outward focus such as problem solving, processing information and feeling anxious (Schutter & Van Honk, 2005). Furthermore, this rhythm can be associated with the motor movement or imagery. During the motor activities, the rhythms are desynchronized and symmetrical distributions of the rhythms are altered.

e) Gamma rhythm

Gamma rhythm belongs to frequency range from 30Hz to 100Hz and the fastest brainwave. It is most evident in the somatosensory cortex during cross modal sensory processing that combines two different senses such as sound and sight (Müller, Keil *et al.*, 1999). A high gamma rhythm can be observed in individual with superior intelligence, enhanced memory and compassion. Contrarily, the deficiency of this rhythm is related to the learning difficulties, cognitive decline and diminished perceptual processing (Saeid Sanei & Chambers, 2008).

2.2.4 Artifacts in EEG

The EEG is highly susceptible to various artifacts that are non-cerebral origin. Technical artifacts are caused by equipment or environment and mainly attributed to

power-line noises (50/60Hz artifacts), cable movements or changes in electrode impedances. Also, interference of high frequency transmitted from other electronic devices can overload the EEG amplifiers. These technical artifacts can be prevented by proper electrode setup and shielding the amplifier.

Physiological artifacts that originate from the ocular, muscle and heart activity can introduce significant alterations in brain signals and ultimately affect the neurological phenomenon. For example, blinking generates high amplitude pattern in the brain signal that is larger in the frontal and decrease rapidly towards the posterior areas (Lins, Picton *et al.*, 1993) as shown in Figure 2.3. EOG activity is most prominent over the anterior regions and frequency below 4Hz (McFarland, Sarnacki *et al.*, 2005).

Movement of the head, body or jaw can result in a substantial distortion in the EEG signal and high in amplitude as the intensity of the movement is increased (Waterink & Van Boxtel, 1994). Finally, ECG artifacts present in the EEG signal due to heartbeats or respiration.
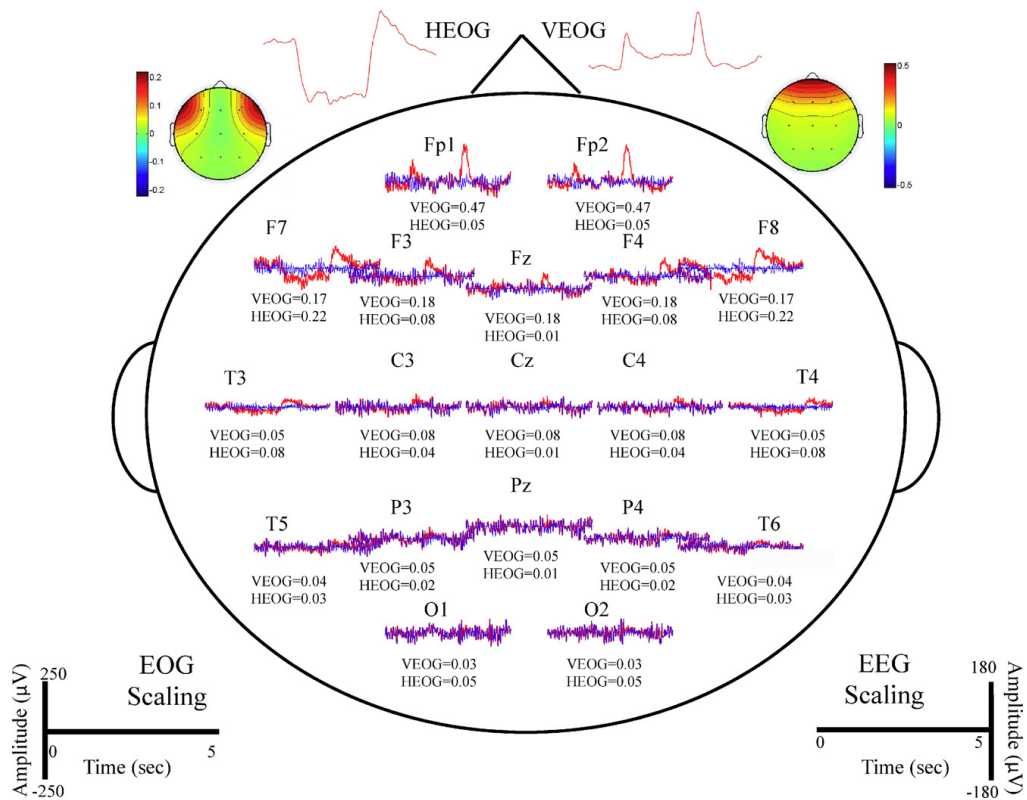
Figure 2.3: Contamination of vertical EOG (VEOG) and horizontal EOG (HEOG) in EEG signals are depicted in red color (Klados, Papadelis *et al.*, 2011).

2.3 Electrooculography

The EOG signal is an electrical signal generated by eye movement from the potential difference between the cornea and retina. Its amplitude is relatively high in the EOG signals recorded from the outer canthi ranging between 15-3500μV and easy to detect. Bandwidth of VEOG and HEOG recorded from the outer canthi was located in the range of 0.5–35 Hz. The EOG signal corresponding to gaze right, left, blink and closed eye is presented in Figure 2.4. In VEOG, natural blink and intentional blink can be distinguished by the strength and duration of the signal. A closed eye is formed by two pulses as a positive and negative pulse representing the moment of the eyelid is

closed and open. From Figure 2.4 (a) and (b), it can be observed that the HEOG is lateralized ipsilateral to the eyeball movement and also reflected in EEG signals. Therefore, the same characteristics of horizontal gaze are registered in HEOG and EEG.
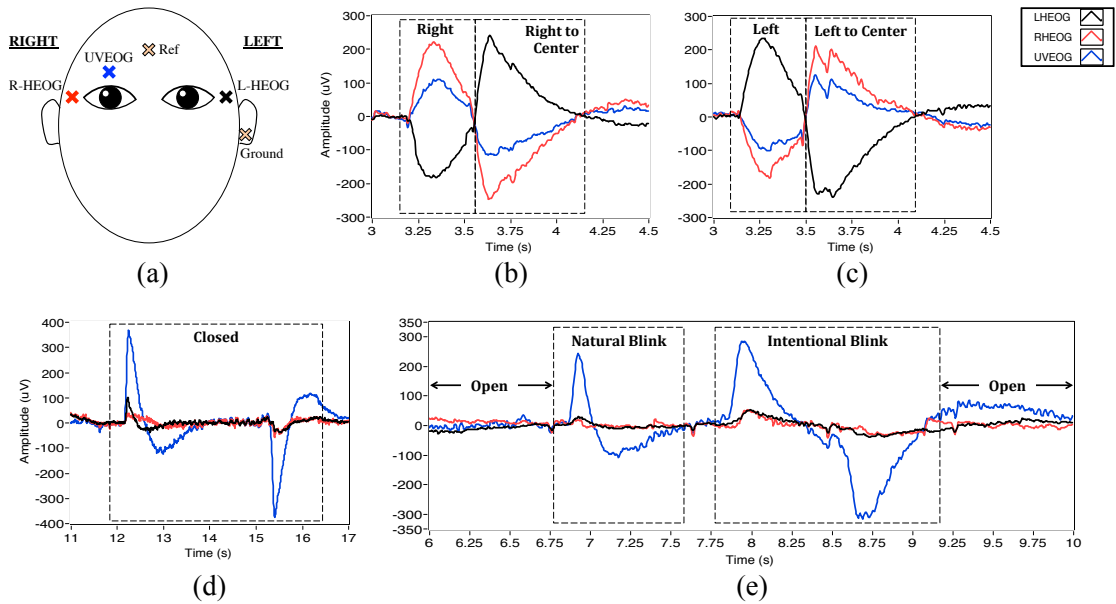
Figure 2.4: The EOG signal in the range of 0.5–35 Hz. (a) The electrode placement. (b), (c) HEOG is lateralized ipsilateral to eyeball direction. (d) A closed eye is represented by two pulses in VEOG during eyelid closed and open. (e) Distinction between natural and intentional blink in VEOG.

2.4   Human Machine Interface

Many alternative strategies of HMI using non-biosignal and electrophysiological signal have been proposed to operate assistive device (Latif *et al.*, 2008; Nguyen & Jo, 2012; Thorsten O. Zander *et al.*, 2010). The assistive device that operates from non-biosignal is normally received the hands free signals in the form of sip and puff (Mougharbel, El-Hajj *et al.*, 2013), eye tracking control (Nguyen & Jo, 2012), tongue

control (Kim, Park *et al.*, 2013), head gesture (Halawani, ur Réhman *et al.*, 2012) and chin control. These strategies are easy to execute, accurate and require less training. However, sufficient ability to move part of the body is required to control them, which are not in the case of severe motor disabilities.

In situations where the user with locked-in syndrome, approaches using electrophysiological signals that demand lesser control of the body functions are more suitable. Access to the device can be made by means of EMG (Xu, Zhang *et al.*, 2013), EOG and EEG (Kaufmann, Herweg, & Kubler, 2014).

2.4.1 Brain Computer Interface

EEG based HMI is also known as BCI, can translate the user's intention into computer commands. Various neurophysiological signals, such as, P300 wave, sensorimotor rhythms (mu and beta rhythms) and SSVEP can be recorded from the scalp using electrical brain signals or EEG. Many applications have been developed using P300, mu and beta rhythms and SSVEP as control signals such as character selection (Townsend, LaPallo *et al.*, 2010), virtual object movement (Piccione, Giorgi *et al.*, 2006), controlling robotic arm (Blasco, Ianez *et al.*, 2012), cursor control (Yu, Li *et al.*, 2012), word speller (Hwang, Lim *et al.*, 2012), wheelchair navigation (P. F. Diez, Mut *et al.*, 2011; Huang, Qian *et al.*, 2012; I. Iturrate, J. M. Antelis *et al.*, 2009; Kus, Valbuena *et al.*, 2012; Parini, Maggi *et al.*, 2009; B. Rebsamen, C. T. Guan *et al.*, 2010) and cursor movement (Lederman & Tabrikian, 2012) to assist physically challenged patients.

Compared to other neurophysiological signal to control BCI, SSVEP based BCI has the advantage of higher information transfer rate (ITR) with short training time. A

general comparison of different neurophysiological signal to drive BCI is summarized in Table 2.5.

Table 2.5: Comparison of the common neurophysiological signals used to drive BCI.

Brain Signals	Stimulus	Concentration	Training Time	Command Interval	ITR (bits/min)	No. of choices
SSVEP	Flickering lights	High	Short (Minutes)	Short (2–4s)	60–100	High
P300	Oddball paradigm	High	Short (Minutes)	Long (10–20s)	20–25	High
Sensorimotor rhythms	None	High	Long (Weeks)	Short (0.5–4s)	3–35	Low

a) SSVEP

SSVEP is a response to visual stimulation at specific frequencies observed in the occipital region as shown in Figure 2.5. SSVEP based BCI allow users to select a target by visually fixes attention on a flickering light with frequency above 4Hz and a higher ITR up to 100bits/min can be achieved with a little training. The SSVEP response differs between stimulus properties such as light, graphic and pattern (Zhu, Bieger *et al.*, 2010). Increasing the number of available frequencies will increase the number of targets, however, the accuracy and speed will be affected.

The advantage of SSVEP based BCI is high ITR and requires no significant training to operate. However, the flickering stimulus can be annoying for certain individuals and produces fatigue. A higher frequency stimulus has been utilized to reduce these issues, but makes the SSVEP harder to detect.
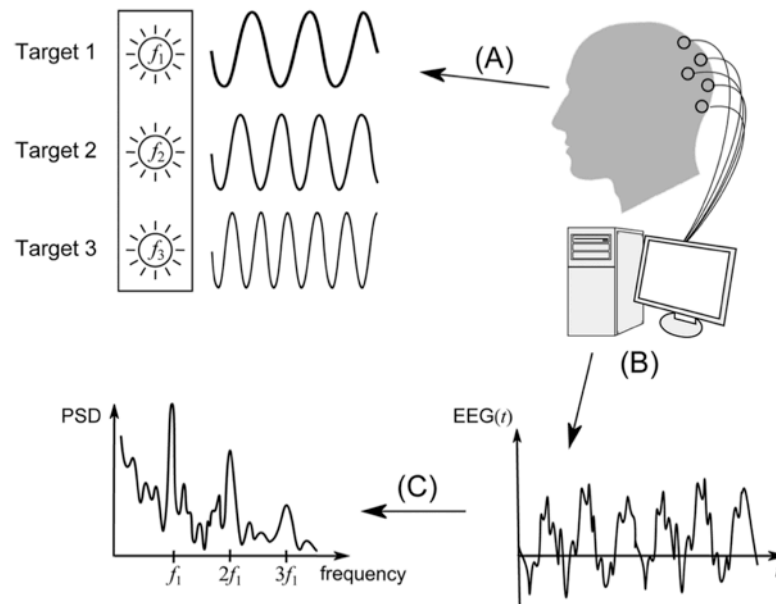
Figure 2.5: SSVEP decoding approach (A) Subject focus on Target 1, stimulus flickering at frequency f_1 (B) EEG is processed to obtain its power spectral density (C) The salient peak at f_1 imply that Target 1 as the selection (Chumerin, Manyakov *et al.*, 2013).

b) *P300*

The P300 wave is an event related potential (ERP) elicited by visual stimuli as a reaction to oddball paradigm. The largest P300 amplitude occurs when desired items are flashed in front of the participants (Polich, Ellerson, & Cohen, 1996) as the signal is related to individuals' motivation (Kleih, Nijboer *et al.*, 2010). The P300 is effective for both able (Minett, Zheng *et al.*, 2012) and disabled (Mak, McFarland *et al.*, 2012) bodies as no training is required and has been shown to have a relatively robust performance.

Many studies have been conducted to improve the interface paradigm (Jin, Allison *et al.*, 2012; Park & Kim, 2012) and signal processing techniques (Jin, Sellers, & Wang, 2012; Speier, Arnold *et al.*, 2012) for the analysis of P300 signal. For instance, the

checkerboard interface paradigm is reported to be superior to the standard row or column paradigm in terms of accuracy and speed (Townsend *et al.*, 2010) as shown in Figure 2.6.

(a)   (b)
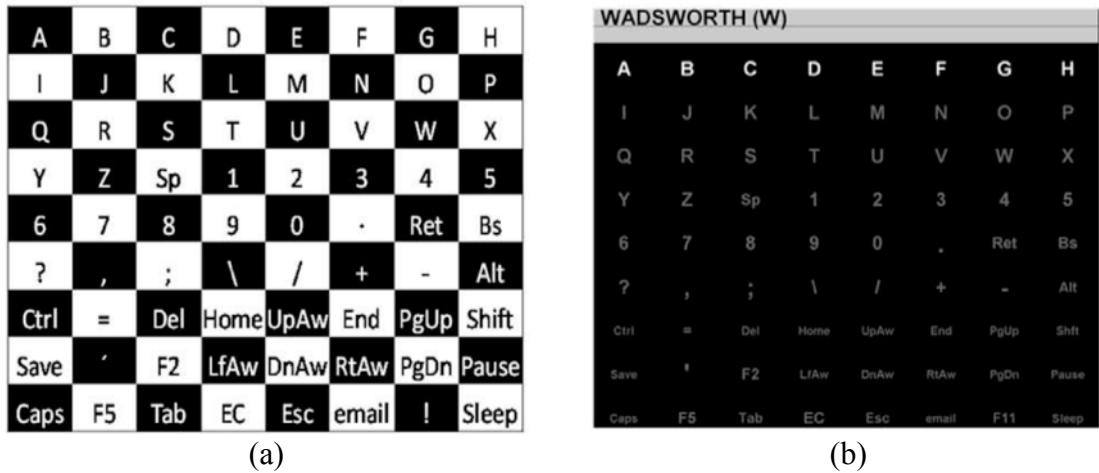
Figure 2.6: P300 paradigms containing 72 items presented in 8x9 matrix (a) checkerboard paradigm (b) row–column paradigm (Townsend *et al.*, 2010).

c)   *Sensorimotor rhythms*

Another neurophysiological signal used to control BCI is sensorimotor rhythm (mu rhythm), which can be generated by sensory stimulation, motor behavior and mental imagery. It is a known fact that imagination of actual movement can generate sensorimotor rhythms without the actual movement taking place (B. Blankertz, Sannelli *et al.*, 2010). The capacity of motor imagery varies between individuals with most individuals find it difficult (McAvinue & Robertson, 2008). Therefore, training needs to be implemented to extend the individuals' ability to imagine the actual movement (J. H. Li & Zhang, 2012). However, the effectiveness of mental training depends on the

presence or absence of disturbances of proprioception (Dettmers, Benz *et al.*, 2012) and physical fatigue (Di Rienzo, Collet *et al.*, 2012).

2.4.2 EOG based HMI

Due to advancement in technology, the acquisition of EOG signal can be simplified by the used of wearable EOG goggles (Bulling, Roggen, & Troster, 2009). The linearity between EOG and eye movements are stable in patients suffering from neurological disorders such as amyotrophy lateral sclerosis (ALS) (Ball, Nordness *et al.*, 2010) and muscular dystrophy (Kaminski, Al-Hakim *et al.*, 1992) with the exception of cerebral palsy (Woo, Ahn *et al.*, 2011) and multiple sclerosis (Prasad & Galetta, 2010), has attracted much attention as a source of information to control assistive devices. From directional eye movements, these signals can be used as an input platform for HMI devices such as remote control TV (Deng, Hsu *et al.*, 2010), virtual keyboard (Usakli & Gurkan, 2010) and robotic arm (Ianez, Ubeda *et al.*, 2012; Postelnicu, Barbuceanu *et al.*, 2012) to provide support to disabled person.

2.5 HMI Controlled Mobile Robots

HMI controlled mobile robots can serve as a powerful assistive device to help severely disabled people to gain mobility. Details of well-known wheelchair navigation systems using EEG, EOG and their hybrid are listed in Table 2.7. In the early systems of wheelchair navigation using these signals, the wheelchair could only be steered in forward direction (Cao *et al.*, 2014; B. Choi & Jo, 2013; K. Choi & Cichocki, 2008; Pablo F. Diez, Torres Müller *et al.*, 2013; Galan, Nuttin *et al.*, 2008; Hai, Van Trung, & Van Toi, 2013; I. Iturrate *et al.*, 2009; Kaufmann *et al.*, 2014; Khare, Santhosh *et al.*,

2011; Lamti, Ben Khelifa *et al.*, 2013; A. C. Lopes, Pires, & Nunes, 2013; Ning, Li *et al.*, 2012; B. Rebsamen *et al.*, 2010; Scherer, Lee *et al.*, 2008; C. S. L. Tsui, Gan, & Hu, 2011; Wang *et al.*, 2014). Later, the movement in the backward direction was introduced as an additional feature (Hai *et al.*, 2013; Kaufmann *et al.*, 2014; Khare *et al.*, 2011; A. C. Lopes *et al.*, 2013; Ning *et al.*, 2012; Wang *et al.*, 2014).

Table 2.6: Summary of relevant research works using EEG, EOG and their hybrid for wheelchair navigation systems.

Author(s)	System	Input	Available Command	Accuracy (%)	Execution Time (s)
(B. Rebsamen *et al.*, 2010)	Asynchronous	Imagery, P300	Destination selection	100	15
(Cao *et al.*, 2014)	Synchronous	Imagery, SSVEP	Forward, Left, Right, Deceleration, Acceleration, Constant Speed, Start, Stop	98.77	–
(Huang *et al.*, 2012)	Synchronous	Imagery	Forward, Left, Right, Stop	98.4	–
(Postelnicu, Girbacia, & Talaba, 2012)	Asynchronous	EOG	Forward, Backward, Left, Hard Left, Right Hard Right, Stop	95.63	–
(Pablo F. Diez *et al.*, 2013)	Synchronous	SSVEP	Forward, Left, Right, Stop	95	(44.6 bits/min)
(I. Iturrate *et al.*, 2009)	Synchronous	P300	Forward, Left, Right, Stop	94	–
(Hai *et al.*, 2013)	Asynchronous	EOG Artifacts	Forward, Backward, Left, Right, Stop	93.5	–
(Zhijun *et al.*, 2013)	Asynchronous	Imagery, EMG	Forward, Left, Right, Stop	92.5	–
(Long *et al.*, 2012; Wang *et al.*, 2014)	Asynchronous	Imagery, P300, Eye Blinking	Forward, Backward, Left, Right, Deceleration, Acceleration, Stop	92	2 ~ 5
(A. C. Lopes *et al.*, 2013)	Asynchronous	P300	Forward, Backward, Left 90°, Left 45°, Right 90°, Right 45°, Stop	88	4.7
(Galan *et al.*, 2008)	Asynchronous	Imagery	Forward, Left, Right, Stop	86.7	–
(Kaufmann *et al.*, 2014)	Synchronous	ERP	Forward, Backward, Left, Right	85.5	28
(Scherer *et al.*, 2008)	Asynchronous	Imagery	Forward, Left, Right, Stop	62	2

Recently, semi-autonomous wheelchair using shared-control between the operator and the wheelchair was introduced to provide assistance as well reduce the workload of the user (Al-Haddad, Sudirman, & Omar, 2011; Galan *et al.*, 2008; I. Iturrate *et al.*, 2009; C. Mandel, T. Luth *et al.*, 2009; J. Philips, del R.Millan *et al.*, 2007; B. Rebsamen, E. Burdet *et al.*, 2006; Vanacker, del R Millán *et al.*, 2007). However, wrongly interpreted commands may instruct the semi-autonomous wheelchair to perform unwanted moves.

2.5.1 BCI Controlled Mobile Robots

The first BCI developed for wheelchair navigation system or mobile robots was proposed by Millan et al. in 2004 (Millan, Renkens *et al.*, 2004). Since then, many researchers have contributed their efforts in developing and improving the brain-controlled wheelchair. In early studies, the wheelchair navigation was introduced in forward direction (B. Rebsamen, Burdet *et al.*, 2007; B. Rebsamen *et al.*, 2006) until recently the backward direction was introduced as an important feature in brain-controlled wheelchair (Khare *et al.*, 2011; Ning *et al.*, 2012; Wang *et al.*, 2014). Brain-controlled wheelchair requires higher safety aspect compared to other assistive device since they are used to transport disabled people. Therefore, high accuracy with fast computational time is preferable in translating the brain signals in this BCI.

Using shared-control approach, an autonomous system, which drives the wheelchair to the desired locations, can filter out the possible erroneous mental commands acquired by analyzing brain signals. The experimental results show the possibility of the shared control system being able to improve the overall driving

performance (Galan *et al.*, 2008; C. Mandel *et al.*, 2009; Vanacker *et al.*, 2007). This intelligent controller can be utilized to drive the wheelchair in predefined locations (B. Rebsamen *et al.*, 2006) or unknown environment (I. Iturrate *et al.*, 2009). However, the overall performance of these brain controlled wheelchair are mainly depends on the performance of the noninvasive BCIs, which are currently slow and uncertain. In addition, artifacts caused by eye movements or EOG are undesired signals in brain-controlled wheelchair that can introduce significant changes in brain signals and ultimately affect the performance of the BCI.

2.5.2 EOG Controlled Mobile Robots

One of the applications demonstrating the potential of the EOG signal for control is to navigate a wheelchair through eye movements (Barea, Boquete *et al.*, 2002b; Hashimoto, Takahashi, & Shimada, 2009; Postelnicu, Girbacia*, et al.*, 2012). In the early development of EOG controlled wheelchair, eye blink was detected to control robots (Kong & Wilson, 1998). Later, the direction of the eyeball was utilized to operate and change the direction of wheelchair accordingly (Barea *et al.*, 2002b; Ki-Hong, KIM, & Soo-Young, 2006). The direction of eye movement can be realized in four directional eye movements (left, right, up and down) including diagonal directions. However, it is difficult for the user to execute the diagonal eye movement. Therefore, from horizontal and vertical eye movements, finite state machine can be used to increase the number of signals to control a device (Gandhi, Trikha *et al.*, 2010; Trikha, Gandhi *et al.*, 2007).

It is a known fact that the performance of EOG controlled wheelchair is fast and high in accuracy compared with EEG as a control mechanism. An automatic navigation method with shared control can reduce the human efforts as well as to avoid obstacles in

the path to the desired destination (Al-Haddad *et al.*, 2011). However, the occurrence of constant eye movement will result in Midas touch problem and difficult to keep the system in idling state.

2.5.3 Hybrid BCI Controlled Mobile Robots

The BCI systems that rely on only one type of brain signals to translate user intentions into commands does not work for all users (B. Z. Allison, Wolpaw, & Wolpaw, 2007; Benjamin Blankertz, Losch *et al.*, 2008; Nijholt & Tan, 2008). Certain user finds it difficult to modulate brain signals in a way to control the BCI systems. Therefore, to broaden the user coverage and improve the performance of the brain-controlled wheelchair, hybrid BCI systems are proposed.

Hybrid BCI combines brain signal with one or more additional signal from EEG or other physiological sources such as EOG or EMG for real world applications (B Z Allison, Brunner *et al.*, 2010; Gert Pfurtscheller, Allison *et al.*, 2010). This strategy can improve the BCI performance, as the false positive from two sources would be needed for misclassification to occur. The hybrid BCI is typically processed simultaneously (Figure 2.7 (a), (b)) or operate two systems sequentially (Figure 2.7 (c), (d)), with the first system can act as either a "brain switch" or as "selector".

Multiple inputs into the interface can provide multiple commands for multi control direction for wheelchair navigation system (Cao *et al.*, 2014; Yuanqing *et al.*, 2013). Moreover, multi inputs allowed the user to control speed during navigating wheelchair in the open area or in narrow places (Long *et al.*, 2012). In a familiar environment, implementation of motion guidance or shared control will provide driving assistance as well reducing the workload of the user (B. Rebsamen *et al.*, 2010).

However, wrongly detected or executed commands will instruct the autonomous controller to unwanted moves.

SIMULTANEOUS PROCESSING   SEQUENTIAL PROCESSING

(a)

(b)

(c)

(d)
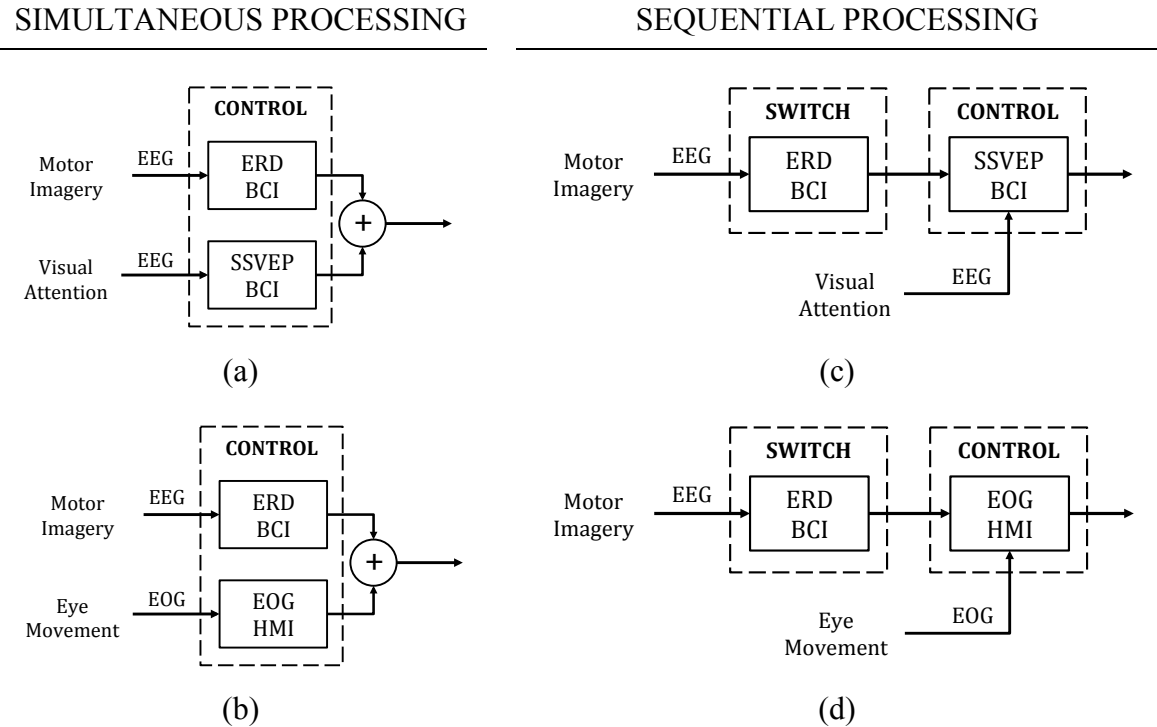
Figure 2.7: Examples of hybrid BCIs with at least one of the input signals must be a signal recorded directly from the brain. (a), (b): Simultaneous processing. (c), (d): Sequential processing.

Thus, an effective brain-controlled wheelchair is able to stop the wheelchair as fast as possible once the user gives the instruction. Therefore, several studies have contributed significantly to improve the response time of this command. In Rebsamen et al. (B. Rebsamen *et al.*, 2010) an average response time of 5.9s and 5.5s are achieved for fast P300 and mu/beta rhythm respectively. Then, Li et al. (Yuanqing *et al.*, 2013) proposing to combine P300 and SSVEP for the stop command and achieved an average response time of 5.28s. Blinking proposed in (Wang *et al.*, 2014) achieved a faster average response time of 2s to activate the stop command.

2.6 Signal Processing in BCI

After the EEG signals have been acquired, the artifacts from the power line and other unwanted signals can be removed in pre-processing. Then, the features can be extracted from the clean signals. Finally, these features can be classified accordingly and used as inputs to external devices.

2.6.1 Pre-processing

In the pre-processing, filtering technique using lowpass, highpass, bandpass and notch filtering is the most frequent technique used to remove frequency specific artifacts from power line and non-cerebral origin signals. However, this filtering technique only suitable to remove artifacts those are in the different frequency range as the component of interest in EEG signals. In most analyses, mixture of artifacts and signals is inevitable.

Therefore, independent component analysis (ICA) has been introduced to remove the artifacts that in the same frequency range as component of interest and have demonstrated its efficacy in several studies (K. Choi & Cichocki, 2008; James & Gibson, 2003; Lin, Ko *et al.*, 2006). However, this technique requires high computational complexity compared to filtering. Thus, ICA is unsuitable to eliminate artifacts in BCI for external devices that demand a fast response time such as wheelchair.

2.6.2 Feature Extraction

Once the EEG signals have been cleaned, the significant features can be extracted in time or frequency domain. Typically, the domain is selected with regards to the neurophysiological signals used in the BCI. For example, the P300 (Pires, Castelo-Branco, & Nunes, 2008) based BCI employed temporal features while event related desynchronization (ERD) (B. Z. Allison, Brunner *et al.*, 2012) and SSVEP (Sanchez, Diez *et al.*, 2011) based BCI use frequency features. Other features that had been utilized in designing BCI systems were time-frequency features (Yamawaki, Wilke *et al.*, 2006) and autoregressive parameters (Schlögl, Lugger, & Pfurtscheller, 1997).

2.6.3 Classification

In a BCI system, feature vector that has distinctive brain activity of user's intention can be classified accordingly. A variety of classifiers have been proposed to translate the features and generally it can be categorized into linear and non-linear classifiers as listed in Table 2.7.

Linear classifier such as LDA and SVM normally categorizes the features into two classes. In mobile robot applications, LDA has been adopted by numerous studies as a translation algorithm in their BCI system. The extended multiclass version exists with improved algorithms of linear classifier. This classifier is simple and has low computational complexity with acceptable accuracy. However, this classifier is susceptible to the presence of strong noise, thus, requires regularization.

Table 2.7: Classifiers used in BCI research.

Linear	Non Linear
Linear Discriminant Analysis (LDA)	Radial Basis Function SVM (RBF-SVM)
Fisher's LDA (FLDA)	Multi Layer Perceptron (MLP)
Regularized FLDA (RFLDA)	Bayesian logistic regression neural network (BLR NN)
Linear-Support Vector Machine (Linear-SVM)	Time-Delay Neural Network (TDNN)
Perceptron	Finite Impulse Response Neural Network (FIRNN)
	Gamma Dynamic Neural Network (GDNN)
	Gaussian Neural Network
	Vector Quantization Neural Network (VQ NN)
	Probability Estimating Guarded Neural Classifier (PeGNC)
	Fuzzy
	Hidden Markov Model (HMM)
	Input–output HMM (IOHMM)
	Bayes Quadratic
	Bayes Graphical
	K Nearest Neighbors (kNN)
	Mahalanobis Distance

Nonlinear classifier such as artificial neural network (ANN) and k-NN produce nonlinear decision boundaries in the training data. This classifier is generative and outperforms the linear classifier in rejection of uncertain samples. Furthermore, this classifier is efficient with low dimensional feature vectors, but very sensitive to the dimensionality of the feature vectors.

The performance of nonlinear classifiers applied to EEG signals produces only slightly better classification results over linear classifiers (Garrett, Peterson *et al.*, 2003). However, utilizing linear classifier can result in fast computational time, which is favorable in designing BCI system for a mobile robot application. The typical classifiers

that are applied in the study of brain controlled mobile robots are summarized in Table

2.8.

Table 2.8: Typical classifiers applied in P300, ERD/ERS and SSVEP-based BCI for controlled mobile robots (Bi, Fan, & Liu, 2013).

Classifier	Author (s)
P300-based	
LDA	(Escolano, Antelis, & Minguez, 2009; Escolano, Murguialday *et al.*, 2010; Iturrate, Antelis, & Minguez, 2009; Iñaki Iturrate, Javier Mauricio Antelis *et al.*, 2009)
SVM	(Bell, Shenoy *et al.*, 2008; Guan, Teo, & Zeng, 2007; Brice Rebsamen, Etienne Burdet *et al.*, 2006; B. Rebsamen, C. Guan *et al.*, 2010; Brice Rebsamen, Teo *et al.*, 2007; Shin, Kim, & Jo, 2010)
Statistical Classifiers	(Ana C Lopes, Pires *et al.*, 2011; Pires *et al.*, 2008; Zhang, Guan, & Wang, 2008)
ERD/ERS-based	
LDA	(Chae, Jo, & Jeong, 2011; Fan, Ng *et al.*, 2008; Geng, Dyson *et al.*, 2007; Geng, Gan, & Hu, 2010; Guan *et al.*, 2007; Leeb, Friedman *et al.*, 2007; Brice Rebsamen *et al.*, 2006; Brice Rebsamen *et al.*, 2010; Brice Rebsamen *et al.*, 2007; Ron-Angevin, Velasco-Alvarez *et al.*, 2011; Chun Sing Louis Tsui & Gan, 2007; Chun Sing Louis Tsui, Gan, & Roberts, 2009; Velasco-Álvarez, Ron-Angevin *et al.*, 2011)
SVM	(K. Choi, 2012; K. Choi & Cichocki, 2008; André Ferreira, Bastos-Filho *et al.*, 2010; Gomez-Rodriguez, Grosse-Wentrup *et al.*, 2011)
Statistical Classifiers	(Galán, Nuttin *et al.*, 2008; Millán, Galán *et al.*, 2009; Millan *et al.*, 2004; Johan Philips, del R Millan *et al.*, 2007; Vanacker *et al.*, 2007)
ANN	(Barbosa, Achanccaray, & Meggiolaro, 2010; Craig & Nguyen, 2007; C. Hema, Paulraj *et al.*, 2010; C. R. Hema & Paulraj, 2011; A. Satti, D. Coyle, & G. Prasad, 2011; Stamps & Hamam, 2010)
SSVEP-based	
LDA	(Christian Mandel, Thorsten Luth *et al.*, 2009; Ortner, Guger *et al.*, 2010; Prueckl & Guger, 2009, 2010)
SVM	(Dasgupta, Fanton *et al.*, 2010)

2.6.4 Finite State Machine

A finite state machine is an abstraction representation of mathematics that used in computer programs. Briefly, a finite state machine is a set of states which are connected by transitions. Transitions represented by arrows are the detection of BCI for state selection and this state can only be activated one at a time, called the current state. The finite state machine changes its state according to rules that specify the action when a new input is arrived. Figure 2.8 shows an example of a finite state machine in a diagram consists of two states and two inputs. Basically, the diagram of a finite state machine always accompanies by truth table that record the information of the state transition as presented in

Table 2.9.
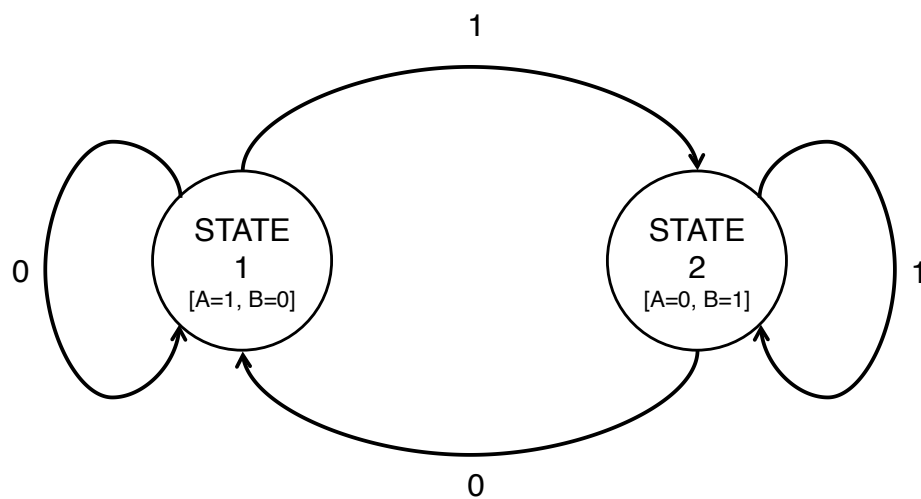
Figure 2.8: Example of a finite state machine. States are represented by bubbles while the transitions by arrows.

Table 2.9: The truth table for the state transition in Figure 2.8.

Current State	Input	Next State	Output	
			A	B
STATE 1	0	STATE 1	1	0
STATE 1	1	STATE 2	1	0
STATE 2	1	STATE 2	0	1
STATE 2	0	STATE 1	0	1

One benefit of finite state machine is the number of instructions to the machine can be maximized with a limited number of commands from BCI. In mobile robot applications, the state is associated with motion instructions to the wheelchair such as turn left, turn right, going forward or stop. Figure 2.9 shows an example of finite state machine in mobile robot application presented in (Teymourian, Lüth *et al.*, 2008). Two input signals from SSVEP are used as transition between states resulting in four types of instructions to the wheelchair, which are STRAIGHT, LEFT, RIGHT, and STOP.
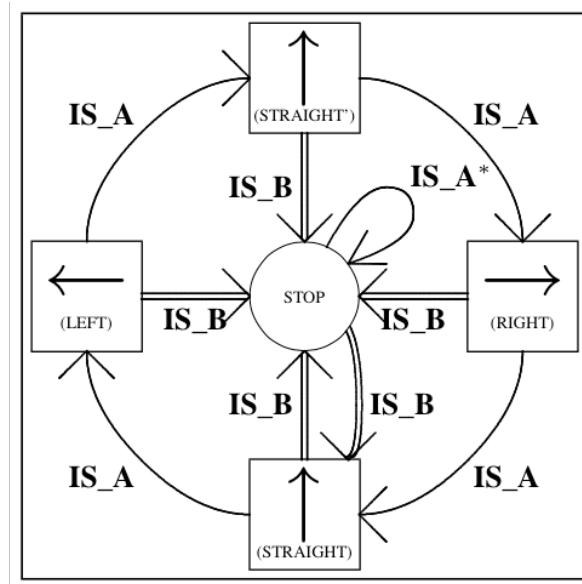
Figure 2.9: Example of finite state machine implemented in mobile robot application (Teymourian *et al.*, 2008).

Other published work that applied finite state machine technique in mobile robot application are listed in Table 2.10.

Table 2.10: Studies related to mobile robot application that implemented finite state machine in their work.

BCI	Author(s)
P300	(Escolano, Antelis, & Minguez, 2012) (I. Iturrate *et al.*, 2009) (Gentiletti, Gebhart *et al.*, 2009)
SSVEP	(Pablo F. Diez *et al.*, 2013; Teymourian *et al.*, 2008)
Imagery	(A. R. Satti, D. Coyle, & G. Prasad, 2011)
ERD/ERS	(Cheein, De La Cruz *et al.*, 2009)
Hybrid BCI	(Andre Ferreira, Celeste *et al.*, 2008)

Another used of finite state machine is to overcome the Midas touch problem. This problem commonly occurs in the studies that involving eye control (Abe, Ohi, & Ohyama, 2013). For example in EOG signals, the same patterns of signals are recorded during looking around the environment and invoking the action to command a wheelchair. If the HMI is unable to distinguish between natural and intentional eye movement, the signals will be translated as intent to move the wheelchair. This unwanted movement would upset the user as well as endangering their safety. Distinguishing two nearly identical signals will require a complex algorithm thus, high computation time.

Conversely, implementation of finite state machine as secondary control can overcome the Midas touch problem by applying a set of simple rules in state transition (Barea, Boquete *et al.*, 2002a). For instance, if a transition between the current state to the next can be made by a closed eye, any eye movement such as look left, right or blink performed by the user will not trigger the transition. Therefore, any unintentional command can be prevented.

2.7 Summary

Various neurophysiological signals can be recorded in EEG signals such as P300 wave, mu and beta rhythms and SSVEP. These signals can be used as control mechanism for physically disabled individuals to operate assistive device. However, controlling these signals require a high degree of concentration and unsuitable for individual with presence of cognitive impairments.

Therefore, hybrid BCI is introduced to provide an efficient channel for interaction for patients who are partially lost control over muscular activity. This type of BCI combines EEG signals with other physiological signals such as EOG, EMG or ECG (Gert Pfurtscheller *et al.*, 2010). Moreover, hybrid BCI can be utilized to combines multiple neurophysiological signals sequentially or simultaneously for various applications. However, it remains a challenge to design a fast and high-efficiency hybrid BCI for wheelchair navigation system.

In this thesis, alpha rhythm and EOG artifacts in the EEG are utilized as inputs to the hybrid BCI. These signals are fast, stable and easy to generate that are suitable for physically disabled with cognitive impairments. Nevertheless, the Midas touch problem always associated with the application that relies on eye control as input. Furthermore, only a limited number of eye movements can be realized to control the wheelchair. To overcome these limitations, finite state machine is employed in this work. A finite state machine is a representation of mathematical abstraction applied in computer programming. In this work, states in the finite state machine are representing the action of the wheelchair while the transitions are the outcome from the hybrid BCI.

Currently, there are limited studies that employing alpha and delta rhythm as input to BCI, thus, limited information on their signal processing. Therefore, the processing techniques employed in this work are based on the previous work that using different neurophysiological signals. As this work will be tested in actual navigation task, any selected processing technique must result in high accuracy rate as well as fast computational time. Therefore, the selection of processing techniques is based on following general requirements, ability to analyze in time series domain, linear classifier and low computational complexity. This result in selection of variance (Ahn, Ahn *et al.*,

2013), 2nd order difference plot and central tendency measurement (CTM) (Thuraisingham, Tran *et al.*, 2007), and area under the signal (Luck, 2004) for alpha rhythm analysis. For delta rhythm, LDA (Aloise, Schettini *et al.*, 2012), K-Means (Kaur, Soni, & Rafiq, 2014), and area under the signal are selected.

CHAPTER 3

METHODOLOGY

3.1 Introduction

The research work begins by collecting data from healthy participants during Recording Session to study the properties of the alpha rhythm and EOG artifacts in EEG signals. Then, the collected data are processed and classified accordingly in Offline Session. The performances of the processing techniques are compared in Online Session with real-time experiment without actual wheelchair movement. The processing techniques with the highest score are used as input into the navigation system. The system is designed as a finite state machine and used fuzzy rules for the state transition. This is followed by the implementation of the proposed navigation system to the wheelchair. Finally, the system is tested and evaluated with actual navigation experiment in Navigation Session. The process of research work can be summarized as in Figure 3.1.

DATA COLLECTION
• Recording Session

SIGNAL PROCESSING
• Offline Session
• Online Session

NAVIGATION SYSTEM DESIGN
• Finite State Machine

HARDWARE IMPLEMENTATION
• Wheelchair Interface

TESTING PHASE
• Navigation Session
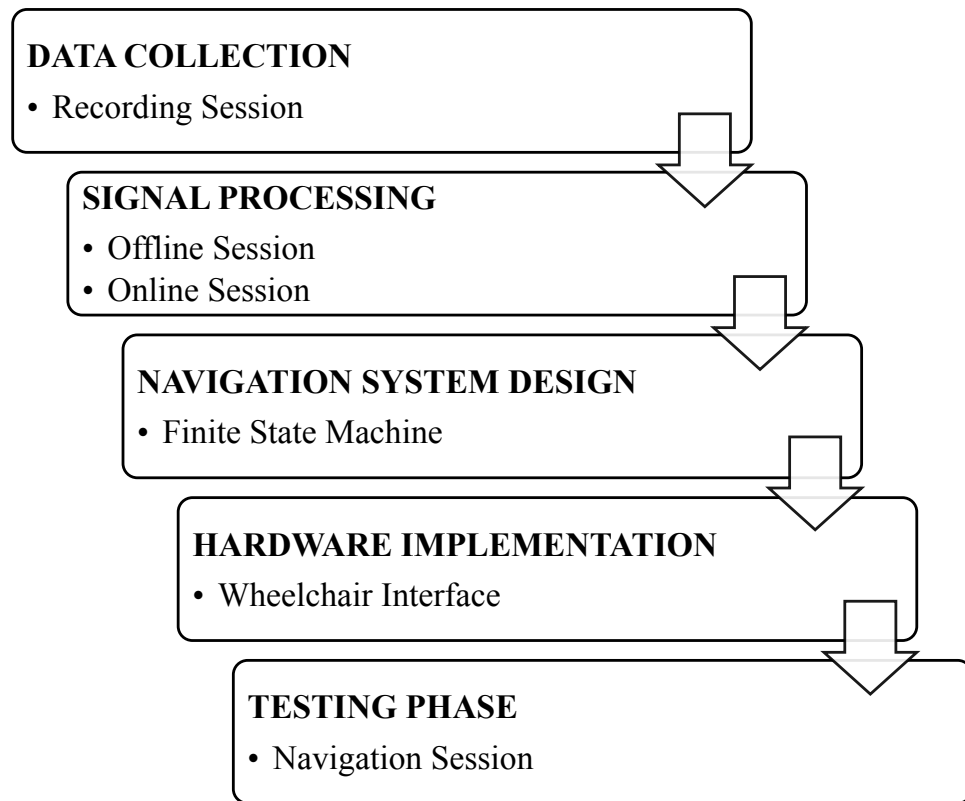
Figure 3.1: Process of developing navigation system in this work.

3.2 Data Collection

3.2.1 Participants

A total of 20 healthy participants (12 females, 8 males) between 23 to 27 years old (Mean = 25.15, SD = 1.69) with no prior experience with EEG recording were selected in this study. The selection of the participants is made based on young adult group age from 20 to 30 years old to avoid the age effect on alpha rhythm responses in EEG (Kolev, Yordanova *et al.*, 2002; Nombela, Nombela *et al.*, 2014). All participants are students and colleagues from the University of Malaya, who had normal or corrected to normal vision. The participants are briefed on the purpose and nature of the study and asked to sign a consent form before the EEG recording began.

3.2.2 EEG Signal Acquisition System

The EEG signals are acquired using wireless g.Mobilab from Guger Technologies at a sampling rate of 256Hz. The gold electrodes of monopolar montage are placed at C3, C4, O2 with reference connected to Cz and the ground attached to the forehead (FPz). The electrode arrangement followed the International 10-20 system and the impedance is measured before, during and after the experiment to maintain below $10\,\Omega$. Since the experiment is conducted in unshielded room, the laptop is powered by the batteries to minimize electrical interferenced in the EEG data. The EEG signals are acquired and then analyzed using LabVIEW software from National Instrument.

3.2.3 Recording Session

The objectives of this session are to record the EEG signals and study the characteristics of eyelid position and horizontal gaze in alpha and delta rhythm respectively. During the Recording Session, the visual stimulus is given to participants as shown in Figure 3.2.

Each trial is recorded in 10 seconds duration and the tasks are issued in pairs as shown in Figure 3.3. The participants are instructed to open their eyes for the first half of the trial, and performed four possible tasks of blink, closed eye, left or right gaze that were randomly assigned in the second half of the trial. Each task is repeated for five times and evenly issued in 20 trials for every subject.
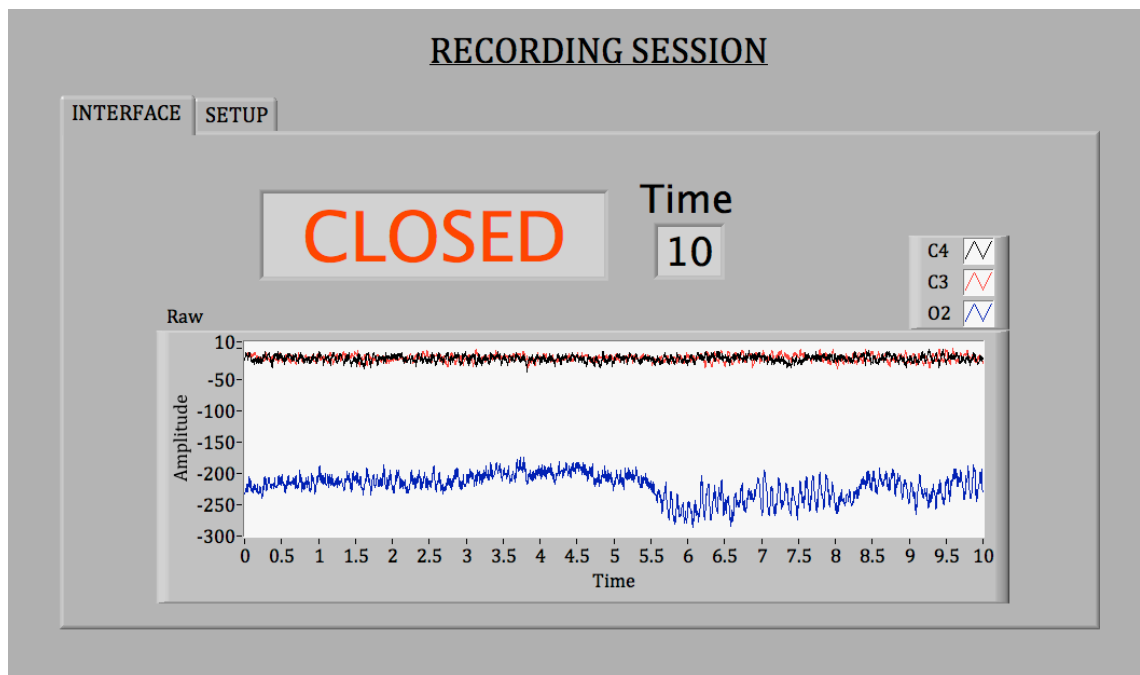
Figure 3.2: Graphical user interface of visual stimuli during Recording Session.

In each trial, the participant is expected to respond within 2 seconds after the onset of instruction and 15 seconds rest is given between trials. Their performances are manually validated during the session and if any of the instructions are wrongly executed, the instruction pair is repeated. At the end of the session, a total of 400 trials of EEG signals were collected from 20 participants.

The blink recorded in this session is in the form of quick closed eye or hard blink that performed for approximately 0.5s. In opposite, the closed eye is performed for 1 second or longer. Throughout the session, natural blink is allowed and the participants are asked to stay still by minimizing any muscle movement.
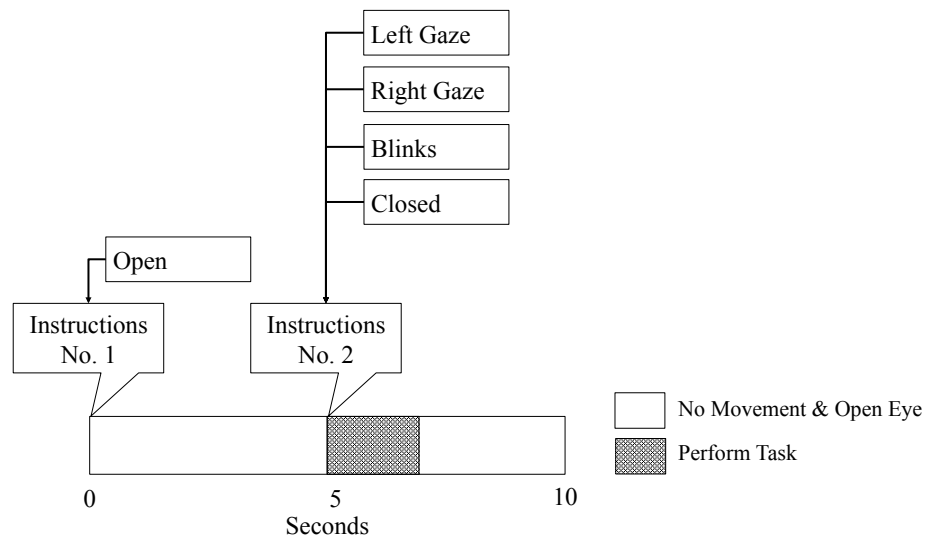
Figure 3.3: Instructions in a trial are issued in pair with time allocated for each task is only 5 seconds during the Recording Session.

3.2.4 Signal Properties

The EEG signals related to eyelid position and horizontal gaze are recorded during Recording Session. These signals can be described as follows.

a)   *Eyelid Position in EEG*

The common amplitude of the alpha rhythm is around $5 - 10$uV when the eyes are open and it increases to $20 - 50\mu V$ when they are closed as shown in Figure 3.4. These signal patterns are most obvious in the occipital region, thus, signal acquired from channel O2 is used to determine the eyelid position. Since the blink is a formed of closed eye, the same fluctuation of alpha rhythm is observed during blink and closed eye with regard to their duration. Furthermore, the presence of EOG artifacts such as natural blink and horizontal gazes in alpha rhythm are negligible with an exception in the frontal region (Hagemann & Naumann, 2001).
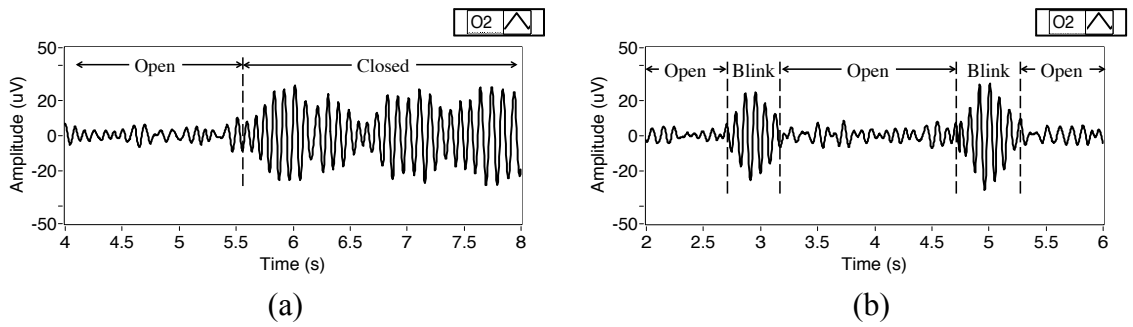
Figure 3.4: Alpha rhythm signals observed in channel O2 at the occipital during (a) closed eye and (b) blink.

b) *Vertical and Horizontal Gaze in EEG*

EOG artifacts are caused by ocular activity such as blinking and eye movements. EOG activity is most prominent over the anterior regions and in frequency below 4Hz (McFarland *et al.*, 2005). Both vertical and horizontal gaze generate substantial activity in the delta rhythm that is larger in the frontal and decrease rapidly towards the posterior region (Lins *et al.*, 1993). Further, vertical gaze and natural blink has minimal effect laterally, while horizontal gaze is lateralized ipsilateral to eyeball direction (Klados *et al.*, 2011). The delta rhythm signals from channel C3 and C4 contained less contamination of vertical gaze compared to the frontal region but preserved significant artifacts of horizontal gaze. For this reason, these channels are selected to determine the horizontal gaze in this work.

The artifact of horizontal gazes appears in the delta rhythm as a pulse that localized in time. The gaze from the center to the left will induce a strong positive pulse at C3 and weaker negative pulse at C4. In opposite, when the gaze is moved from the center to the right, a strong positive pulse at C4 and weaker negative pulse at C3 are observed. The gaze from left to center will register a positive pulse at C4 and a negative

pulse at C3 same as gaze from the center to the right. The same principle can be observed for the gaze from right to center with gaze from the center to the left. However, these pulses between gaze to the corner and from corner to center are not identical that differ in strength and duration. Generally, the gaze to left or right produced a strong pulse for 0.5s while the gaze from left or right to center produced a weaker pulse for 1.5s as shown in Figure 3.5.
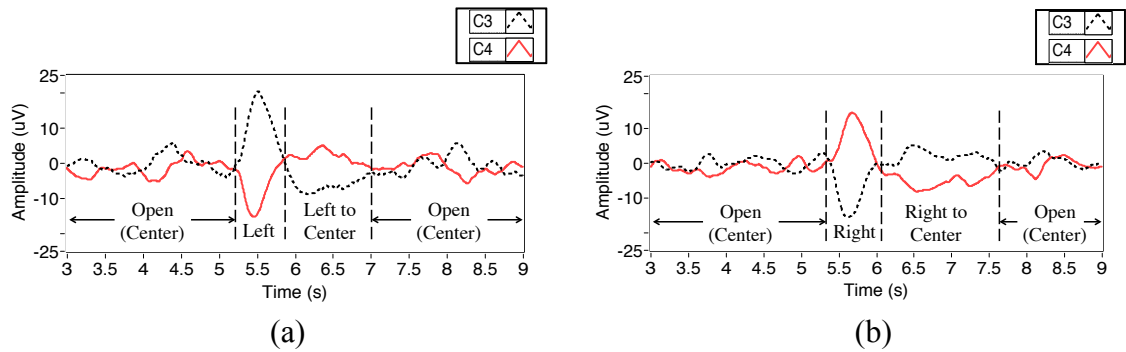
Figure 3.5: EEG signals at channel C3 and C4 of delta rhythm during (a) left gaze and (b) right gaze.

3.3 Signal Processing (Offline Session)

The Offline Session involves analyzing the recorded EEG signals in Recording Session and calculating parameters in processing technique for each participant. The flow of data processing and classification for eyelid position and horizontal gaze detection is summarized in Figure 3.6. First, the alpha signal is examined to determine whether the eyes are open or closed. If the eyes are open, the delta signal is used to monitor the eye gaze movement to the left and right.

3.3.1 Filtering

After acquiring the EEG signals, they are filtered to remove noise. For the alpha rhythm, a Butterworth bandpass filter is used to capture the information within 8-13Hz since this frequency range contains information related to the open or closed eye condition. For the delta rhythm, a Butterworth lowpass filter with a cutoff frequency of 3Hz is utilized. For each signal, a sliding window containing 128 samples is analyzed consecutively.
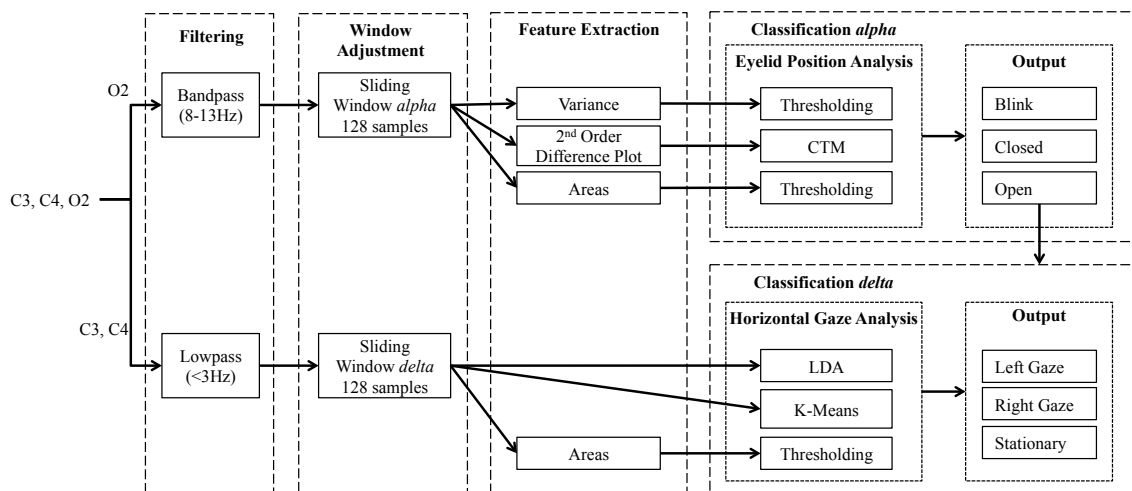
Figure 3.6: The flow of signal processing for detection of eyelid position in alpha rhythm and horizontal gazes in delta rhythm. This architecture will be implemented in Online Session.

3.3.2 Sliding Window

A conventional and overlapping window is rigidly positioned that may split important cues in signals. In contrast, a sliding window is able to adjust its position so that the cue will be captured entirely within it. In this study, when a blink or gaze movement is performed, a short accompanying cue is registered in alpha and delta

signals. For example, while analyzing the alpha signal, the conventional and overlapping window frame might capture an interval when the eyes are just about to open or closed. During this short period, the signal is in transition from low amplitude to high or vice versa. In this case, the samples in the window will be a mixture of those with low and high amplitudes as shown in Figure 3.7 (a), (b).
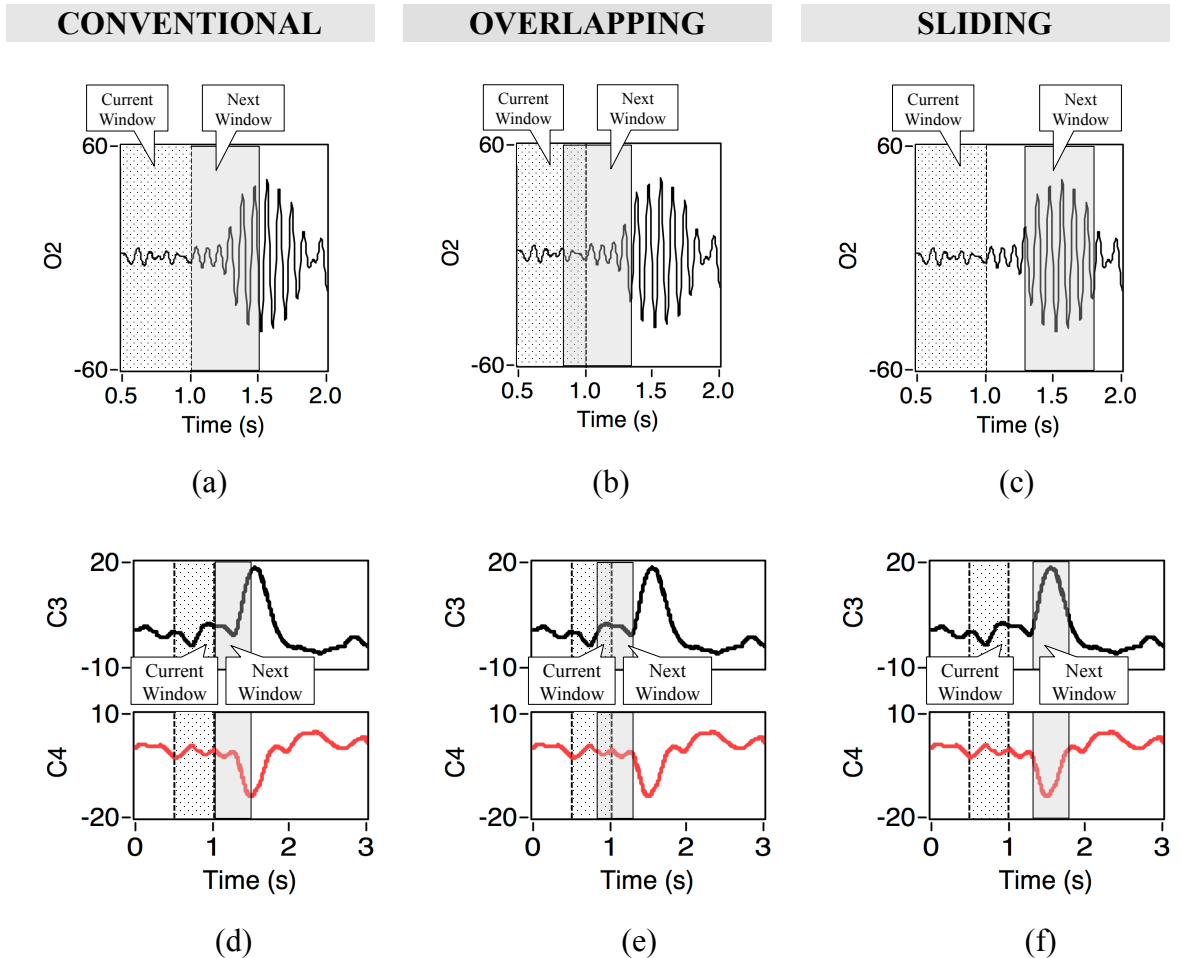
Figure 3.7: (a), (b), (d), (e) The conventional and overlapping window will lose part of the crucial features in signal. Insufficient information in a window, will lead to misclassification. (b), (d) Sliding window will automatically adjust its position so that the full cue is captured within its interval.

In the analysis of the alpha signal, the position of the sliding window is adjusted as follows. First, the absolute values of the samples in the window are divided into eight adjoining subintervals where each subinterval contains 16 samples. Then the average of samples in each subinterval is calculated and the averages of the first and last subinterval are compared. If the absolute difference of the two averages is more than a specified threshold (called *threshold_alpha*), the window is shifted to the right by 16 samples. The process of calculating and comparing the averages of the first and last subinterval is repeated until their difference is less than the *threshold_alpha*. In our experiment, the *threshold_alpha* was set at half of the mean absolute values of closed eye samples of the user. Once this condition is met, the window position is fixed and the features can be extracted. The procedure to adjust the window position is illustrated in Figure 3.8.

For capturing important cues in the delta signals of C3 and C4, the position of the window is also adjusted to find the best location where that cue is fully captured by the window as shown in Figure 3.7 (d). First, the samples in the window are divided into eight non-overlapping subintervals where each subinterval contains 16 samples like before. Then the average values of the subintervals are calculated and compared to a threshold (called *threshold_delta*). If all of them are below the *threshold_delta* then it is assumed that no gaze shift occurs and the position of the window is maintained. Otherwise, the position of the window is adjusted so that the subinterval that records the highest average is placed at the center of the window. Since the peak of the pulse is associated with the highest average, it should be positioned either in the 4th or 5th subinterval, whichever position that incurs the least shift in the new window position.

This step is necessary to obtain high classification accuracy if the data in the window are used as inputs. Here, the *threshold_delta* is taken as the midpoint of the average amplitude of the peaks recorded during horizontal gaze. In open eye condition, once the window in the C3 and C4 delta signal is adjusted, the one in alpha signal will obey accordingly.
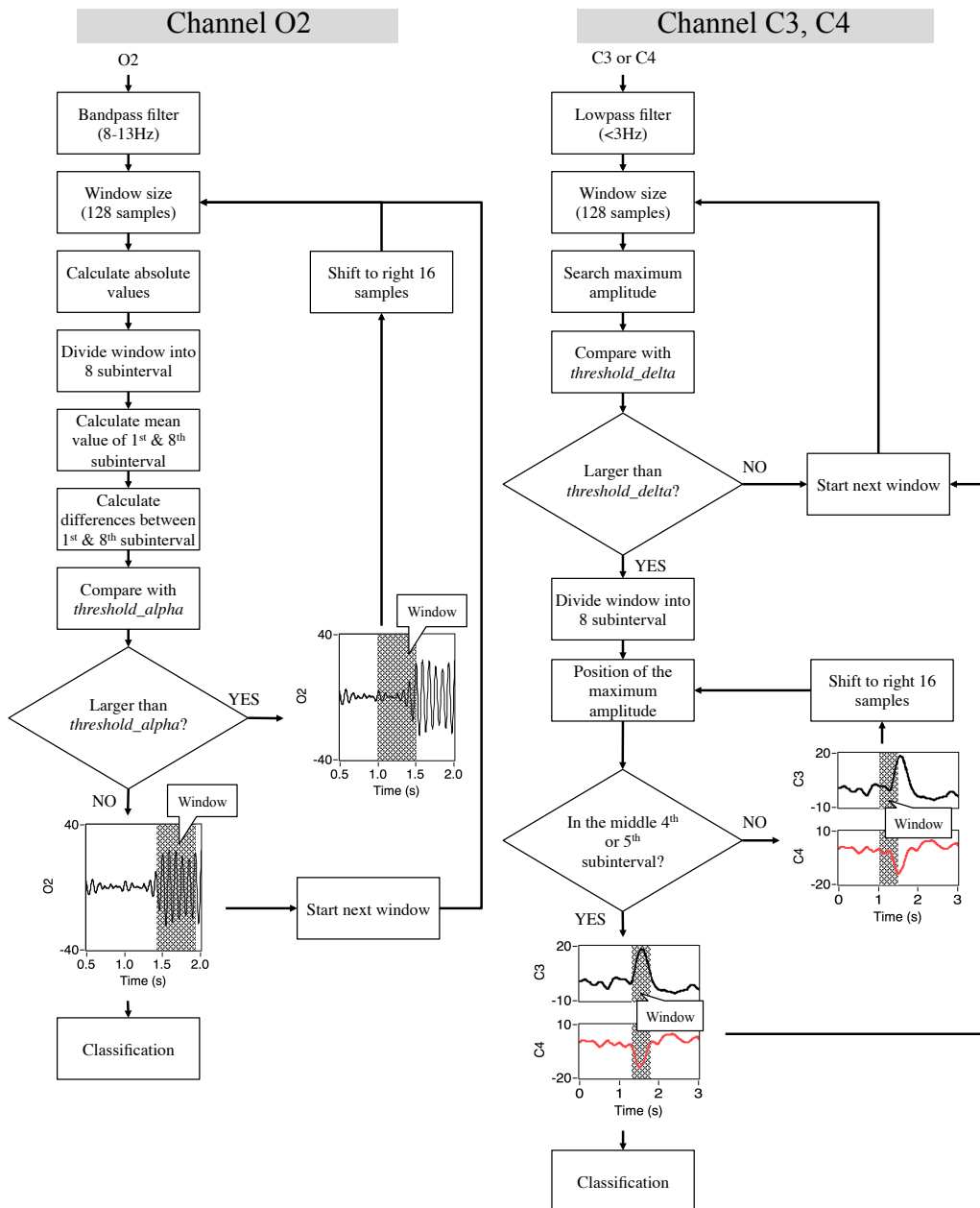
Figure 3.8: The process to reposition the sliding window during Online and Navigation Session.

3.3.3 Eyelid Position Analysis

The filtered alpha rhythm signal in channel O2 exhibits relatively higher amplitude of fluctuation when the eyes are closed than when they are open. Features can

be extracted from the alpha signal and classified to determine the eyelid position of blink, closed and open eye. In eyelid position analysis, three types of features are studied, there are variance, 2nd order difference plot and area. Then, these features will be classified by thresholding and CTM.

a) *Variance and Thresholding*

Variance (σ^2) is a measurement of variability of data set from their mean or expected value. The variance of alpha signal in O2 can be computed as in equation (3.1) taking account of mean of 128 samples in a window (μ), number of sample in a window ($N = 128$) and value of each sample ($x(t)$).

$$\sigma^2 = \frac{1}{N} \sum_{k=0}^{N-1} (x(t) - \mu)^2 \qquad (3.1)$$

In this study, a mean variance of alpha signal during open eye (called *threshold_variance*) was computed over open eye trials from the recorded data. The alpha signals from a particular window in O2 will be classified as an open eye if the calculated variance was equal or smaller than the *threshold_variance*, while larger variance will be classified as blink or closed eye with regard to the duration of closed eye.

b) *2nd Order Differential Plot and Central Tendency Measurement*

In this approach, the 128 samples of alpha signal in a O2 window are plotted as second-order difference plot to display the successive rates of variability against each other as in equation (3.2).

$$[x(n+1) - x(n)] \text{ is plotted against } [x(n+2) - x(n+1)] \tag{3.2}$$

Where, $x(n)$ is denoted as sample value of alpha signal at discrete time n. The examples of second-order difference plotted for five EEG rhythms are shown in APPENDIX B.

Then, the CTM is used to measure the variability in the second-order difference plot by counting points (x) that fall within the radius (r) and divide by the total samples in a window $(n = 128)$ as describe below in equation (3.3) and (3.4):

$$\text{CTM} = \frac{\sum_{i=1}^{n-2} \delta(d_i)}{n - 2} \tag{3.3}$$

$$\delta(d_i) = \begin{cases} 1 \; if \; ([x(i+2) - x(i+1)^2] + [x(i+1) - x(i)]^2)^{0.5} < r \\ 0 \; otherwise \end{cases} \tag{3.4}$$

The CTM value represents the fraction of the total points lie within the radius without distinguishes between sign. In this study, the optimum radius was chosen when CTM reaches a value of 0.90 to avoid spurious high frequency noisy components at larger radius value as suggested in (Thuraisingham *et al.*, 2007). Then, the radius difference (r_d) between the radius of the current window $r(0.90, eye)$ and mean radius of open eye $r_{mean}(0.90 \; open)$ when CTM reached 0.90 can be defined as follows:

$$r_d = r(0.90, eye) - r_{mean}(0.90 \; open) \tag{3.5}$$

The mean radius of open eye, $r_{mean}(0.90 \; open)$ for each participant are calculated over collected data.

The classification of open and closed eye was based on the sign of r_d value from the equation (3.5). The alpha signal of the closed eye contains higher variability

compared to the open eye, thus, the positive value of r_d will yield closed eye condition while a negative value yield open eye condition. Again, the distinction between blink and closed eye are made with regard to their duration.

c)   *Area in Alpha Rhythm and Thresholding*

This technique used the concept of area calculation and threshold to classify alpha signal in O2 into closed, blink and open eye. First, the absolute value of the sample ($|x_i|$) is calculated between the envelope and the x-axis at 0μV. Then, the area ($Area_{O2}$) in a single window frame is represented by summing the absolute values of all 128 samples ($N = 128$ samples) as in equation (3.6):

$$Area_{O2} = \sum_{i=1}^{N} |x_i| \tag{3.6}$$

This value will be compared with a mean area of open eye (called *threshold_area$_{O2}$*) that determined from individual's trial. Exceeding the *threshold_area$_{O2}$* will denote as blink and closed eye due to higher fluctuation of alpha rhythm, while low $Area_{O2}$ value will denote as the open eye.

3.3.4 Horizontal Gaze Analysis

The horizontal gaze direction can be inferred from the delta rhythm signals in channels C3 and C4. In this analysis, feature such as the area is extracted from the C3 and C4 signals and used to determine the change in gaze direction by thresholding. Otherwise, the delta rhythm contained in the windows of C3 and C4 signals can be directly used as inputs to K-Means and LDA.

a) *Linear Discriminant Analysis*

LDA is a supervised learning that required data assigned to the respective group at the beginning of the analysis as a model. Three groups of data; left gaze, right gaze and stationary were assigned to LDAs to create the predetermined model that unique for each subject. A total of 15 signals for each participant are assigned into these groups evenly. Then, the global mean (μ) and group mean (μ_k) vector of delta signals in C3 and C4 window are computed. In this analysis, the vector represents by $X_{(x,y)}$ are the combination of delta rhythm samples from C3 on the y-axis and C4 on x-axis. Details algorithm of LDA is presented in APPENDIX C.

In this work, two LDA classifiers are used to classify the changes of eyeball direction. The first LDA decides whether the eyeballs move to the left or remain stationary while the second LDA decides whether the eyeballs move to the right or remain stationary. The combination of these outputs from two LDAs will determine the current gaze as shown in Figure 3.9.
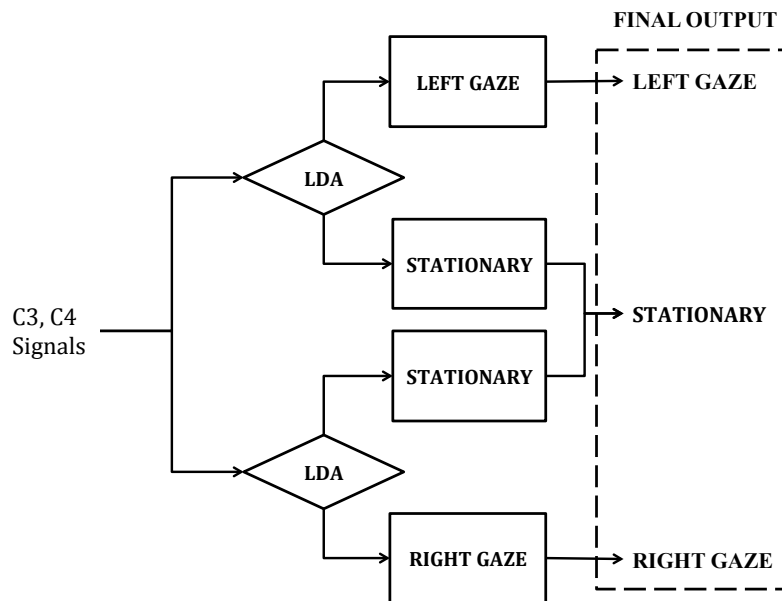
Figure 3.9: The gaze shifts were determined using two LDA classifiers.

b) *K-Means*

A K-Means is a clustering algorithm that assigns k-dimensional data into a number of groups. The dimension of the data, k, is equal to the number of samples in the window which is 128. It is possible to use only one of the signals (C3 or C4) as they both display pulses of opposite amplitudes when the eyes move in the opposite directions from the middle. Another alternative is to combine the signals to form a longer signal and use it with a single K-Means. However, a better classification result is obtained when they are used separately with two K-Means to determine the centroid of horizontal gaze signals. In this case, the number of output groups is two for each K-Means. The first K-Means takes C3 signal as input and cluster it into left gaze (L) and no movement (NM). Likewise, the second K-Means assigns C4 signal into right gaze (R) and no movement (NM).

Prior to Online Session, the group centroids for particular horizontal gaze are determined from trials collected in Recording Session. These centroids are unique for each individual. During real-time classification in Online Session, the Euclidean distance is used to determine the minimum distance between the data in a window (128 samples) to the predetermined group centroids and assigned the data to the respective group. The Euclidean distance from channel C3 and C4 are combined to reach the final classification as listed in Table 3.1.

Table 3.1: Classification outputs of Euclidean distance.

EUCLIDEAN 1 C3	EUCLIDEAN 2 C4	FINAL CLASSIFICATION
L	R	Error
L	NM	Left
NM	R	Right
NM	NM	No change in gaze or eyeball stationary

c) *Area in Delta Rhythm and Thresholding*

The area in delta rhythm analysis is using the similar area calculation as in alpha analysis. However, the delta rhythm has two channels to be analyzed and the area is calculated between channel C3 and C4 as follows:

$$Area_{C3,C4} = \sum_{i=1}^{N} x_{C3,i} - x_{C4,i}$$

(3.7)

The value of the difference between samples in C3 ($x_{C3,i}$) and C4 ($x_{C4,i}$) in a window of 128 samples ($N = 128$) are summed to get the area lies between signal C3 and C4. This

value will be compared to a range of area during eyeball stationary (called *threshold_area$_{C3, C4}$*) that predetermined and unique to each individual. The *threshold_area$_{C3, C4}$* is set between half of the mean area during right gaze in the lower limit and half of the mean area during left gaze in the upper limit. The calculated area will represent the gazes to left, right and stationary as follows. If the calculated area is less than the defined *threshold_area$_{C3, C4}$*, then the right gaze is detected, while a higher area value will represent a left gaze. An area that in the range of *threshold_area$_{C3, C4}$* will recognize as stationary or no movement of t eyeball.

3.3.5 Online Session

This session is conducted to test the efficiency of the signal processing technique in real-time with no actual wheelchair movement is involved. A short training was given to 20 participants prior to Online Session to ensure that the interface and data acquisition were fully functioning. Once the participants were familiar with the experimental protocol, the session is commenced. Throughout the session, the instructions are given in visual stimulus as depicted Figure 3.10.
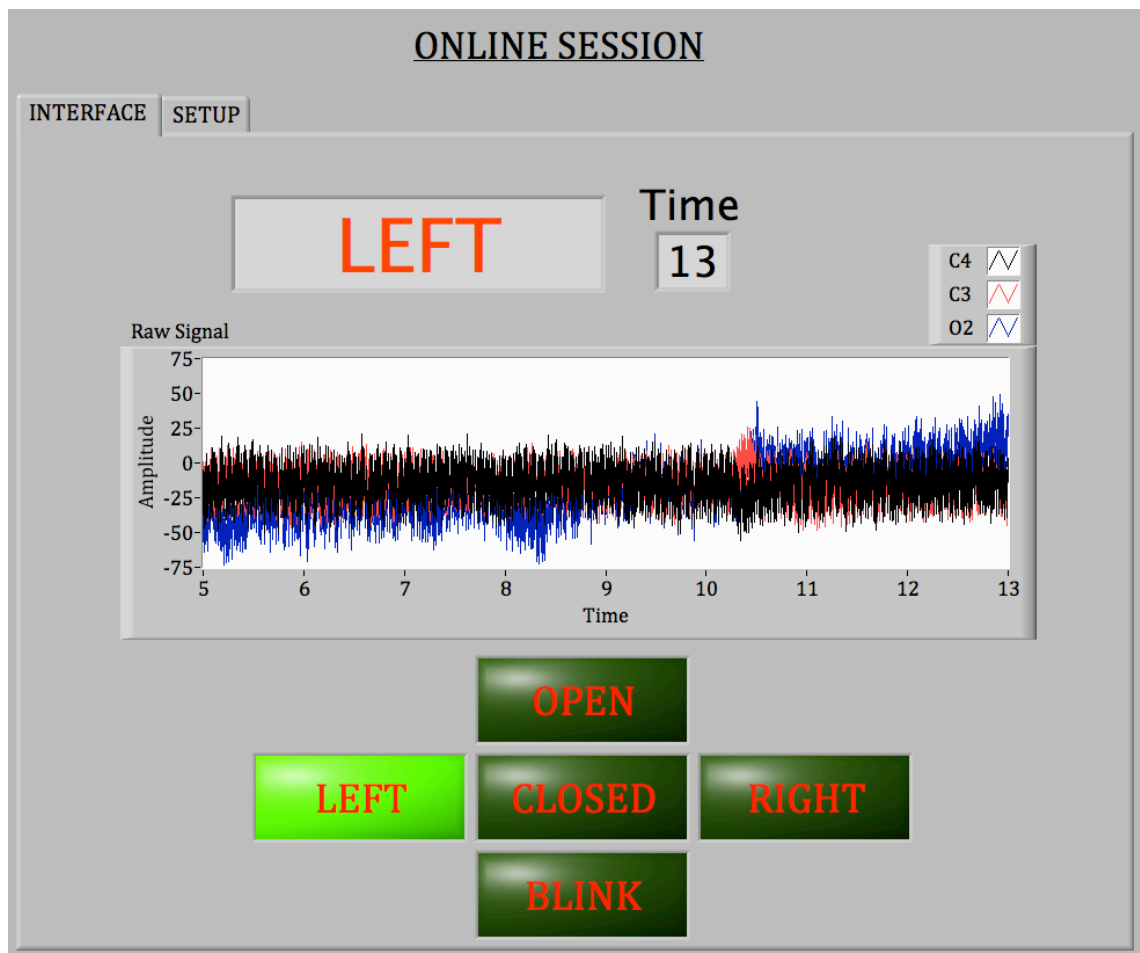
Figure 3.10: Graphical user interface of visual stimuli and feedback during Online Session.

In a trial, five possible tasks of open, blink, closed eye, left gaze and right gaze are randomly assigned every 10 seconds continuously for 260 seconds as shown in Figure 3.11. A total of 500 instructions were issued to the 20 participants in this session. Upon the onset of the stimulus, the participant is expected to direct his gaze or move his eyelids accordingly. For instance, an open eye instruction will require the participants to open their eyes and stay stationary. During the session, natural blink is allowed as it has a minimal effect in alpha and delta signal of EEG. An instruction is considered successfully executed if the participant responds correctly in less than 2 seconds after

the onset of the stimulus. At the end of the session, the best processing techniques that recorded the highest score will be used as input to the navigation system and evaluated in real navigation task.
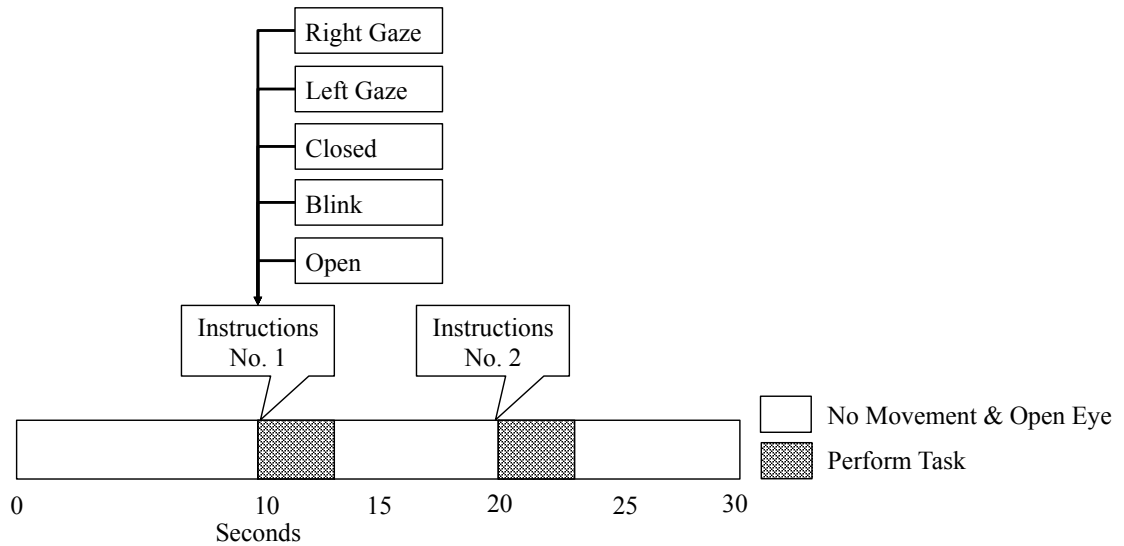
Figure 3.11: Five instructions of horizontal gaze and eyelid position are assigned every 10 seconds during the Online Session.

3.4 Navigation System Design using Finite State Machine

In this section, the navigation system that modeled as a finite state machine is described. The overview of the system architecture is illustrated in Figure 3.12. The features such as variance and minimum distance are extracted from alpha and delta rhythm respectively. Then, these features are fed to the fuzzy state transitions for classification to determine the final output of hybrid BCI. Once the eye gaze is determined, the navigation controller that modeled as a finite state machine will be instructed accordingly and followed by the wheelchair movement.
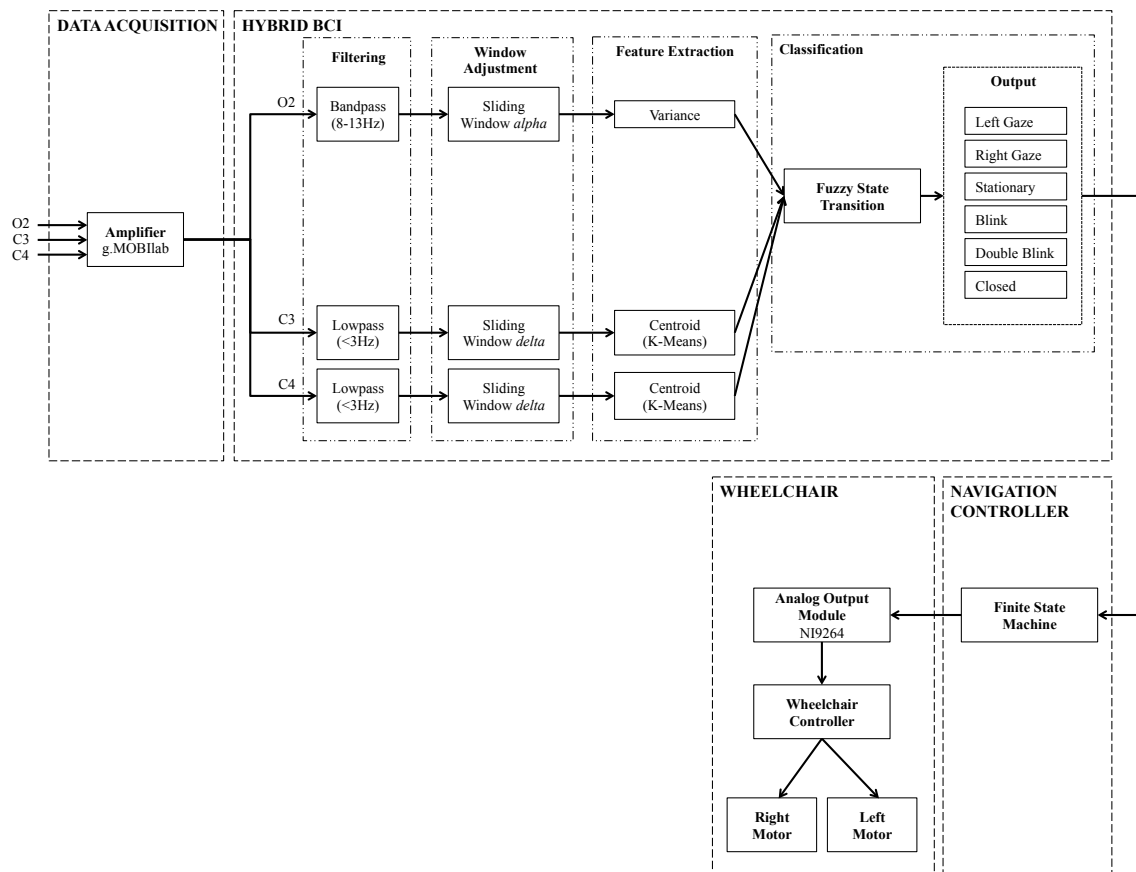
Figure 3.12: Overview of the system architecture for navigation controller.

3.4.1 Fuzzy State Transitions

The implementation of the fuzzy logic technique in the state transition is described in three steps: fuzzification, fuzzy inference process and defuzzification. Two techniques that recorded the highest score in Online Session will be implemented as inputs to fuzzy rules for classification, which are variance for eyelid position and K-Means for horizontal gaze.

The fuzzification process converts two inputs (*variance_O2* and *distance_centroid*) and output (*gaze_shift*) to the associated linguistic variables. The *variance_O2* input is associated with the calculated variance value in channel O2. The

linguistic variables of this input are defined as *Small, Medium* and *Large*. The second input of the *distance_centroid* represents the Euclidean distance between the centroid of NM class determined by K-Means and the delta rhythm signal from C3 and C4 in a window of 128 samples. This input can be described in three linguistic variables; *Short, Medium* and *Long*. The grade of membership of both inputs in fuzzy sets is defined through trapezoidal functions as shown in Figure 3.13 (a) and (b).
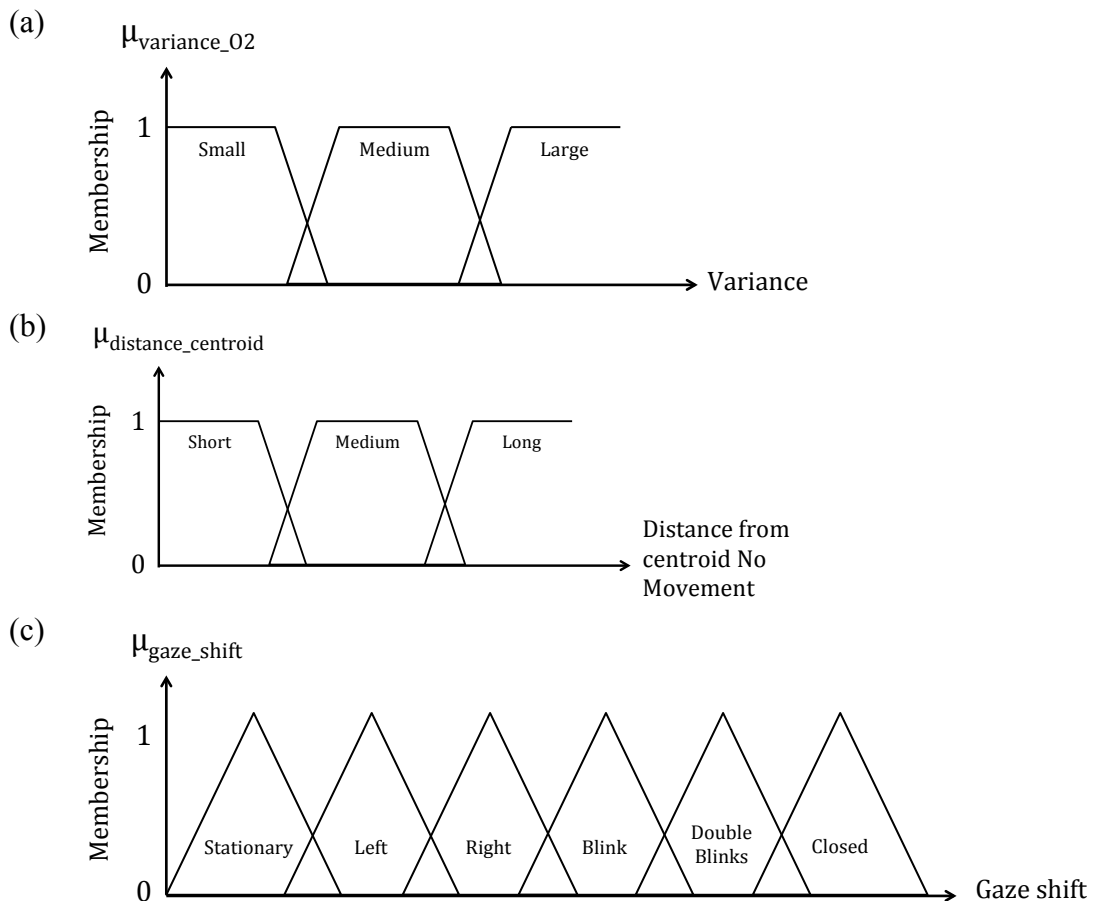
Figure 3.13: Membership function for two inputs (a) *area_O2* (b) *distance_centroid* and an output (c) *gaze_shift*.

The fuzzy set of the *gaze_shift* output is defined by the triangle functions consist of six variables which are *Stationary, Left, Right, Blink, Double Blink* and *Closed*. Due to their

computational efficiency, both triangular and trapezoidal membership function have been used in this study. The output represents the eyelid position and gaze direction.

Next, the fuzzy inference process combines the membership functions with the control rules to derive the control output. These control rules can be characterized using IF-THEN statements as follows:

Rule 1   :   IF *<variance_O2 is small>* AND *<distance_centroid is short>* THEN *<gaze_shift is Left>*

Rule 2   :   IF *<variance_O2 is small>* AND *<distance_centroid is medium>* THEN *<gaze_shift is Stationary>*

Rule 3   :   IF *<variance_O2 is small>* AND *<distance_centroid is long>* THEN *<gaze_shift is Right>*

Rule 4   :   IF *<variance_O2 is medium>* AND *<distance_centroid is short>* THEN *<gaze_shift is Blink>*

Rule 5   :   IF *<variance_O2 is medium>* AND *<distance_centroid is medium>* THEN *<gaze_shift is Blink>*

Rule 6   :   IF *<variance_O2 is medium>* AND *<distance_centroid is long>* THEN *<gaze_shift is Blink>*

Rule 7   :   IF *< variance_O2* is large> AND *<distance_centroid is short>* THEN *<gaze_shift is Closed>*

Rule 8   :   IF *< variance_O2* is large> AND *<distance_centroid is medium>* THEN *<gaze_shift is Closed>*

Rule 9   :   IF *< variance_O2* is large> AND *<distance_centroid is long>* THEN *<gaze_shift is Closed>*

For example in Rule 2, when the variance calculated in alpha rhythm from O2 is *Small* and the Euclidean distance computed between centroids of NM class and delta rhythm from C3 and C4 is *Medium*, the current eye gaze are determined as stationary. In this

case, the AND operator is used to condition two inputs, wherein the minimum membership degree will be selected and applied to the output membership function. All the *gaze_shift* outputs triggered by the *variance_O2* and *distance_centroid* are mapped in Table 3.2.

Table 3.2: Fuzzy mapping rules for the fuzzy state transition. The rows and columns represent two inputs, *area_O2* and *distance_centroid*. The cross point of each row and column represents the output.

AND	*distance_centroid*		
variance_O2	**SHORT**	**MEDIUM**	**LONG**
SMALL	*Left*	*Stationary*	*Right*
MEDIUM	*Blink*	*Blink*	*Blink*
LARGE	*Closed*	*Closed*	*Closed*

Defuzzification converts linguistic variables back to crisp value. This process begins by combining all the outputs from all fuzzy rules to obtain one fuzzy output distribution using operator OR. Then, the mean of maximum as in equation (3.8) of the fuzzy output distribution is computed to obtain one crisp value.

$$z = \sum_{j=1}^{k} \frac{z_j}{k} \tag{3.8}$$

The mean of maximum, z, is an outcome of the point at which the membership function is maximum, z_j, over the number of times the output distribution reaches the maximum level, k.

The implementation of the fuzzy logic technique in the state transition can be simplified as illustrated in Figure 3.14. The output value represents the eyelid position and gaze direction. It is worth mentioning that small value of *gaze_shift* output may

indicate the occurrence of fatigue. For instance, the value range for *Left* in *gaze_shift* is between 20 to 40 with the highest at 30. If the outcome of defuzification shows the *Left* value is 23, this indicates that the user performs the gaze in slower motion as a result of fatigue. In this work, if this condition is detected more than three times continously, the LED showing fatigue sign will be activated to alert the user. It is important for the user to aware of their condition as fatigue may compromise their concentration as well as their safety.
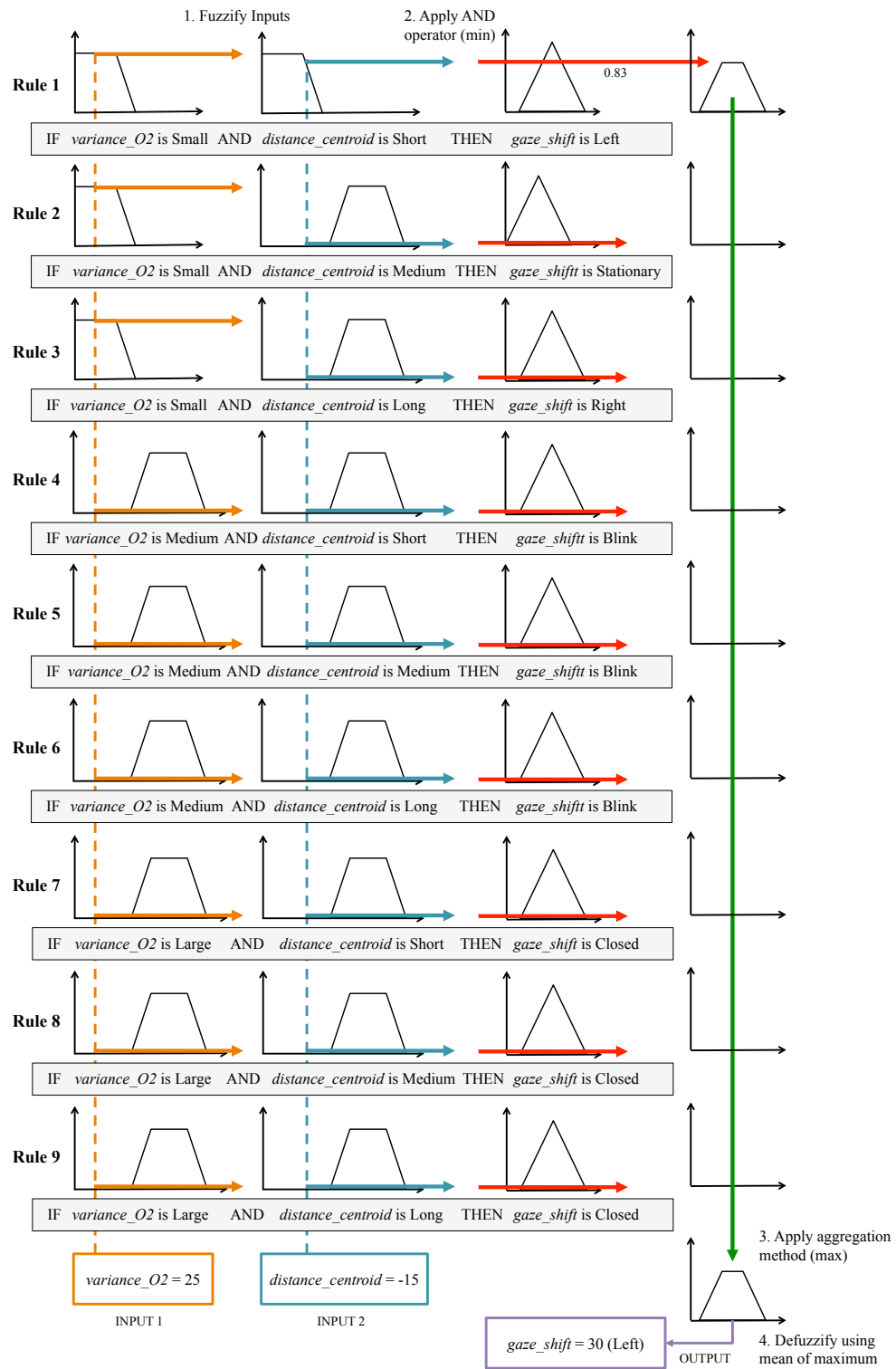
Figure 3.14: Implementation of the fuzzy inference diagram for the fuzzy state transitions.

3.4.2 Finite State Machine

In this work, the proposed system can be regarded as a finite state machine with fuzzy state transitions. Basically, its operation can be divided into two modes, namely READY and RUN MODEs. Both modes contain three identical states, which are LEFT, MIDDLE and RIGHT as shown in Figure 3.15. By default, the process starts at the MIDDLE state of the READY MODE where the EEG signals of the alpha and delta rhythm are sampled at 256 samples per second. The READY MODE is intended for the user to check the system functionality while the wheelchair is stationary. It also enables the user to select either FORWARD or BACKWARD, as the direction the wheelchair will go when the system enters RUN MODE.
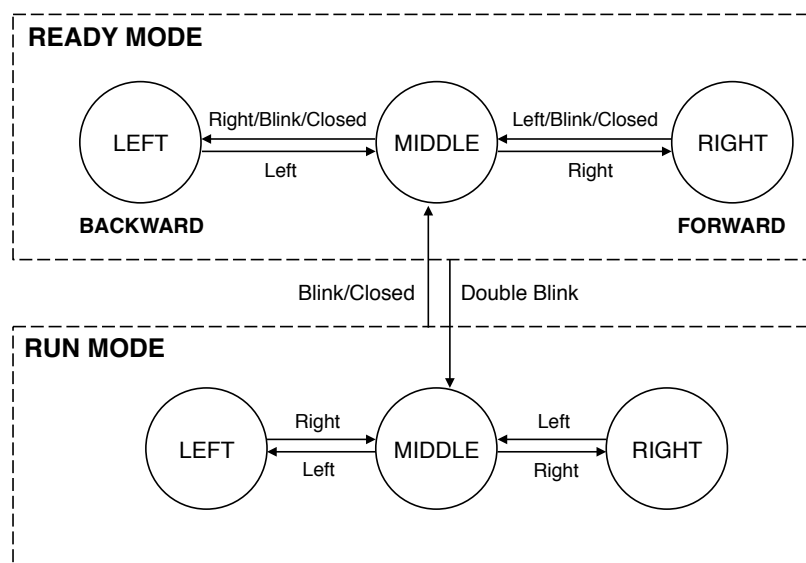
Figure 3.15: The modes and states of the proposed system. The READY MODE is intended for the user to check the system functionality while the wheelchair is stationary and function as a stop. In RUN MODE, the wheelchair will be executed into left, straight and right direction.

In READY MODE, a window containing 128 samples of the alpha signal is analyzed to inspect the condition of closed or open eyes and the occurrence of blink. Delta signal of the same length is also examined to check the gaze direction of the eyes.

From MIDDLE state, if the user gazes to the right or left, the state will follow accordingly. If the state is already LEFT, moving the gaze from the center to the left will not affect the state anymore. This action is known as a null act. However, if the state is LEFT and the user wants to shift it to RIGHT, he will have to move his gaze from the center to the right twice so that the state will shift from LEFT to MIDDLE and then from MIDDLE to RIGHT. This is to avoid an abrupt change in the direction of the wheelchair as sudden change in its direction might topple it over when it is moving. The converse is also true if the user wants to shift the state from RIGHT to LEFT. Another thing to note in READY MODE is that a blink or closed eye will move the system to the MIDDLE state.

As stated earlier, in READY MODE no motor movement is executed yet as this mode is designed to allow the user to test the system operation before the actual motor commands start as shown in Table 3.3. However, once the user is familiar with the system, he may want to start moving the wheelchair.

The first step is to choose either FORWARD or BACKWARD as the direction the wheelchair will go when activated. This is done by shifting the state to the RIGHT or LEFT for FORWARD or BACKWARD move direction respectively. Once the user is sure of the movement direction and ready to enter the RUN MODE, he should lock the chosen move direction by repeating the null act twice. This is done by moving his gaze from the center to the chosen direction (left or right) twice in 2 seconds. If he wishes to change the locked direction, he should move his gaze in the opposite direction and

repeat the null act twice. However, if the user changes his mind and wants to unlock the chosen move direction without replacing it with the opposite one, he simply has to close his eyes for more than 1 second. This action will return the system to MIDDLE state of READY MODE and unlock the move direction. If the user blink his/her eyes, the state will go to the MIDDLE but the locked direction will not be affected.

Table 3.3: State transition of the proposed system.

CURRENT		INPUT		NEXT		WHEELCHAIR
MODE	STATE	O2	C3, C4	MODE	STATE	MOVEMENT
READY	MIDDLE	Open	Straight	READY	MIDDLE	None
		Closed	Straight/ Left/ Right	READY	MIDDLE	
		Blink	Straight/ Left/ Right	READY	MIDDLE	
		Open	Right	READY	RIGHT	
		Open	Left	READY	LEFT	
	LEFT	Open	Right	READY	MIDDLE	None
		Closed	Straight/ Left/ Right	READY	MIDDLE	
		Blink	Straight/ Left/ Right	READY	MIDDLE	
		Open	Left (Null Act)	READY	LEFT	
		Open	Double Left (Double Null Act)	LOCKED	MIDDLE	(Locked Backward)
	RIGHT	Open	Left	READY	MIDDLE	None
		Closed	Straight/ Left /Right	READY	MIDDLE	
		Blink	Straight/ Left/ Right	READY	MIDDLE	
		Open	Right (Null Act)	READY	RIGHT	
		Open	Double Right (Double Null Act)	LOCKED	MIDDLE	(Locked Forward)
RUN	MIDDLE	Open	Straight	RUN	MIDDLE	Move straight
		Open	Right	RUN	RIGHT	Turn Right
		Open	Left	RUN	LEFT	Turn Left
		Closed	Straight/ Left /Right	LOCKED	MIDDLE	Stop
		Blink	Straight/ Left/ Right	READY	MIDDLE	Stop
	LEFT	Open	Right	RUN	MIDDLE	Move straight
		Open	Left	RUN	LEFT	Turn Left
		Closed	Straight/ Left /Right	LOCKED	MIDDLE	Stop
		Blink	Straight/ Left/ Right	READY	MIDDLE	Stop
	RIGHT	Open	Left	RUN	MIDDLE	Move straight
		Open	Right	RUN	RIGHT	Turn Right
		Closed	Straight/ Left /Right	LOCKED	MIDDLE	Stop
		Blink	Straight/ Left/ Right	READY	MIDDLE	Stop

Once the move direction is locked, the system is ready to enter RUN MODE. This is done by performing a double blink in 2 seconds. After that the system will enter RUN MODE immediately. Upon entering the RUN MODE, the system is automatically assigned to the MIDDLE state, but the user is given 5 seconds to change his gaze direction to the left or right before it is taken as the first command to move the wheelchair. In this mode, the state is viewed as an instruction to move the wheelchair. If there is no change of gaze direction in the grace period, the wheelchair will move in a straight direction forwardly or backwardly according to the locked move direction.

While in RUN MODE, the state changes in accordance with the gaze direction, and the wheelchair follows the state. Each instruction will be executed for at least 2 seconds to maintain the stability of the moving wheelchair and avoid confusion caused by command overcrowding. Another restriction is that the wheelchair will stop before turning or changing direction. And finally, only a gradual change of direction is allowed.

At all time, the wheelchair is moving at 5km/h, which is an average walking speed and turns at 0.4rad/s. If a user wishes to stop the wheelchair, all he has to do is blink or closes his eyes. Once blink or closed eye is detected, the system will terminate whatever command it is executing, exit RUN MODE and return to MIDDLE state of READY MODE. For a blink, the locked direction is not affected, but for a closed eye it will be unlocked and the user has to choose one before returning to READY MODE by double blinking. This feature is also useful when an error occurs due to misclassification or distraction. For example, while moving straight the user's attention is drawn to something in the environment and therefore accidentally delivers an incorrect navigation command to turn left. The new state will be displayed on the user interface

panel and the user can simply gaze to the opposite direction (right) to shift the state back to the MIDDLE. Another solution is to blink so that the wheelchair will stop before executing the left turn and the state will move to the MIDDLE of READY MODE. Double blinking will send the system back to MIDDLE state of RUN MODE. These options show that the system is flexible and forgiving. Finally, in a span of two second, only one instruction is kept while the wheelchair is executing the current command. If the user generates another instruction, only the latest is kept as the next command to be executed.

3.5   Hardware Implementation

Based on the state of the finite state machine, a command to the wheelchair used in (Mokhtar, 2012) is identified and issued. The system checks whether it is the same command currently being executed. If it is the same ones, the execution of the current command is prolonged. If it is different, a new instruction in the form of a digital command is sent to a digital to analog module that converts the digital signal to an analog voltage level. The module used in our experiment is NI9264 by National Instrument. The analog output is then sent to a motor controller that controls the right and left motors of the wheelchair as shown in Figure 3.16. The controller will switch on the right, left or both motors if the command is turn left, turn right or move forward respectively. If a blink or closed eye is detected, both motors will stop and the system will exit RUN MODE and enter MIDDLE state in READY MODE.
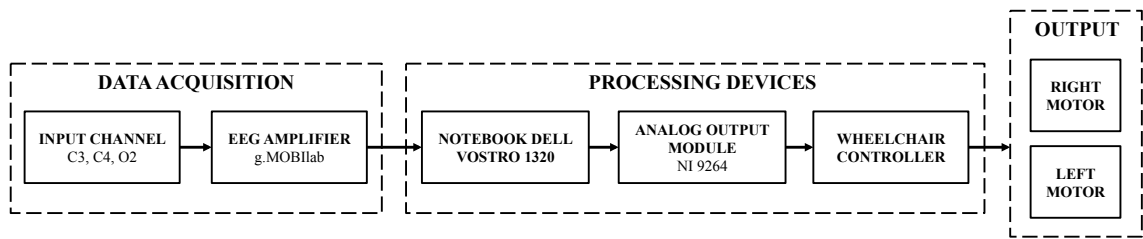
Figure 3.16: Flow of the hardware implementation consists of three main components; data acquisition, processing devices and output to wheelchair motor.

3.6 Navigation Session

In this session, the performance of the proposed navigation system is investigated in the indoor environment. Participants are required to steer the wheelchair using the proposed navigation controller along the designated routes. Since the proposed navigation system is untested in real navigation task, their performance is uncertain and might risk the safety of the participants. Therefore, only participants that show the best competency in performing eyelid position and horizontal gaze tasks in Online Session with score higher than 98% will be selected. This result in five participants is selected to perform the navigational tests.

Prior to Navigation Session, a short training session was commenced to check the system functionality and the participant is given 30 minutes to perform as many commands as he wishes to obtain more familiarity with the system in READY MODE. Two routes are designed with the passage width in the range of 4.5m to 1.8m as shown in Figure 3.17.

Route 1 has a total optimal path length of 17.7m with three checkpoints of A_1, B_1 and C_1 while Route 2 has a total optimal path length of 22.7m with four checkpoints of A_2, B_2, C_2 and D_2. Participants are responsible for maneuvering the wheelchair to pass

through these checkpoints starting from the first point back to the same point. However, when the participants reach the dead end points of C_1 and D_2, they are expected to reverse the wheelchair backward to exit the tight end and only make a turn at point B_1 and C_2 respectively. Each participant is given 3 attempts to repeat the task and at the end of the session they are asked to answer a set of questionnaires regarding their experience (see APPENDIX E).
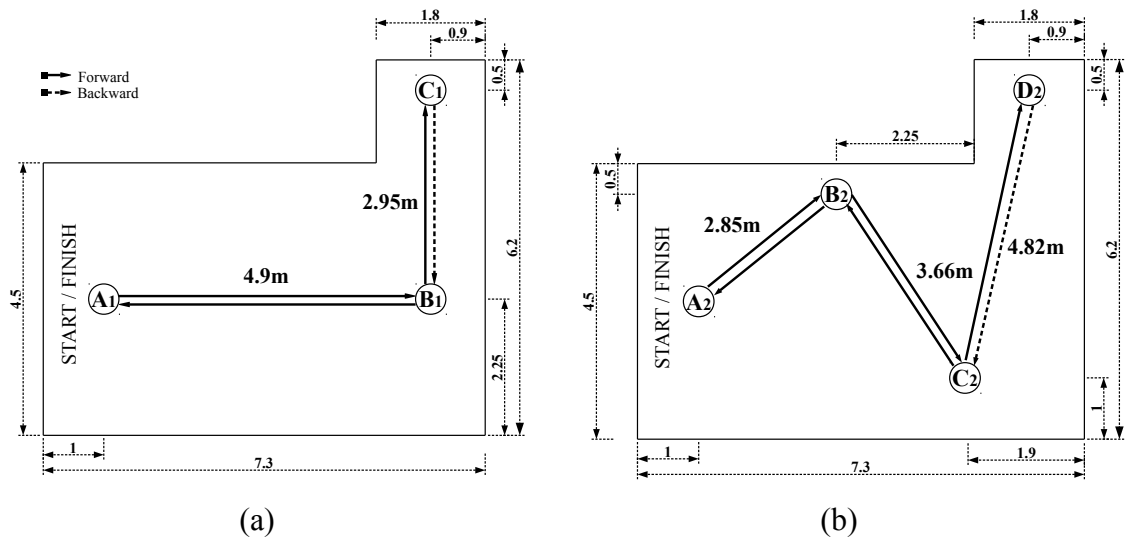
Figure 3.17: The navigation route with checkpoints (a) Route 1 (b) Route 2.

The GUI consists of mode, move direction and current state are all displayed in front of the user by LED lights as shown in Figure 3.18 (c).
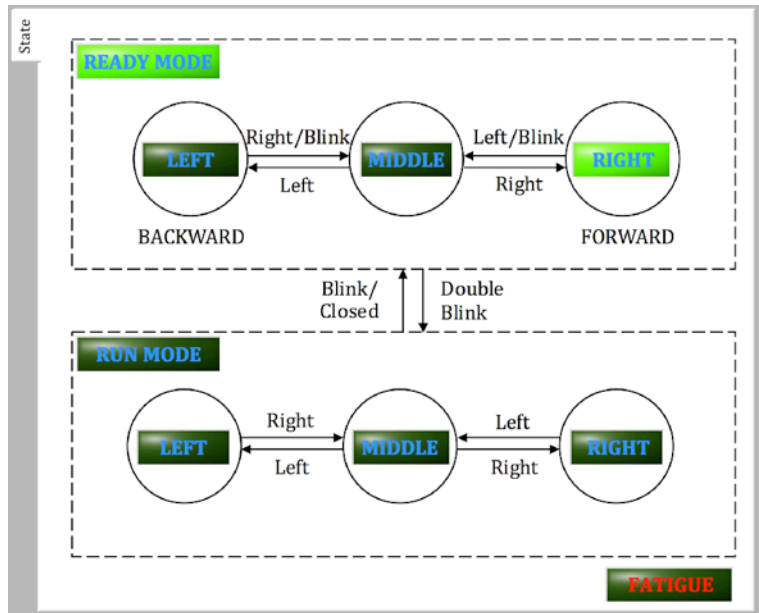
Figure 3.18: (a) A participant undergoing the experiment during Navigation Session (the participant has given written informed consent for the photograph) (b) Print screen of the graphical user interface.

CHAPTER 4

RESULTS & DISCUSSIONS

4.1   Introduction

In this chapter, the results obtained during Online Session and Navigation Session are presented and discussed. The performance between conventional and sliding window are compared during Online Session. The evaluation of navigation system during Navigation Session is described in three parts, overall, navigation performance and individual performance.

4.2   Online Session

The efficiency of the signal processing techniques are evaluated in Online Session with no actual wheelchair movement is involved. In total, 500 commands of eyelid position and horizontal gazes were issued continuously every 5 seconds to 20 participants. Prior to the session, the values of *threshold_alpha, threshold_delta, threshold_variance*, $r_{mean}(0.90\ open)$, *threshold_area$_{O2}$*, *threshold_area$_{C3,\ C4}$* and K-Means centroids for every participant are determined from the recorded signals.

4.2.1 Sliding Window

The filtered alpha and delta signals are examined in 0.5s window containing 128 samples. During this short period, a sliding window is used to adjust the position of the window so that it will contain samples of eye movements exclusively.

In the analysis of the alpha signal in O2, the position of the sliding window is adjusted until the difference between the averages of the first and last subinterval is less than the *threshold_alpha*. In our experiment, the *threshold_alpha* is set at half of the mean absolute values of closed eye samples. When the difference value is less than *threshold_alpha*, it indicates that the window contains samples of open or closed eye exclusively. Then, the window position is fixed and the feature such as variance, 2nd order difference plot or area of the samples in the whole window can be calculated. Values of *threshold_alpha* that determined for each participant prior to Online Session are listed in Table 4.1.

Table 4.1: A sliding window in channel O2 is adjusted if the difference between the averages of the first and last subinterval is less than the *threshold_alpha*. The *threshold_alpha* is determined from half of the average absolute values of closed eye samples for each participant.

Participant	1	2	3	4	5	6	7	8	9	10
threshold_alpha	6.91	7.11	7.03	7.97	7.97	8.98	5.72	7.61	11.22	7.04
Participant	11	12	13	14	15	16	17	18	19	20
threshold_alpha	6.61	8.29	10.69	10.64	8.72	9.21	10.48	8.28	11.00	7.26

For capturing the horizontal gaze in the delta signals of C3 and C4, average values of eight subintervals in a window are calculated and compared to *threshold_delta*. The *threshold_delta* is set at the midpoint of the average amplitude of the peaks recorded during left and right gaze for every participant as listed in Table 4.2. Once the values of the subintervals are greater than the *threshold_delta*, the position of the highest subinterval is adjusted to the center of the window. Otherwise, the position of the window is maintained as no gaze is occurred. Then, the area or the filtered delta signal

in the whole window can be analyzed by the thresholding, K-Means and LDA for the detection of horizontal gaze respectively.

Table 4.2: A sliding window in channel C3 and C4 is adjusted if the eight subintervals in a window are greater than *threshold_delta*. The *threshold_delta* is determined from the half of the average peaks recorded during horizontal gaze.

Participant	1	2	3	4	5	6	7	8	9	10
threshold_delta	7.41	7.93	7.60	6.95	7.84	7.08	6.84	8.32	6.92	6.28
Participant	11	12	13	14	15	16	17	18	19	20
threshold_delta	10.54	9.99	9.65	9.36	9.97	7.90	9.62	9.37	9.20	8.18

The positioning of sliding window in channel C3 and C4 are according to O2 at all time unless the values of the subintervals in C3 or C4 are greater than *threshold_delta*. In this case, the sliding window in O2 is adjusted according to the one in C3 or C4 as summarized in Table 4.3.

Table 4.3: Rules of the sliding window adjustment.

| LESS THAN | | GREATER THAN | | WINDOW ADJUSTMENT |
threshold_alpha	*threshold_delta*	*threshold_alpha*	*threshold_delta*	WILL FOLLOWED:
O2	C3	-	-	O2
O2	C4	-	-	O2
O2	-	-	C3	C3
O2	-	-	C4	C4
-	C3	O2	-	O2
-	C4	O2	-	O2
-	-	O2	C3	O2
-	-	O2	C4	O2

4.2.2 Eyelid Position Analysis

Analysis of eyelid position classified three features extracted from alpha rhythm in channel O2 using thresholding and CTM. The features are variance, 2nd order differential plot and area. These techniques are evaluated in Online Session and the feature recorded the highest classification accuracy will be implemented in the Navigation Session. The confusion matrix presented in Table 4.4 shows the overall performance using conventional and sliding window of three techniques in classifying 300 instructions issued in Online Session for eyelid position analysis. The metrics used in the evaluation are described as follows:

1) *Positive Predictive Value (PPV)***:** Rate of correctly identifies a condition.

2) *Negative Predictive Value (NPV)*: Rate of correctly excludes a condition.

3) *Accuracy*: Overall ability to identify and exclude correctly.

4) *Sensitivity***:** Overall ability to identify correctly.

5) *Processing Time (s)*: Time taken in second from extracting the feature until the output of classification.

It can be observed that, implementation of sliding window improves the accuracy for approximately 10% and sensitivity for approximately 9% for all techniques compared to the conventional window.

Table 4.4: Confusion matrix for eyelid position analysis using conventional and sliding window during Online Session.

	Task	Recognized Eyelid Position			PPV	NPV	Accuracy	Sensitivity	Processing Time (s)
		Open	Blink	Closed					
CONVENTIONAL WINDOW	Variance & Threshold								
	Blink	18	82	0	0.77	0.91	0.84	0.89	0.45
	Closed	0	15	85	0.92	0.93	0.93	0.93	0.45
	Open	84	9	7	0.82	0.92	0.87	0.91	0.45
	Mean				**0.84**	**0.92**	**0.88**	**0.91**	**0.45**
	2nd order difference plot & CTM								
	Blink	27	73	0	0.71	0.86	0.79	0.84	0.62
	Closed	6	18	76	0.92	0.89	0.90	0.89	0.62
	Open	81	12	7	0.71	0.90	0.80	0.87	0.62
	Mean				**0.78**	**0.88**	**0.83**	**0.87**	**0.62**
	Area & Threshold								
	Blink	22	78	0	0.72	0.88	0.80	0.86	0.42
	Closed	0	19	81	0.92	0.91	0.92	0.91	0.42
	Open	81	12	7	0.79	0.90	0.84	0.89	0.42
	Mean				**0.81**	**0.90**	**0.85**	**0.89**	**0.42**
SLIDING WINDOW	Variance & Threshold								
	Blink	4	95	1	1	0.98	0.98	0.98	0.45
	Closed	0	0	100	0.96	1	0.98	1	0.45
	Open	97	0	3	0.96	0.98	0.97	0.98	0.45
	Mean				**0.97**	**0.99**	**0.98**	**0.99**	**0.45**
	2nd order difference plot & CTM								
	Blink	6	91	3	1	0.96	0.98	0.96	0.62
	Closed	11	0	89	0.94	0.95	0.94	0.95	0.62
	Open	97	0	3	0.85	0.98	0.92	0.98	0.63
	Mean				**0.93**	**0.96**	**0.95**	**0.96**	**0.62**
	Area & Threshold								
	Blink	5	92	3	1	0.96	0.98	0.96	0.42
	Closed	7	0	93	0.94	0.97	0.95	0.96	0.42
	Open	97	0	3	0.89	0.98	0.94	0.98	0.42
	Mean				**0.94**	**0.97**	**0.96**	**0.97**	**0.42**

a) *Variance & Thresholding*

The value of variance is bigger when a large scale of fluctuation in alpha rhythm is detected as shown in Figure 4.1. Utilizing variance and thresholding in eyelid position analysis recorded the highest overall accuracy of 98% with 0.45s of processing time.

During the experiment, four blink instructions are wrongly identified as open eye and one as closed eye.
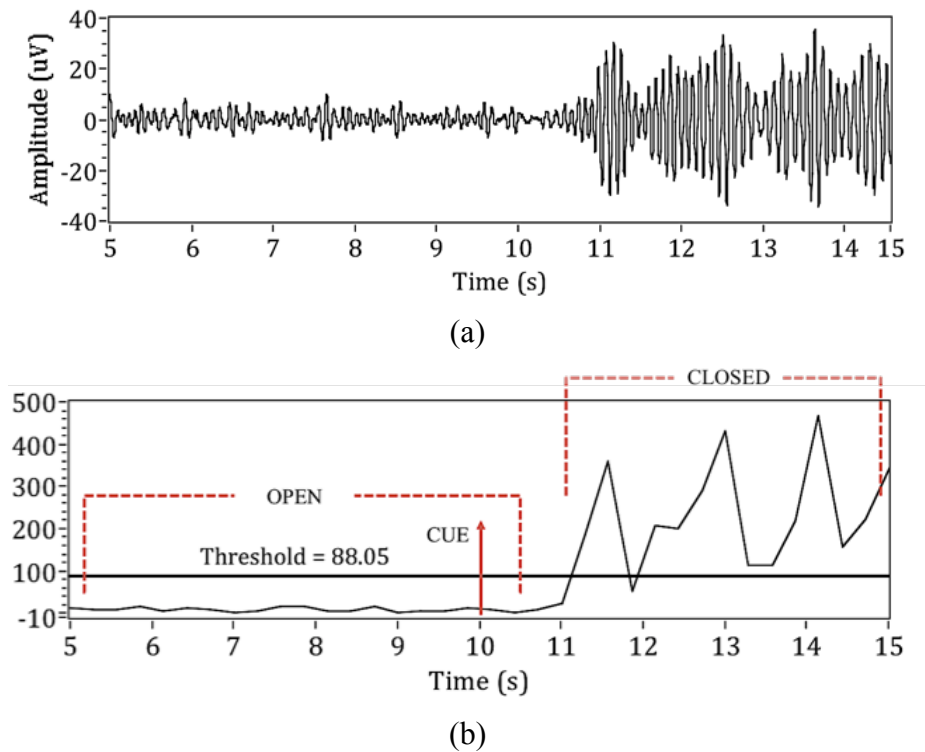
Figure 4.1: Alpha rhythm in channel O2 recorded from a Participant 4 during Online Session (a) The participant executed an open eye (5s – 10s) and closed eye (10.5s – 15s) (b) Variance and mean variance of the open eye represented by a straight line at y = 88.05 parallel to x-axis.

The *threshold_*variance is computed from the open eye data collected during Recording Session and assigned uniquely for each participant as listed in Table 4.5. For example, the mean variance of the open eye (*threshold_variance*) for Participant 4 is represented by a straight line at y = 88.05 parallel to x-axis. If the calculated variance in the particular O2 window is equal or smaller than the defined *threshold_variance* at y = 88.05, the signal will be classified as an open eye while larger variance will be classified as blink or closed eye with regard to the duration of closed eye.

Table 4.5: *threshold_variance* **determined from the open eye data for each participant.**

Participant	1	2	3	4	5	6	7	8	9	10
threshold_variance	48.34	44.45	44.01	88.05	44.85	34.32	46.56	39.41	91.04	41.65
Participant	11	12	13	14	15	16	17	18	19	20
threshold_variance	121.39	39.81	46.46	33.69	44.15	74.32	50.27	42.99	124.54	76.13

b) 2nd *Order Difference Plot & CTM*

2nd order difference plot shows the variation of successive rates. The distributions of alpha rhythm in a window of 128 samples for open and closed eye display in the 2nd order difference plot are shown in Figure 4.2. This variation was measured by CTM within an optimum radius (r) that determined once CTM reaches a value of 0.90.

For example, the optimum radius obtained for Participant 3 during open eye is $r(0.90 \, open) = 2.42$ and closed eye is $r(0.90 \, closed) = 7.83$ as shown Figure 4.3. Generally, the closed eye contains higher variability of alpha rhythm and will yield larger optimum radius compared to open eye.
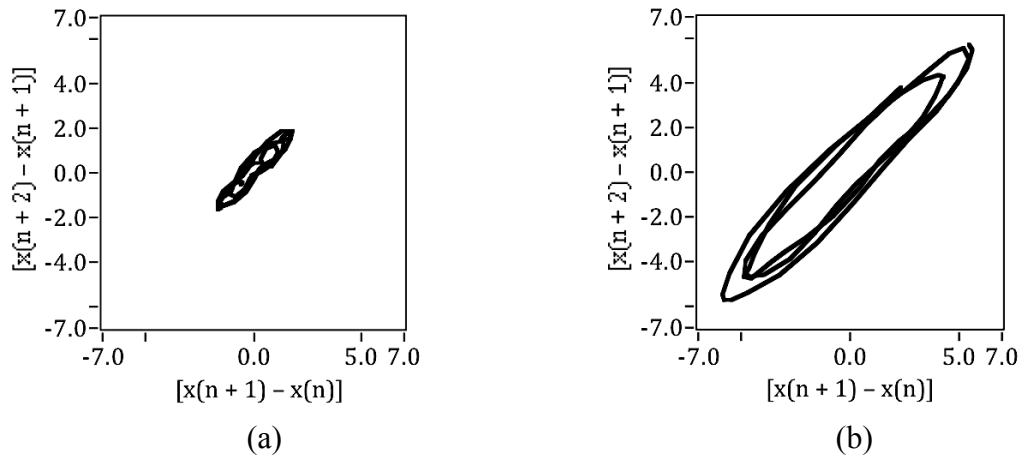
Figure 4.2: Second-order difference plot during (a) open eye and (b) closed eye in alpha rhythm (8-13Hz) in a window of 128 samples.
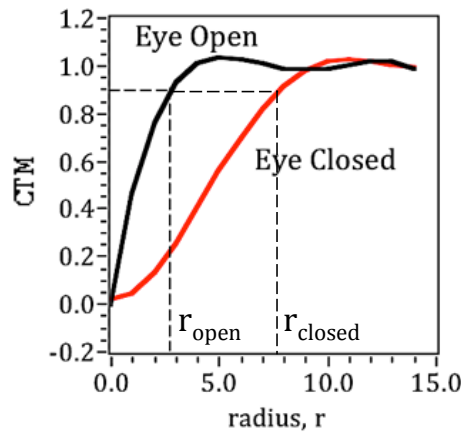
Figure 4.3: The optimum radius of $r_{open} = 2.42$ and $r_{closed} = 7.83$ at x-axis is determined from open eye radius when the CTM reach 0.90 for Participant 3.

The classification of open and closed eye was based on the radius difference (r_d) between the optimum radius obtained in a window of 128 samples and $r_{mean}(0.90 \ open)$, a mean value of open eye radius calculated from the recorded data as listed in Table 4.6. A closed eye condition is represented by the positive value of r_d, while open eye condition is represented by negative value.

Table 4.6: The mean of open eye radius, $r_{mean}(0.90\ open)$ for each subject.

Participant	1	2	3	4	5	6	7	8	9	10
$r_{mean}(0.90\ open)$	3.43	2.66	2.48	5.47	2.92	1.44	3.29	2.13	5.52	2.27
Participant	11	12	13	14	15	16	17	18	19	20
$r_{mean}(0.90\ open)$	5.98	2.14	3.07	1.41	2.58	5.36	3.96	2.39	6.18	5.42

2nd order difference plot and CTM has denoted to low overall accuracy of 95% with six blink are recognized as open and three as closed. Also, 11 closed eye signals are mistakenly recognized as open while three open eye signals are recognized as closed. The analysis of 2nd order difference plot and CTM utilized the time series signals from O2 to calculate the radius of its variation without amplification. Therefore, in the case when the intensity of the alpha rhythm was low during closed eye, CTM might recognized it as open eye due to a slight difference between radiuses of open and closed eye. The recorded processing times showed approximately 0.62s was required to analyzed a window of 128 samples and the highest among the three techniques tested in this analysis.

c)   ***Area in Alpha Rhythm***

This feature used the concept of area calculation by summing the absolute value of alpha signal samples as shown in Figure 4.3. Then, this area was compared with a *threshold_area_{O2}*, a mean area of open eye for each participant as listed in Table 4.7. If the compared value is less than *threshold_area_{O2}*, the area will denote as open eye while larger value will denote as blink or closed eye with regard to its duration.

(a)   (b)
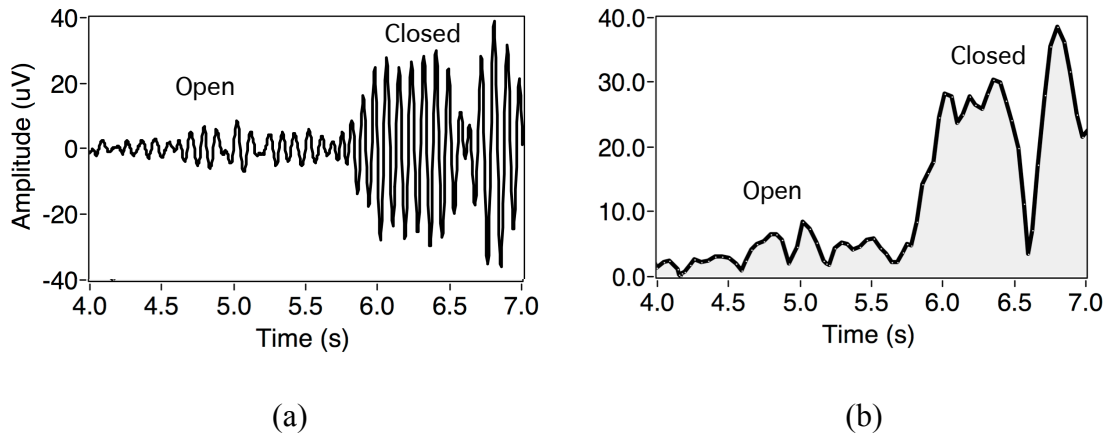
Figure 4.4: (a) Alpha rhythm in channel O2 (b) Area of closed and open eye is calculated from the absolute value.

Utilizing area in alpha signals as feature for eyelid position analysis has recorded overall accuracy of 96%. Five blink has mistakenly identified as open eye and three as closed eye while seven closed eye signals as open. As the rigid threshold is employed, the low intensity of alpha rhythm during blink or closed eye might be detected as open. The recorded processing times show only fragment of time required for detection with approximately 0.42s.

Table 4.7: The mean of open eye area, *threshold_area$_{O2}$* for each participant.

Participant	1	2	3	4	5	6	7	8	9	10
threshold_area$_{O2}$	269	227	425	400	263	513	232	276	411	207
Participant	11	12	13	14	15	16	17	18	19	20
threshold_area$_{O2}$	888	400	761	480	364	433	759	467	1068	553

d)   *Uncontrolled Factors*

The analysis of eyelid position during Online Session was influenced by the uncontrolled factors either from the participants or the environment as followed. First,

the strength of alpha rhythm during closed eye is weaker when the subjects are excited with anticipation and high in alertness. However, the rigid *threshold_variance*, $r_{mean}(0.90\ open)$ and *threshold_area$_{O2}$* level cannot be changed to accommodate the change in signal strength. This contributed to misclassification of blink and closed eye as open.

Second, when the participants are in relaxation, tired and inattentive at the beginning of the session, alpha rhythm signal in O2 during open eye increases and sometimes its amplitude encroaches the domain of the closed eye signal. In this case, three open eye signals are recognized as closed by all methods using sliding window due to this condition as shown in Table 4.4. Figure 4.5 shows an example of the alpha rhythm recorded during the excited period.

Finally, the blink is defined as a form of closed eye, which is less than 1s while closed eye with longer than 1s. However, during the experiment when the participants are unintentionally blink for a longer than 1s, the blink is mistakenly recognized as closed eye. If the blink is too short, the strength of alpha rhythm will be weaker and identical as open eye signal.
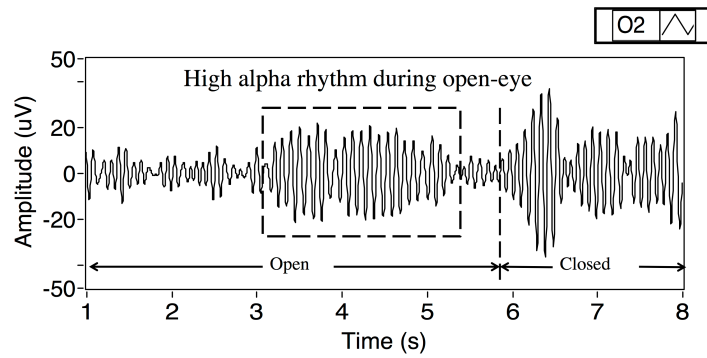
Figure 4.5: High alpha rhythm occurs during open eye due to high anticipation and alertness.

4.2.3 Horizontal Gaze Analysis

Analysis of horizontal gaze extracted feature such as area in delta signal between channel C3 and C4 and classified using tresholding. In LDA and K-Means the delta rhythm signals from C3 and C4 are directly fed to classifier. These techniques are evaluated in Online Session and the feature recorded the highest classification accuracy will be implemented in the Navigation Session.

The confusion matrix presented in Table 4.8 shows the overall performance of the system in classifying the 300 instructions using conventional and sliding window issued in Online Session for horizontal gaze detection. In this analysis, the open eye instructions issued in eyelid position analysis are examined and denoted as stationary. The implementation of sliding window in horizontal gaze analysis improves the accuracy for all techniques for approximately 3% while sensitivity for approximately 1% compared to conventional window.

Table 4.8: Confusion matrix for horizontal gaze analysis using conventional and sliding window during Online Session

	Task	Recognized Gaze			PPV	NPV	Accuracy	Sensitivity	Processing Time (s)
		Stationary	Left	Right					
CONVENTIONAL WINDOW	LDA								
	Stationary	100	0	0	0.68	1	0.84	1	0.49
	Left gaze	26	74	0	1	0.93	0.97	0.94	0.49
	Right gaze	22	0	78	1	0.94	0.97	0.95	0.49
	Mean				**0.89**	**0.96**	**0.93**	**0.96**	**0.49**
	K-Means								
	Stationary	100	0	0	0.78	1	0.89	1	0.48
	Left gaze	12	88	0	1	0.93	0.97	0.94	0.48
	Right gaze	17	0	83	1	0.94	0.97	0.95	0.48
	Mean				**0.93**	**0.96**	**0.94**	**0.96**	**0.48**
	Area & Threshold								
	Stationary	100	0	0	0.68	1	0.84	1	0.42
	Left gaze	26	84	0	1	0.93	0.97	0.94	0.42
	Right gaze	22	0	81	1	0.94	0.97	0.95	0.42
	Mean				**0.89**	**0.96**	**0.93**	**0.96**	**0.42**
SLIDING WINDOW	LDA								
	Stationary	100	0	0	0.79	1	0.90	1	0.49
	Left gaze	14	86	0	1	0.93	0.97	1	0.49
	Right gaze	12	0	88	1	0.94	0.97	0.95	0.49
	Mean				**0.93**	**0.96**	**0.95**	**0.96**	**0.49**
	K-Means								
	Stationary	100	0	0	0.92	1.00	0.96	1	0.48
	Left gaze	5	95	0	1	0.98	0.99	0.98	0.48
	Right gaze	4	0	96	1	0.98	0.99	0.98	0.48
	Mean				**0.97**	**0.99**	**0.98**	**0.99**	**0.48**
	Area & Threshold								
	Stationary	100	0	0	0.85	1.00	0.93	1	0.42
	Left gaze	11	89	0	1	0.95	0.97	0.95	0.42
	Right gaze	6	0	94	1	0.97	0.99	0.97	0.42
	Mean				**0.95**	**0.97**	**0.96**	**0.97**	**0.42**

It can be observed that the stationary instructions are perfectly executed for all three techniques tested in this analysis. This indicates that the anticipation and high in alertness during the experiment that altered the alpha rhythm in open eye signal, has a minimal effect in delta rhythm.

a) ***Linear Discriminant Analysis (LDA)***

LDAs has detected 14 left gaze and 12 right gaze as stationary that contributed to the overall accuracy of 93%. Moreover, the LDA recorded 0.49s of processing time to obtain the final output from two LDA classifiers. Figure 4.6 shows the projection of the LDA in 1D subspace during execution of left and right gaze in a window of 128 samples. In the case where the gaze was not done rapidly by the participant, LDA will rule the weak pulses as stationary that contributed to the lowest overall accuracy in the horizontal gaze analysis.

(a)   (b)
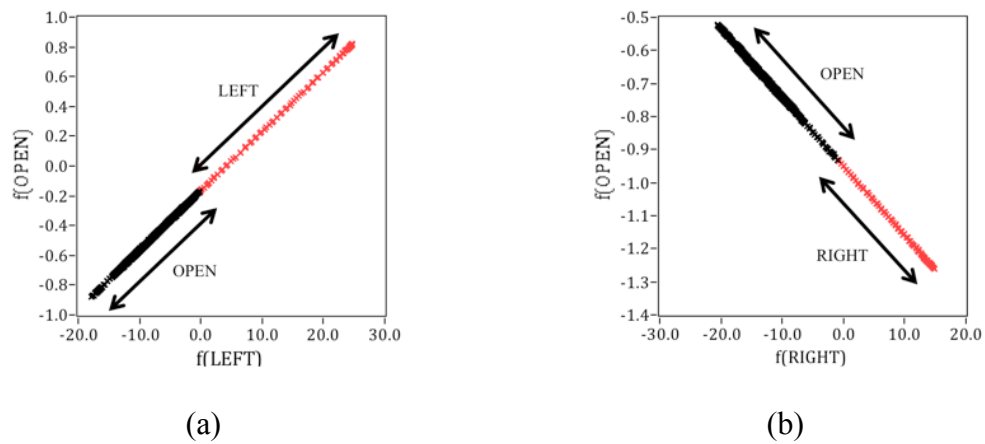
Figure 4.6: Projection of LDA in 1D subspace (a) left gaze (b) right gaze

b) ***K-Means & Euclidean Distance***

Among the three techniques, K-Means and Euclidean distance recorded the highest overall accuracy of 98% with five left gaze and four right gaze instructions are wrongly executed as stationary. The processing time requires approximately 0.48s to obtain the minimum distance between centroid from a window and the predetermined centroid of each group. The predetermined centroids that calculated from recording data

are presented in the Table 4.9. The minimum distance from centroids in K-Means 1 and K-Means 2 are combined to reach the final classification as listed in Table 3.1.

Table 4.9: K-Means centroids obtained for each participant.

Participant	K-Means 1		K-Means 2	
	Left	Stationary	Stationary	Right
1	8.9024	0.8211	0.3937	11.5058
2	10.8833	0.4934	1.0186	14.1659
3	9.9662	0.3318	1.2894	13.8899
4	9.5955	1.3828	1.5664	11.3481
5	11.5054	0.5615	-0.1302	11.9542
6	9.7842	-0.9461	0.3956	11.7507
7	10.7908	0.7316	0.5986	11.0119
8	10.8428	-0.1711	1.3422	13.9627
9	9.66	1.3924	2.4418	11.5321
10	7.9459	-0.3438	1.8518	11.0432
11	16.183	1.775	-0.8713	16.5271
12	16.0006	-0.0202	-0.3665	14.549
13	16.2557	0.6049	0.2312	14.4966
14	18.8997	-0.9463	-0.6492	12.7471
15	16.7951	0.4163	-0.3774	14.7554
16	15.2134	1.2661	0.1956	11.0271
17	17.0682	0.9985	0.1529	13.6501
18	14.6868	0.3342	0.4834	14.7461
19	14.9007	1.9424	0.2733	13.7922
20	16.9446	1.2542	0.2124	10.432

c)   *Area in Delta Rhythm*

Area is analyzed between delta signal in C3 and C4 as shown in Figure 4.7. Then, the area will be compared to *threshold_area$_{C3, C4}$*, a range between half of the mean area during right gaze at the lower limit and half of the mean area during left gaze at the upper limit. The calculated area will be recognized as right gaze if the area is under the lower limit and left gaze if exceeding the upper limit. However, if the area is in the

range of *threshold_area$_{C3, C4}$* in between lower and upper limit, the current window will recognize as stationary or no movement of eyeball.

(a) Center to Left　　　(b) Center to Right　　　(c) Stationary
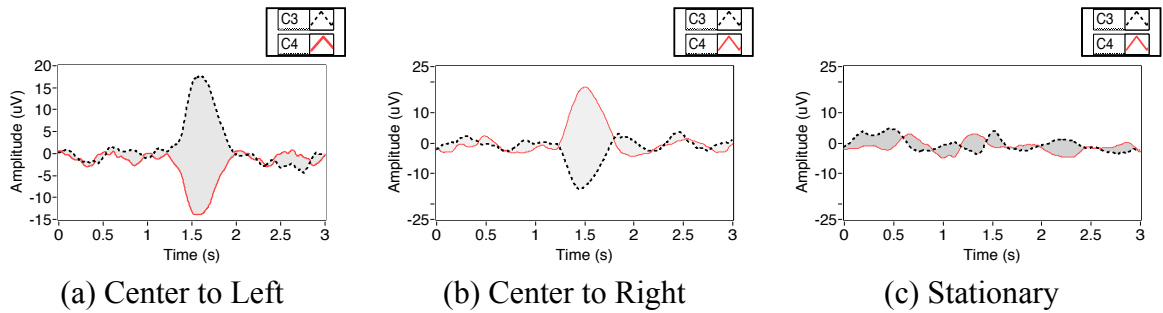
Figure 4.7: Area in delta rhythm are calculated between signals in C3 and C4.

This technique has recorded overall accuracy of 96% with 11 left gazes and six right gazes are mistakenly recognized as stationary. Implementation of area and thresholding in Online Session has recorded approximately 0.42s of processing time to examine a window of 128 samples.

Table 4.10: The upper and lower limits of *threshold_area$_{C3, C4}$* for each participant. An area that lies in between lower and upper limit will recognize as stationary. If the area is below the lower limit, then the right gaze is detected, while exceeding the upper limit will represent a left gaze.

Participant	1	2	3	4	5	6	7	8	9	10
Upper Limit	798	932	871	1059	1109	858	1033	966	843	633
Lower Limit	-1234	-1364	-1422	-1268	-1297	-1073	-1296	-1399	-1208	-1224
Participant	11	12	13	14	15	16	17	18	19	20
Upper Limit	1407	1337	1436	1709	1561	1336	1361	1248	1417	1404
Lower Limit	-1524	-1392	-1344	-1303	-1361	-1171	-1346	-1424	-1290	-1204

d)   Uncontrolled Factors

Generally, the uncontrolled factor that contributes to the wrongly executed horizontal gaze is mainly due to the operator failing to execute the instruction within 2s after the command is issued. Another reason is because the shift in gaze is not done rapidly. This generates weak pulses in C3 and C4 that are difficult to detect. These errors are caused by fatigue, lack of focus and familiarity, disturbance and confusion.

4.3   Navigation Session

In this session, features such as variance and centroids from K-Means are used as input to the fuzzy state transition. These two features are selected as they score the highest overall accuracy in Online Session. Furthermore, five participants with score higher than 98% in Online Session are chosen to perform the navigational tests.

This session requires the participants to navigate the wheelchair along two routes passing through checkpoints in the same indoor area. Then, the performances of the wheelchair system and the participant are evaluated. The evaluation metrics are described as follows (I. Iturrate *et al.*, 2009; Montesano, Diaz *et al.*, 2010):

1) ***Clearance Min (m)*:** Minimum clearance distances between the wheelchair and obstacles during the Navigation Session.

2) ***Clearance Mean (m)*:** Average of clearance distances between the wheelchair and obstacles at all time.

3) ***Collisions*:** Total number of collisions during the task.

4) ***ITR (bits/min):*** Information transfer rate defined by Wolpaw et. al (Wolpaw, Ramoser et al., 1998).

5) **Mission Time (s):** Mean time to perform one mission.

6) **No. Of Missions:** Total missions to complete the task. A mission is a navigation going straight FORWARD, BACKWARD, TURN LEFT, RIGHT and STOP. A few commands or selections would be required to execute a mission such as left, right gaze, blink or closed eye. These commands or selections are also known as state transitions in the modeled state machine.

7) **Path Length (m):** Distance traveled to complete the task.

8) **Path Optimality Ratio:** Ratio of the path length to the optimal path (the optimal path was 17.7m for Route 1 and 22.7m for Route 2. See Figure 3.17)

9) **Real Accuracy:** Ratio of correct selections to the total number of selections.

10) **Task Success:** Completion of the navigation task. The task is considered a failure for the following reasons: user desertion, wheelchair misoperation or unable to reach the finish line.

11) **Time in Motion (s):** Total time wheelchair in moving condition during task.

12) **Time Optimality Ratio:** Ratio of the time taken to the optimal time to complete the task (the optimal time was approximately 17s for Route 1 and 24s for Route 2 based on maximum and rotational velocities of 1.39m/s and 0.4rad/s)

13) **Total Errors:** Total of incorrect selections during navigation tasks.

14) **Total Time (s):** Time taken to complete the task from start to finish line.

15) **Useful Accuracy:** Ratio of correct selections and useful error to the total number of selections.

16) **Useful Errors:** Incorrect selections that the participants decide to use it.

17) **Useless Errors:** Incorrect selections that the participants decide not to use.

18) **Velocity (m/s):** Total length over the total time taken for a task.

4.3.1 Wheelchair System Performance

The navigation system performance is represented by the overall, signal processing and navigation performance as follows.

a)   *Overall Performance*

The criteria used in evaluating the overall performance are shown in Table 4.11. All participants managed to complete the navigation task successfully through Route 1 and 2 without collision. On average, the participants took 76 seconds and 167 seconds to navigate Route 1 and 2 respectively. The average distances covered by the participants were 18.79m for Route 1 and 26.84m for Route 2. The low path optimality ratio of 1.06 for Route 1 and 1.18 for Route 2 indicates that the participants were able to travel close to the designated paths. However, the actual time taken to complete the task is much higher than the optimal time, with a maximum ratio of 7.76 for Route 1 and 9.74 times for Route 2. The participants took a longer time to navigate Route 2 as it has more turns. The high actual time includes the waiting period during mode changing, command selection and computational time. The useful accuracy of the Navigation Session is satisfying with a mean of 98% and 96% for Route 1 and Route 2 respectively. These performances could be translated into an average ITR of 89.16bits/min for Route 1 and 83.15% for Route 2. In general, a narrow performance gap observed among the participants signifies the system usability and consistency to navigate and maneuver the wheelchair in small and indoor spaces.

Table 4.11: Metrics to evaluate the overall performance in Navigation Session.

	Route 1				Route 2			
	min	max	mean	std	min	max	mean	std
Task Success	1	1	1	0	1	1	1	0
Path Length (m)	17.90	19.55	18.79	0.49	25.80	27.50	26.84	0.52
Total Time (s)	53	132	76	21	103	173	125	18
Path Optimality Ratio	1.01	1.10	1.06	0.03	1.14	1.21	1.18	0.02
Time Optimality Ratio	3.11	7.76	4.47	1.23	4.24	7.11	5.16	0.75
Collisions	0	0	0	0	0	0	0	0
Useful Accuracy	0.94	1	0.98	0.02	0.93	1	0.96	0.02
ITR (bits/min)	78.04	96.55	89.16	2.77	72.05	95.30	81.28	3.97

b) Signal Processing Performance

The performance of the signal processing or fuzzy state transition during Navigation Session is outlined in Table 4.12 and described in two groups: real accuracy and useful accuracy. The real accuracy is the ratio of correctly recognized command according to the participants' selection to the total recognized command while the useful accuracy is the mixture of real accuracy and useful errors. The average real accuracy recorded during the session is 93% for Route 1 and 90% for Route 2. However, the average useful accuracy recorded, 98% for Route 1 and 96% for Route 2, were higher when the useful errors were taken into consideration.

Table 4.12: Metrics to evaluate the signal processing performance in Navigation Session.

	Route 1				Route 2			
	min	max	mean	std	min	max	mean	std
Real Accuracy	0.86	1	0.93	0.04	0.83	0.97	0.90	0.04
Useful Accuracy	0.94	1	0.98	0.02	0.93	1	0.96	0.02
Total Errors	0	4	1	1	1	7	4	2
Useless Errors	0	1	0.47	0.52	0	3	1.60	0.83
Useful Errors	0	3	0.93	0.80	1	5	2.27	1.10
Mission Time (s)	4.50	8	5.89	1.17	3.17	4.41	3.93	0.31

Here, not all errors occur during the experiment were unusable. Some of the errors were actually used by the participants to reach the target (Baker, Casey *et al.*, 2004; I. Iturrate *et al.*, 2009). For instance, the wheelchair may stop when triggered by false closed eye signal caused by high alpha rhythm due to high anticipation and alertness. In this case, if the participant used this error to rethink the strategy to reach the target, the error is considered useable and counted as a successful command. In contrast, a useless error is unusable and only interferes with the wheelchair movement. For instance, when the user command the system to turn left by left gaze, the system recognized it as going straight instruction as no gaze is detected. This error is counted as useless error.

An average time required to accomplish a mission is approximately 5.89 second for Route 1 and 3.93 second for Route 2. The lower mission time for Route 2 indicates the increasing competency of the participants in maneuvering the wheelchair while the distance traversed for each mission was shorter.

c)   *Navigation Performance*

In total, six attempts were given to the participants to accomplish both tasks and the participants successfully completed each of the attempts. The metrics to evaluate the navigation system is presented in Table 4.13. The participants required an average of 9.67 missions to travel the 18.79m of Route 1 and an average of 24 missions to travel the 26.84m of Route 2. Route 2 was designed with more checkpoints, thus it requires more missions than Route 1 such as going straight forwardly, turn left or right to complete the route. In total, 501 missions were executed along 684.4m during the Navigation Session and in general, the wheelchair traveled 1.37m for every mission with a mean velocity of 0.9m/s.

Table 4.13: Metrics to evaluate the navigation performance.

	Route 1				Route 2			
	min	max	mean	std	min	max	mean	std
Task Success	1	1	1	0	1	1	1	0
No. Of Missions	8	15	9.67	1.63	19	39	24	5.52
Collisions	0	0	0	0	0	0	0	0
Path Length (m)	17.90	19.55	18.79	0.49	25.80	27.50	26.84	0.52
Velocity (m/s)	0.88	1.08	1.06	0.05	0.80	0.84	0.82	0.01
Time in Motion (s)	17	22	18	1	32	34	33	0
Clearance Min (m)	0.38	0.74	0.54	0.10	0.43	0.69	0.55	0.08
Clearance Mean (m)	0.92	1.22	1.10	0.08	0.77	0.93	0.83	0.05

In this study, we designed all the checkpoints to be close to the obstacles with a minimum distance of 0.5m. Under space constraint in indoor environment, it is important to have a fast system response to avoid collision. During the Navigation Session, the mean of the minimum clearance is approximately 0.54m for Route 1 and 0.55m for Route 2 while mean clearance is approximately 1.10 and 0.83m for Route 1 and Route 2 accordingly. Here, the proposed system demonstrates the ability to stop responsively as the participants were able to reach the points close to the walls and avoid collisions with good safety margins.

Also, usability of the backward maneuver was proven when the wheelchair reversed from tight checkpoints of C_1 and D_2 without collisions. Without this ability, the wheelchair would be stuck, as there was no space to turn.

4.3.2 Individual Performance

The metrics evaluation shown in Table 4.14 is a summary of the individual performance from three attempts performed for each route during the experiment. Participant P4 executed the least missions with 8.67 (Route 1) and 20 (Route 2) while

the participant P1 executed the most missions with 11.67 (Route 1) and 30 (Route 2). Fewer missions executed during the task shows the competency level of the participants to control and command the wheelchair effectively. Also, participant P4 travelled the shortest path length of 18.10m in Route 1 and 26.49m in Route 2 with path optimality length of 1.02 in Route 1 and 1.17 in Route 2. In contrast, participant P1 required a longer path length of 19.56m in Route 1 and 27.87m in Route 2. Participant P4 demonstrated the skill to navigate the wheelchair near the perfect path and in contrary participant P1 took the longer path length to reach the finish line. Here, the path length reflects the total time taken to finish the tasks with participant P4 the fastest and participant P1 the slowest.

Table 4.14: The performance of each participant in Navigation Session.

	Route 1					Route 2				
	P1	P2	P3	P4	P5	P1	P2	P3	P4	P5
Task Success	1	1	1	1	1	1	1	1	1	1
No. Of Missions	11.67	9	9.67	8.67	9.33	30	23.33	24.33	20	21
Path Length (m)	19.56	18.52	18.97	18.10	18.83	27.87	26.84	27.13	26.49	26.67
Path Optimality Length	1.11	1.05	1.07	1.02	1.06	1.23	1.18	1.20	1.17	1.17
Total Time (s)	106	68	79	59	70	150	119	129	114	117
Useful Accuracy	0.97	0.98	0.97	0.98	0.98	0.94	0.95	0.96	0.97	0.96

The total time consists of the idle time during which the wheelchair is stationary and in-motion time as shown in Figure 4.8. Idle time accounts for the time taken by the participants to plan and execute the commands while in-motion time represents the time the wheelchair is moving. In both tasks, participant P1 required more time than others to plan and execute commands with 87 seconds in Route 1 and 112 second in Route 2.

However, all participants managed to complete both navigational tasks without collision.
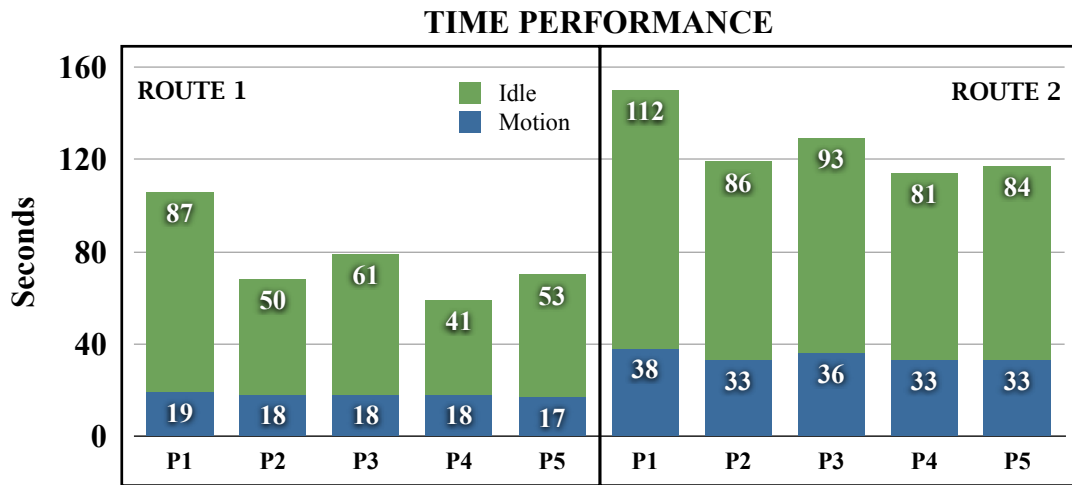
Figure 4.8: The total time taken during the navigation task.

Output from the fuzzy state transition will indicate if the participant performed the gaze in a slower motion resulting in a weaker signal due to fatigue, lack of focus, disturbance or confusion. During the Navigation Session, this fatigue warning was recorded in every attempt as outlined in Table 4.15. It can be seen that the number of fatigue warning was increased over attempts and higher in Route 2 than in Route 1. Also, participant P1 recorded the highest mean of fatigue warning and participant P4 the lowest. This also reflects the performance rate of the participants, as this warning can be an indication of their concentration.

Table 4.15: Fatigue warning during the navigation experiment.

	Route 1					Route 2				
	P1	**P2**	**P3**	**P4**	**P5**	**P1**	**P2**	**P3**	**P4**	**P5**
Attempts 1	1	0	1	0	0	3	2	1	1	1
Attempts 2	2	1	1	0	0	4	2	2	1	1
Attempts 3	2	1	2	1	1	6	4	2	1	2
Mean	1.67	0.67	1.33	0.33	0.33	4.33	2.67	1.67	1	1.33

At the end of the navigational session, the participants were given a set of questionnaire (see APPENDIX E) to express their navigational experience in three metrics of workload, learnability and confidence as presented in Figure 4.9 for every attempt (I. Iturrate *et al.*, 2009). The metrics were measured in scale between 0 to 5 from the least to the most. The workload metrics denotes the effort to accomplish the tasks. All participants agreed that it took a higher workload to complete Route 2 than Route 1. Also, all participants verified that the workload decrease over attempts and this correlates with the adaptation of the participants to learn. Participant P1 recorded the most effort required to operate the wheelchair in both routes. The learnability metrics indicates that the participants adapted to control the navigation system based on their experience from the previous attempt thus increasing their confidence to perform the task.
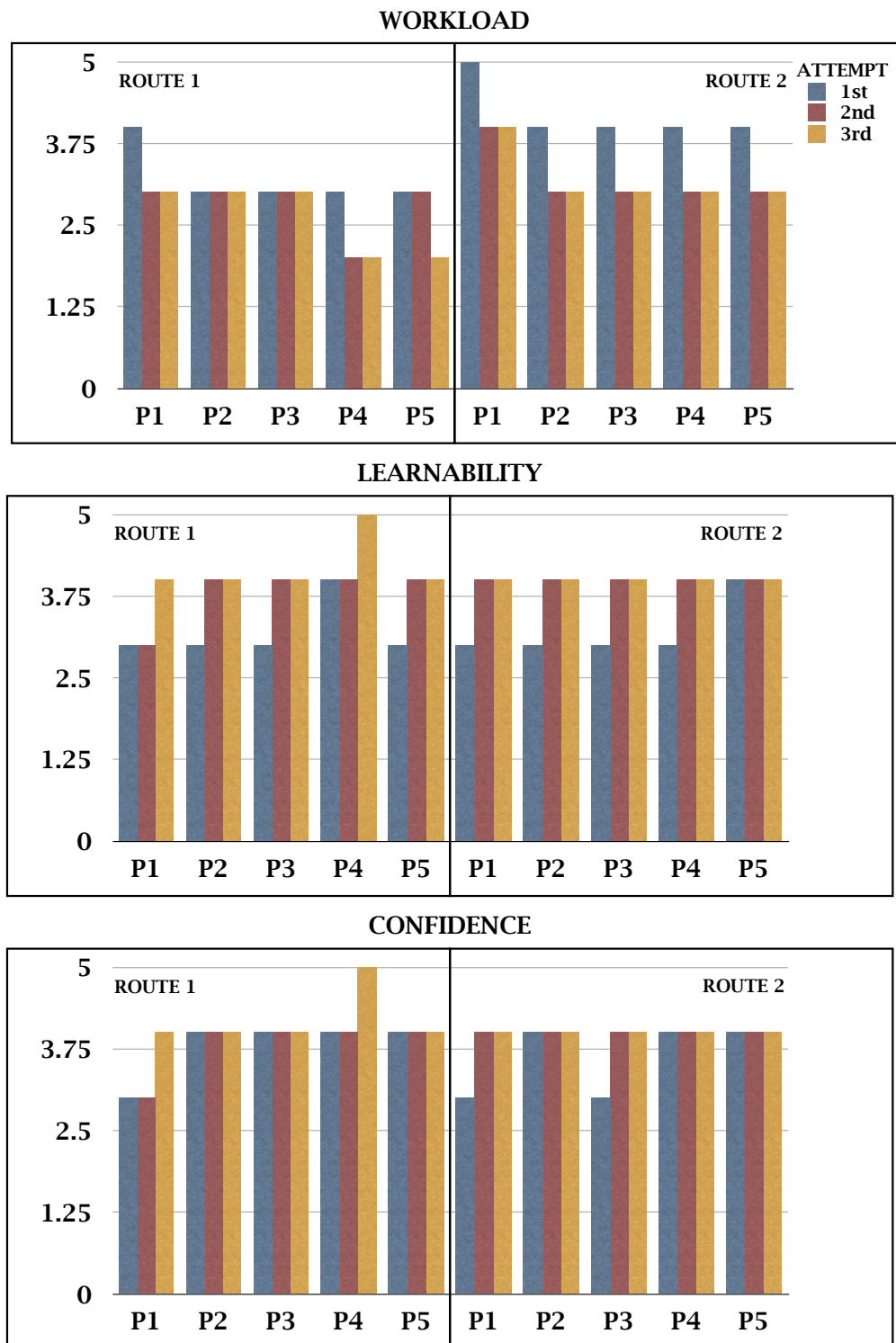
Figure 4.9: The assessment of the participants' navigational experience. The scale of 0–5 (least to the most) was used to express the metrics.

4.4   Comparison Study

A comparison of similar studies involving HMI for wheelchair navigation is presented in Table 4.16. The studies are categorized either BCI, hybrid BCI or other HMI. Overall, (B. Rebsamen *et al.*, 2010) recorded the highest classification rate while (Cao *et al.*, 2014) recorded the fastest execution time in wheelchair navigation studies. However, both studies employed synchronous system, which requires the user to follow the system pace.

In opposite, asynchronous system received the commands at the user pace offering more natural control experience. Utilizing this system, (Parini *et al.*, 2009) recorded the highest classification accuracy and the fastest in BCI studies while our proposed studies recorded the best performance and the fastest in hybrid BCI studies. Compared to all studies, our proposed work is ranked in 4th place for the highest accuracy and 2nd place for the fastest execution time.

Table 4.16: Comparison between this study and other HMI system used for wheelchair navigation.

Author	Input	System	Feature	Classifier	Accuracy	*Execution Time (s)
BCI						
(B. Rebsamen *et al.*, 2010)	P300	Synchronous	Epochs	SVM	99.78%	6
(Parini *et al.*, 2009)	SSVEP	Asynchronous	CSP	LDA	97.5%	2.38
(I. Iturrate *et al.*, 2009)	P300	Synchronous	(Krusienski, Sellers *et al.*, 2006)	SWLDA	94%	5.40
(Huang *et al.*, 2012)	Imagery	Synchronous	Power Spectra	MLD	84.3%	60.4
(P. F. Diez *et al.*, 2011)	SSVEP	Asynchronous	Power Spectra	Fast Fourier Transform (FFT)	81.68%	4.48
(Kus *et al.*, 2012)	Imagery	Asynchronous	Power Spectra	MLD	74.84%	8.81
Hybrid BCI						
(Cao *et al.*, 2014)	Imagery, SSVEP	Synchronous	CSP	RBF-SVM, CCA	98.77%	295 bits/min
Proposed study	EEG, EOG Artifact	Asynchronous	Variance, K-Means	Fuzzy Logic	97%	0.98 (85 bits/min)
(Wang *et al.*, 2014)	Imagery, P300, EOG	Asynchronous	CSP	SVM	95%	3
(B. Choi & Jo, 2013)	Imagery, SSVEP, P300	Asynchronous	CSP	SVM, CCA, Bayesian	84.4 – 91%	27.2
(Thorsten O Zander, Matti Gaertner *et al.*, 2010)	Imagery, EOG	Asynchronous	SpecCSP	LDA	83.3%	5.9
(Long *et al.*, 2012)	Imagery, P300	Asynchronous	CSP	LDA	83.10%	6
(Y. Q. Li, Pan *et al.*, 2013)	P300, SSVEP	Asynchronous	ERP, Power Spectra	SVM, Power Ratios	14.18 true positives/ min	5.28
Other HMI						
(Postelnicu, Girbacia, *et al.*, 2012)	EOG	Asynchronous	Maximum Absolute Values	Fuzzy Logic	95.63%	2.6
(Latif *et al.*, 2008)	Eye-Tracking	Asynchronous		-	80%	-

*Execution Time = time taken from the command initiated by the user until the execution of the wheelchair.

4.5 Summary

In this chapter, the outcome of experiments carried out during Online and Navigation Session is presented. In the Online Session, six methods are evaluated for the detection of eyelid position and horizontal gaze. The study of the eyelid position detection shows that using variance as feature present the highest overall performance with 98%. Also, the fastest processing time recorded during the experimental session is approximately 0.42s due to the small window of 128 samples was utilized in windowing stage.

In the study of the gaze detection, using y K-Means present the highest overall performance with 98%. Overall, all of them required approximately less than 0.5s to process the data. Same as the eyelid position analysis, a small window frame of 128 samples was utilized that contributes to faster computational time. For further evaluation, both techniques that recorded the highest overall accuracy in Online Session are employed as input to fuzzy state transition for navigation system.

In the Navigation Session, evaluation of the performance for the navigation system and individual are presented. The evaluation of the navigation system is categorized into overall performance, signal processing and navigation performance. The participants took an average of 76 seconds and 167 seconds to navigate Route 1 and 2 respectively. The average distances covered by the participants were 18.79m for Route 1 and 26.84m for Route 2. All participants agreed that it took a higher workload to complete Route 2 than Route 1. Also, all participants verified that the workload decrease over attempts and this correlates with the adaptation of the subjects to learn. The result shows that all the subjects successfully complete all the tasks without collision. This suggests that the

proposed strategies are effective. All the metrics evaluation used in this study are outlined and explained.

CHAPTER 5

CONCLUSIONS & RECOMMENDATIONS

5.1 Introduction

This chapter presents the summary of the work reported in this thesis. Contributions made through this work will be highlighted and recommendations to improve the work are given.

5.2 Summary

The primary objective of this study to develop a wheelchair navigation system using an EEG signal and EOG artifacts related to eyelid position and horizontal eyeball movement has been achieved. The system is modeled as a finite state machine whose state transition is governed by fuzzy logic. The EOG artifacts obtained from delta rhythm at motor cortex are used to infer the gaze direction while the alpha rhythm at occipital region is used to imply open or closed eye condition.

A sliding window is employed to position important cues in the input signals of C3, C4 and O2 at the center of the window. Variance are extracted from the O2 signal so that the eye condition can be classified into open, blink and closed eye in real-time. The C3 and C4 data are used directly as inputs to two K-means classifiers so that any horizontal eyeball movement can be detected and classified as not moving or moving to

the left or right. An average accuracy of 98% and an execution time of less than 0.5 second are registered in the Online Session involving 20 participants.

In Navigation Session, five selected participants maneuver the wheelchair along two designated routes. Based on the fuzzy state transition, the wheelchair is actuated to move FORWARD and BACKWARD in three directions, which are LEFT, RIGHT and STRAIGHT. The user can also instruct the wheelchair to STOP when needed. A GUI is developed to allow the user to keep track of the states at all time. The participants managed to complete the tasks without collisions. This experiment also tested the usefulness of the backward movement when the wheelchair was trapped at tight dead ends with no space to make u-turn. The high performance of 98% for Route 1 and 96% for Route 2 were recorded during the experiment. The results suggest that the proposed finite state machine model is effective as a navigation controller for the system.

5.2.1 Contributions

The main contribution of this research work is in the implementation of EEG and EOG artifacts in EEG signals as inputs to control a wheelchair. To the best of our knowledge, this is the first report that documents the use of EOG traces from channel C3 and C4 in the EEG as a control mechanism for asynchronous wheelchair navigation. Even though there have been many studies that combine different EEG signals for wheelchair navigation, the execution time of these studies have never been less than 2 seconds. The execution time of the proposed system is only a fraction of the works presented in Table 4.16. The extracted features of the delta and alpha rhythm are simple enough that a small window of 128 samples is sufficient. This results in a fast execution time.

Moreover, the use of a finite state machine to model the process and track the gaze direction allows the wheelchair to move FORWARD and BACKWARD in three directions from a limited number of distinct horizontal eyeball movements. The system is also designed to have an ability to stop as a safety feature.

Additionally, the implementation of sliding window contributes to the high performance during Online and Navigation Session. The sliding window allows important cues to be positioned at the center so that blink, open, closed eye, left and right eyeball movements can be detected and recognized.

Finally, the use of two simultaneous K-Means for horizontal gaze detection in C3 and C4 data, and variance feature for eyelid position detection in O2 delivers a more consistent result by compensating instability in the signals.

5.3   Future Work & Recommendation

Nevertheless, this system can be further improved to increase its flexibility and safety. First, an adaptive fuzzy logic classifier can be used to replace the hard thresholding to reposition the sliding window and classify the EEG signal of varying strength. Second, dedicated hardware like field-programmable gate array (FPGA) and parallel programming can be used to reduce the data acquisition and computational time. Third, a shared control can be incorporated to assist the movement of the wheelchair in a cluttered and dynamic environment such as when passing through a door so that only a minimum number of commands are required from the operator. Fourth, the speed of the wheelchair can be varied to improve its efficiency especially when going straight. It should be noted that this system has not been tested on patients with motor disorder, since it is still in testing and development phase. A test on real

patients is important as it provides a true measure of the system capability and ideas to improve its operation and user friendliness.

REFERENCES

Abe, K., Ohi, S., & Ohyama, M. (2013). *Eye-Gaze Input System Suitable for Use under Natural Light and Its Applications Toward a Support for ALS Patients.*

Aftanas, L., & Golocheikine, S. (2001). Human Anterior and Frontal Midline Theta and Lower Alpha Reflect Emotionally Positive State and Internalized Attention: High-resolution EEG Investigation of Meditation. *Neuroscience Letters, 310*(1), 57-60.

Ahn, M., Ahn, S., Hong, J. H., Cho, H., Kim, K., Kim, B. S., et al. (2013). Gamma band activity associated with BCI performance: simultaneous MEG/EEG study. *Frontiers in human neuroscience, 7*.

Al-Haddad, A. A., Sudirman, R., & Omar, C. (2011, 20-22 Sept. 2011). *Guiding Wheelchair Motion Based on EOG Signals Using Tangent Bug Algorithm.* Paper presented at the Computational Intelligence, Modelling and Simulation (CIMSiM), 2011 Third International Conference on.

Allison, B. Z., Brunner, C., Altstatter, C., Wagner, I. C., Grissmann, S., & Neuper, C. (2012). A hybrid ERD/SSVEP BCI for continuous simultaneous two dimensional cursor control. *Journal of Neuroscience Methods, 209*(2), 299-307.

Allison, B. Z., Brunner, C., Kaiser, V., Müller-Putz, G. R., Neuper, C., & Pfurtscheller, G. (2010). Toward a Hybrid Brain–Computer Interface based on Imagined Movement and Visual Attention. *Journal of Neural Engineering, 7*(2), 026007.

Allison, B. Z., Wolpaw, E. W., & Wolpaw, A. R. (2007). Brain-computer interface systems: progress and prospects. *Expert Review of Medical Devices, 4*(4), 463-474.

Aloise, F., Schettini, F., Arico, P., Salinari, S., Babiloni, F., & Cincotti, F. (2012). A Comparison of Classification Techniques for a Gaze-Independent P300-Based Brain-Computer Interface. *Journal of Neural Engineering, 9*(4).

Baihan, H., Lo, A. P., & Shi, B. E. (2013, 6-8 Nov. 2013). *Integrating EEG information improves performance of gaze based cursor control.* Paper presented at the Neural Engineering (NER), 2013 6th International IEEE/EMBS Conference on.

Baker, M., Casey, R., Keyes, B., & Yanco, H. A. (2004). Improved Interfaces for Human-Robot Interaction in Urban Search and Rescue. *2004 IEEE International Conference on Systems, Man and Cybernetics, 3*, 2960-2965 vol.2963.

Ball, L., Nordness, A., Fager, S., Kersch, K., Pattee, G., & Beukelman, D. (2010). Eye-gaze access of AAC technology for persons with amyotrophic lateral sclerosis. *Journal of Medical Speech Language Pathology, 18*, 11-23.

Barbosa, A. O. G., Achanccaray, D. R., & Meggiolaro, M. A. (2010). *Activation of a mobile robot through a brain computer interface.* Paper presented at the Robotics and Automation (ICRA), 2010 IEEE International Conference on.

Barea, R., Boquete, L., Mazo, M., & Lopez, E. (2002a). System for Assisted Mobility using Eye Movements Based on Electrooculography. *IEEE Transactions on Neural Systems and Rehabilitation Engineering, 10*(4), 209-218.

Barea, R., Boquete, L., Mazo, M., & Lopez, E. (2002b). Wheelchair Guidance Strategies using EOG. *Journal of Intelligent & Robotic Systems, 34*(3), 279-299.

Bell, C. J., Shenoy, P., Chalodhorn, R., & Rao, R. P. (2008). Control of a humanoid robot by a noninvasive brain–computer interface in humans. *Journal of neural engineering, 5*(2), 214.

Bi, L. Z., Fan, X. A., & Liu, Y. L. (2013). EEG-Based Brain-Controlled Mobile Robots: A Survey. *Ieee Transactions on Human-Machine Systems, 43*(2), 161-176.

Blankertz, B., Losch, F., Krauledat, M., Dornhege, G., Curio, G., & Muller, K.-R. (2008). The Berlin Brain--Computer Interface: accurate performance from first-session in BCI-naive subjects. *Biomedical Engineering, IEEE Transactions on, 55*(10), 2452-2462.

Blankertz, B., Sannelli, C., Haider, S., Hammer, E. M., Kubler, A., Muller, K. R., et al. (2010). Neurophysiological Predictor of SMR-Based BCI Performance. *Neuroimage, 51*(4), 1303-1309.

Blasco, J. L. S., Ianez, E., Ubeda, A., & Azorin, J. M. (2012). Visual Evoked Potential-Based Brain-Machine Interface Applications to Assist Disabled People. *Expert Systems with Applications, 39*(9), 7908-7918.

Brown, L., van de Molengraft, J., Yazicioglu, R. F., Torfs, T., Penders, J., & Van Hoof, C. (2010). *A low-power, wireless, 8-channel EEG monitoring headset.* Paper presented at the Engineering in Medicine and Biology Society (EMBC), 2010 Annual International Conference of the IEEE.

Bulling, A., Roggen, D., & Troster, G. (2009). Wearable EOG goggles: Seamless sensing and context-awareness in everyday environments. *Journal of Ambient Intelligence and Smart Environments, 1*(2), 157-171.

Cao, L., Li, J., Ji, H., & Jiang, C. (2014). A Hybrid Brain Computer Interface System based on The Neurophysiological Protocol and Brain-Actuated Switch for Wheelchair Control. *Journal of Neuroscience Methods, 229*(0), 33-43.

Chae, Y., Jo, S., & Jeong, J. (2011). *Brain-actuated humanoid robot navigation control using asynchronous brain-computer interface.* Paper presented at the Neural Engineering (NER), 2011 5th International IEEE/EMBS Conference on.

Cheein, F. A. A., De La Cruz, C., Bastos, T. F., & Carelli, R. (2009). Slam-based cross-a-door solution approach for a robotic wheelchair. *International Journal of Advanced Robotic Systems, 6*(3), 239-248.

Choi, B., & Jo, S. (2013). A Low-Cost EEG System-Based Hybrid Brain-Computer Interface for Humanoid Robot Navigation and Recognition. *Plos One, 8*(9), e74583.

Choi, K. (2012). Control of a vehicle with EEG signals in real-time and system evaluation. *European journal of applied physiology, 112*(2), 755-766.

Choi, K., & Cichocki, A. (2008). Control of a wheelchair by motor imagery in real time *Intelligent Data Engineering and Automated Learning–IDEAL 2008* (pp. 330-337): Springer.

Chumerin, N., Manyakov, N. V., van Vliet, M., Robben, A., Combaz, A., & Van Hulle, M. (2013). Steady-State Visual Evoked Potential-Based Computer Gaming on a Consumer-Grade EEG Device. *IEEE Transactions on Computational Intelligence and AI in Games, 5*(2), 100-110.

Craig, D. A., & Nguyen, H. (2007). *Adaptive EEG thought pattern classifier for advanced wheelchair control.* Paper presented at the Engineering in Medicine and Biology Society, 2007. EMBS 2007. 29th Annual International Conference of the IEEE.

Dasgupta, S., Fanton, M., Pham, J., Willard, M., Nezamfar, H., Shafai, B., et al. (2010). *Brain controlled robotic platform using steady state visual evoked potentials acquired by EEG.* Paper presented at the Signals, Systems and Computers (ASILOMAR), 2010 Conference Record of the Forty Fourth Asilomar Conference on.

Deng, L. Y., Hsu, C. L., Lin, T. C., Tuan, J. S., & Chang, S. M. (2010). EOG-based Human-Computer Interface system development. *Expert Systems with Applications, 37*(4), 3337-3343.

Dettmers, C., Benz, M., Liepert, J., & Rockstroh, B. (2012). Motor Imagery in Stroke Patients, or Plegic Patients with Spinal Cord or Peripheral Diseases. *Acta Neurologica Scandinavica, 126*(4), 238-247.

Di Rienzo, F., Collet, C., Hoyek, N., & Guillot, A. (2012). Selective Effect of Physical Fatigue on Motor Imagery Accuracy. *Plos One, 7*(10).

Dias, N. S., Carmo, J. P., Mendes, P. M., & Correia, J. H. (2012). Wireless instrumentation system based on dry electrodes for acquiring EEG signals. *Medical engineering & physics, 34*(7), 972-981.

Diez, P. F., Mut, V., Laciar, E., & Avila, E. (2010, Aug. 31 2010-Sept. 4 2010). *A comparison of monopolar and bipolar EEG recordings for SSVEP detection.* Paper presented at the Engineering in Medicine and Biology Society (EMBC), 2010 Annual International Conference of the IEEE.

Diez, P. F., Mut, V. A., Perona, E. M. A., & Leber, E. L. (2011). Asynchronous BCI Control using High-frequency SSVEP. *Journal of Neuroengineering and Rehabilitation, 8.*

Diez, P. F., Torres Müller, S. M., Mut, V. A., Laciar, E., Avila, E., Bastos-Filho, T. F., et al. (2013). Commanding a robotic wheelchair with a high-frequency steady-state visual evoked potential based brain–computer interface. *Medical Engineering & Physics, 35*(8), 1155-1164.

Escolano, C., Antelis, J., & Minguez, J. (2009). *Human brain-teleoperated robot between remote places.* Paper presented at the Robotics and Automation, 2009. ICRA'09. IEEE International Conference on.

Escolano, C., Antelis, J. M., & Minguez, J. (2012). A telepresence mobile robot controlled with a noninvasive brain–computer interface. *Systems, Man, and Cybernetics, Part B: Cybernetics, IEEE Transactions on, 42*(3), 793-804.

Escolano, C., Murguialday, A. R., Matuz, T., Birbaumer, N., & Minguez, J. (2010). *A telepresence robotic system operated with a P300-based brain-computer interface: Initial tests with ALS patients.* Paper presented at the Engineering in Medicine and Biology Society (EMBC), 2010 Annual International Conference of the IEEE.

Fan, T. L., Ng, C., Ng, J., & Goh, S. (2008). *A brain-computer interface with intelligent distributed controller for wheelchair.* Paper presented at the 4th Kuala Lumpur International Conference on Biomedical Engineering 2008.

Fatourechi, M., Bashashati, A., Ward, R. K., & Birch, G. E. (2007). EMG and EOG artifacts in brain computer interface systems: A survey. *Clinical Neurophysiology, 118*(3), 480-494.

Fernández, T., Harmony, T., Rodríguez, M., Bernal, J., Silva, J., Reyes, A., et al. (1995). EEG Activation Patterns During the Performance of Tasks Involving Different Components of Mental Calculation. *Electroencephalography and Clinical Neurophysiology, 94*(3), 175-182.

Ferreira, A., Bastos-Filho, T. F., Sarcinelli-Filho, M., Sánchez, J. L. M., García, J. C. G., & Quintas, M. M. (2010). Improvements of a brain-computer interface applied

to a robotic wheelchair *Biomedical Engineering Systems and Technologies* (pp. 64-73): Springer.

Ferreira, A., Celeste, W., Cheein, F., Bastos-Filho, T., Sarcinelli-Filho, M., & Carelli, R. (2008). Human-machine interfaces based on EMG and EEG applied to robotic systems. *Journal of NeuroEngineering and Rehabilitation, 5*(1), 10.

Galan, F., Nuttin, M., Lew, E., Ferrez, P. W., Vanacker, G., Philips, J., et al. (2008). A brain-actuated wheelchair: Asynchronous and non-invasive Brain-computer interfaces for continuous control of robots. *Clinical Neurophysiology, 119*(9), 2159-2169.

Galán, F., Nuttin, M., Lew, E., Ferrez, P. W., Vanacker, G., Philips, J., et al. (2008). A brain-actuated wheelchair: asynchronous and non-invasive brain–computer interfaces for continuous control of robots. *Clinical Neurophysiology, 119*(9), 2159-2169.

Gandhi, T., Trikha, M., Santhosh, J., & Anand, S. (2010). Development of an Expert Multitask Gadget Controlled by Voluntary Eye Movements. *Expert Systems with Applications, 37*(6), 4204-4211.

Garrett, D., Peterson, D. A., Anderson, C. W., & Thaut, M. H. (2003). Comparison of linear, nonlinear, and feature selection methods for EEG signal classification. *Ieee Transactions on Neural Systems and Rehabilitation Engineering, 11*(2), 141-144.

Geng, T., Dyson, M., Tsui, C., & Gan, J. Q. (2007). *A 3-class asynchronous BCI controlling a simulated mobile robot.* Paper presented at the Engineering in Medicine and Biology Society, 2007. EMBS 2007. 29th Annual International Conference of the IEEE.

Geng, T., Gan, J. Q., & Hu, H. (2010). A self-paced online BCI for mobile robot control. *International Journal of Advanced Mechatronic Systems, 2*(1), 28-35.

Gentiletti, G. G., Gebhart, J. G., Acevedo, R. C., Yanez-Suarez, O., & Medina-Banuelos, V. (2009). Command of a simulated wheelchair on a virtual environment using a brain-computer interface. *IRBM, 30*(5-6), 218-225.

Gomez-Rodriguez, M., Grosse-Wentrup, M., Hill, J., Gharabaghi, A., Scholkopf, B., & Peters, J. (2011). *Towards brain-robot interfaces in stroke rehabilitation.* Paper presented at the Rehabilitation Robotics (ICORR), 2011 IEEE International Conference on.

Guan, C., Teo, C. L., & Zeng, Q. (2007). *Controlling a wheelchair using a BCI with low information transfer rate.* Paper presented at the 2007 IEEE 10th International Conference on Rehabilitation Robotics.

Hagemann, D., & Naumann, E. (2001). The Effects of Ocular Artifacts on (Lateralized) Broadband Power in the EEG. *Clinical Neurophysiology, 112*(2), 215-231.

Hai, N. T., Van Trung, N., & Van Toi, V. (2013). Mean Threshold and ARNN Algorithms for Identification of Eye Commands in an EEG-Controlled Wheelchair. *Engineering, 5*(10), 284.

Halawani, A., ur Réhman, S., Li, H., & Anani, A. (2012). Active vision for controlling an electric wheelchair. *Intelligent Service Robotics, 5*(2), 89-98.

Hashimoto, M., Takahashi, K., & Shimada, M. (2009). Wheelchair Control Using an EOG- and EMG-Based Gesture Interface. *2009 IEEE/ASME International Conference on Advanced Intelligent Mechatronics, Vols 1-3*, 1205-1210.

Hema, C., Paulraj, M., Yaacob, S., Adom, A., & Nagarajan, R. (2010). *Robot chair control using an asynchronous brain machine interface.* Paper presented at the Signal Processing and Its Applications (CSPA), 2010 6th International Colloquium on.

Hema, C. R., & Paulraj, M. (2011). *Control brain machine interface for a power wheelchair.* Paper presented at the 5th Kuala Lumpur International Conference on Biomedical Engineering 2011.

Huang, D. D., Qian, K., Fei, D. Y., Jia, W. C., Chen, X. D., & Bai, O. (2012). Electroencephalography (EEG)-Based Brain-Computer Interface (BCI): A 2-D Virtual Wheelchair Control Based on Event-Related Desynchronization/Synchronization and State Control. *IEEE Transactions on Neural Systems and Rehabilitation Engineering, 20*(3), 379-388.

Hwang, H. J., Lim, J. H., Jung, Y. J., Choi, H., Lee, S. W., & Im, C. H. (2012). Development of an SSVEP-Based BCI Spelling System Adopting a QWERTY-Style LED Keyboard. *Journal of Neuroscience Methods, 208*(1), 59-65.

Ianez, E., Ubeda, A., Azorin, J. M., & Perez-Vidal, C. (2012). Assistive Robot Application based on an RFID Control Architecture and a Wireless EOG Interface. *Robotics and Autonomous Systems, 60*(8), 1069-1077.

Iturrate, I., Antelis, J., & Minguez, J. (2009). *Synchronous EEG brain-actuated wheelchair with automated navigation.* Paper presented at the Robotics and Automation, 2009. ICRA'09. IEEE International Conference on.

Iturrate, I., Antelis, J. M., Kubler, A., & Minguez, J. (2009). A Noninvasive Brain-Actuated Wheelchair Based on a P300 Neurophysiological Protocol and Automated Navigation. *IEEE Transactions on Robotics, 25*(3), 614-627.

Iturrate, I., Antelis, J. M., Kubler, A., & Minguez, J. (2009). A noninvasive brain-actuated wheelchair based on a P300 neurophysiological protocol and automated navigation. *Robotics, IEEE Transactions on, 25*(3), 614-627.

James, C. J., & Gibson, O. J. (2003). Temporally constrained ICA: an application to artifact rejection in electromagnetic brain signal analysis. *Biomedical Engineering, IEEE Transactions on, 50*(9), 1108-1116.

Jin, J., Allison, B. Z., Kaufmann, T., Kubler, A., Zhang, Y., Wang, X. Y., et al. (2012). The Changing Face of P300 BCIs: A Comparison of Stimulus Changes in a P300 BCI Involving Faces, Emotion, and Movement. *Plos One, 7*(11).

Jin, J., Sellers, E. W., & Wang, X. Y. (2012). Targeting an Efficient Target-To-Target Interval for P300 Speller Brain-Computer Interfaces. *Medical & Biological Engineering & Computing, 50*(3), 289-296.

Kaminski, H. J., Al-Hakim, M., Leigh, R. J., Bashar, M. K., & Ruff, R. L. (1992). Extraocular muscles are spared in advanced duchenne dystrophy. *Annals of Neurology, 32*(4), 586-588.

Kaufmann, T., Herweg, A., & Kubler, A. (2014). Toward brain-computer interface based wheelchair control utilizing tactually-evoked event-related potentials. *Journal of Neuroengineering and Rehabilitation, 11*.

Kaur, M., Soni, A., & Rafiq, M. Q. (2014). *Semi-Supervised Clustering Approach for P300 based BCI Speller Systems.* Paper presented at the Int. Conf. on Recent Trends in Information, Telecommunication and Computin.

Khare, V., Santhosh, J., Anand, S., & Bhatia, M. (2011). Brain Computer Interface Based Real Time Control of Wheelchair Using Electroencephalogram. *International Journal of Soft Computing, 1*(5), 41-45.

Ki-Hong, K., KIM, H. K., & Soo-Young, L. (2006). A practical biosignal-based human interface applicable to the assistive systems for people with motor impairment. *IEICE transactions on information and systems, 89*(10), 2644-2652.

Kim, J., Park, H., Bruce, J., Sutton, E., Rowles, D., Pucci, D., et al. (2013). The Tongue Enables Computer and Wheelchair Control for People with Spinal Cord Injury. *Science Translational Medicine, 5*(213), 213ra166-213ra166.

Klados, M. A., Papadelis, C., Braun, C., & Bamidis, P. D. (2011). REG-ICA: A hybrid methodology combining Blind Source Separation and regression techniques for the rejection of ocular artifacts. *Biomedical Signal Processing and Control, 6*(3), 291-300.

Kleih, S. C., Nijboer, F., Halder, S., & Kubler, A. (2010). Motivation Modulates the P300 Amplitude during Brain-Computer Interface Use. *Clinical Neurophysiology, 121*(7), 1023-1031.

Kolev, V., Yordanova, J., Basar-Eroglu, C., & Basar, E. (2002). Age effects on visual EEG responses reveal distinct frontal alpha networks. *Clinical Neurophysiology, 113*(6), 901-910.

Kong, X., & Wilson, G. F. (1998). A new EOG-based eyeblink detection algorithm. *Behavior Research Methods, Instruments, & Computers, 30*(4), 713-719.

Krusienski, D. J., Sellers, E. W., Cabestaing, F., Bayoudh, S., McFarland, D. J., Vaughan, T. M., et al. (2006). A comparison of classification techniques for the P300 Speller. *Journal of neural engineering, 3*(4), 299.

Kübler, A., Kotchoubey, B., Kaiser, J., Wolpaw, J. R., & Birbaumer, N. (2001). Brain–Computer Communication: Unlocking the Locked In. *Psychological Bulletin, 127*(3), 358.

Kus, R., Valbuena, D., Zygierewicz, J., Malechka, T., Graeser, A., & Durka, P. (2012). Asynchronous BCI Based on Motor Imagery with Automated Calibration and Neurofeedback Training. *IEEE Transactions on Neural Systems and Rehabilitation Engineering, 20*(6), 823-835.

Lamti, H. A., Ben Khelifa, M. M., Gorce, P., & Alimi, A. M. (2013). A brain and gaze-controlled wheelchair. *Computer Methods in Biomechanics and Biomedical Engineering, 16*(sup1), 128-129.

Latif, H. O., Sherkat, N., & Lotfi, A. (2008). Telegaze: Teleoperation Through Eye Gaze. *7th IEEE International Conference on Cybernetic Intelligent Systems (CIS 2008)*, 1-6.

Lederman, D., & Tabrikian, J. (2012). Classification of Multichannel EEG Patterns using Parallel Hidden Markov Models. *Medical & Biological Engineering & Computing, 50*(4), 319-328.

Lee, S., Shin, Y., Woo, S., Kim, K., & Lee, H.-N. (2013). Review of Wireless Brain-Computer Interface Systems. In R. Fazel-Rezai (Ed.), *Brain-Computer Interface Systems - Recent Progress and Future Prospects* (pp. 215): InTech.

Leeb, R., Friedman, D., Müller-Putz, G. R., Scherer, R., Slater, M., & Pfurtscheller, G. (2007). Self-paced (asynchronous) BCI control of a wheelchair in virtual environments: a case study with a tetraplegic. *Computational intelligence and neuroscience, 2007*.

Li, J. H., & Zhang, L. Q. (2012). Active Training Paradigm for Motor Imagery BCI. *Experimental Brain Research, 219*(2), 245-254.

Li, Y. Q., Pan, J. H., Wang, F., & Yu, Z. L. (2013). A Hybrid BCI System Combining P300 and SSVEP and Its Application to Wheelchair Control. *Ieee Transactions on Biomedical Engineering, 60*(11), 3156-3166.

Liao, L.-D., Chen, C.-Y., Wang, I.-J., Chen, S.-F., Li, S.-Y., Chen, B.-W., et al. (2012). Gaming control using a wearable and wireless EEG-based brain-computer interface device with novel dry foam-based sensors. *Journal of neuroengineering and rehabilitation, 9*(1), 5.

Lin, C.-T., Chang, C.-J., Lin, B.-S., Hung, S.-H., Chao, C.-F., & Wang, I.-J. (2010). A real-time wireless brain–computer interface system for drowsiness detection. *Biomedical Circuits and Systems, IEEE Transactions on, 4*(4), 214-222.

Lin, C.-T., Ko, L.-W., Chung, I.-F., Huang, T.-Y., Chen, Y.-C., Jung, T.-P., et al. (2006). Adaptive EEG-based alertness estimation system by using ICA-based fuzzy neural networks. *Circuits and Systems I: Regular Papers, IEEE Transactions on, 53*(11), 2469-2476.

Lins, O. G., Picton, T. W., Berg, P., & Scherg, M. (1993). Ocular Artifacts in EEG and Event-Related Potentials I: Scalp Topography. *Brain Topography, 6*(1), 51-63.

Long, J. Y., Li, Y. Q., Wang, H. T., Yu, T. Y., Pan, J. H., & Li, F. (2012). A Hybrid Brain Computer Interface to Control the Direction and Speed of a Simulated or Real Wheelchair. *IEEE Transactions on Neural Systems and Rehabilitation Engineering, 20*(5), 720-729.

Lopes, A. C., Pires, G., & Nunes, U. (2013). Assisted navigation for a brain-actuated intelligent wheelchair. *Robotics and Autonomous Systems, 61*(3), 245-258.

Lopes, A. C., Pires, G., Vaz, L., & Nunes, U. (2011). *Wheelchair navigation assisted by Human-Machine shared-control and a P300-based Brain Computer Interface.* Paper presented at the Intelligent Robots and Systems (IROS), 2011 IEEE/RSJ International Conference on.

Luck, S. (2004). Ten Simple Rules for Designing and Interpreting ERP Experiments.[In:] Event-Related Potentials: A Methods Handbook. *Handy, TC (Ed.)*.

Mak, J. N., McFarland, D. J., Vaughan, T. M., McCane, L. M., Tsui, P. Z., Zeitlin, D. J., et al. (2012). EEG Correlates of P300-Based Brain-Computer Interface (BCI) Performance in People with Amyotrophic Lateral Sclerosis. *Journal of Neural Engineering, 9*(2).

Mandel, C., Luth, T., Laue, T., Rofer, T., Graser, A., & Krieg-Bruckner, B. (2009). *Navigating a smart wheelchair with a brain-computer interface interpreting steady-state visual evoked potentials.* Paper presented at the Intelligent Robots and Systems, 2009. IROS 2009. IEEE/RSJ International Conference on.

Mandel, C., Luth, T., Laue, T., Rofer, T., Graser, A., & Krieg-Bruckner, B. (2009). *Navigating a Smart Wheelchair with a Brain-Computer Interface Interpreting Steady-State Visual Evoked Potentials.* Paper presented at the 2009 IEEE-RSJ International Conference on Intelligent Robots and Systems, St. Louis, MO.

Matthews, R., Turner, P., McDonald, N., Ermolaev, K., Manus, T. M., Shelby, R., et al. (2008). *Real time workload classification from an ambulatory wireless EEG system using hybrid EEG electrodes.* Paper presented at the Engineering in Medicine and Biology Society, 2008. EMBS 2008. 30th Annual International Conference of the IEEE.

McAvinue, L. P., & Robertson, I. H. (2008). Measuring Motor Imagery Ability: A Review. *European Journal of Cognitive Psychology, 20*(2), 232-251.

McFarland, D. J., Sarnacki, W. A., Vaughan, T. M., & Wolpaw, J. R. (2005). Brain-Computer Interface (BCI) Operation: Signal and Noise During Early Training Sessions. *Clinical Neurophysiology, 116*(1), 56-62.

Millán, J., Galán, F., Vanhooydonck, D., Lew, E., Philips, J., & Nuttin, M. (2009). *Asynchronous non-invasive brain-actuated control of an intelligent wheelchair.* Paper presented at the Engineering in Medicine and Biology Society, 2009. EMBC 2009. Annual International Conference of the IEEE.

Millan, J. R., Renkens, F., Mouriño, J., & Gerstner, W. (2004). Noninvasive brain-actuated control of a mobile robot by human EEG. *Biomedical Engineering, IEEE Transactions on, 51*(6), 1026-1033.

Minett, J. W., Zheng, H. Y., Fong, M. C. M., Zhou, L., Peng, G., & Wang, W. S. Y. (2012). A Chinese Text Input Brain-Computer Interface Based on the P300 Speller. *International Journal of Human-Computer Interaction, 28*(7), 472-483.

Mokhtar, N. (2012). *Real Time Control of Wheel Chair Using Eye Direction.* (Doctor of Philosophy), University of Malaya.

Montesano, L., Diaz, M., Bhaskar, S., & Minguez, J. (2010). Towards an Intelligent Wheelchair System for Users With Cerebral Palsy. *IEEE Transactions on Neural Systems and Rehabilitation Engineering, 18*(2), 193-202.

Mougharbel, I., El-Hajj, R., Ghamlouch, H., & Monacelli, E. (2013). *Comparative study on different adaptation approaches concerning a sip and puff controller for a powered wheelchair.* Paper presented at the Science and Information Conference (SAI), 2013.

Müller, M. M., Keil, A., Gruber, T., & Elbert, T. (1999). Processing of Affective Pictures Modulates Right-Hemispheric Gamma Band EEG Activity. *Clinical Neurophysiology, 110*(11), 1913-1920.

Nguyen, Q. X., & Jo, S. (2012). Electric Wheelchair Control using Head Pose Free Eye-Gaze Tracker. *Electronics Letters, 48*(13), 750-752.

Nijholt, A., & Tan, D. (2008). Brain-computer interfacing for intelligent systems. *Intelligent Systems, IEEE, 23*(3), 72-79.

Ning, B., Li, M.-j., Liu, T., Shen, H.-m., Hu, L., & Fu, X. (2012). Human Brain Control of Electric Wheelchair with Eye-Blink Electrooculogram Signal. In C.-Y. Su, S. Rakheja & H. Liu (Eds.), *Intelligent Robotics and Applications* (Vol. 7506, pp. 579-588): Springer Berlin Heidelberg.

Nombela, C., Nombela, M., Castell, P., Garcia, T., Lopez-Coronado, J., & Herrero, M. T. (2014). Alpha-Theta Effects Associated with Ageing during the Stroop Test. *Plos One, 9*(5).

Ortner, R., Guger, C., Prueckl, R., Grünbacher, E., & Edlinger, G. (2010). Ssvep based brain-computer interface for robot control *Computers Helping People with Special Needs* (pp. 85-90): Springer.

Parini, S., Maggi, L., Turconi, A. C., & Andreoni, G. (2009). A Robust and Self-Paced BCI System Based on a Four Class SSVEP Paradigm: Algorithms and Protocols for a High-Transfer-Rate Direct Brain Communication. *Computational Intelligence and Neuroscience, 2009*.

Park, J., & Kim, K. E. (2012). A POMDP Approach to Optimizing P300 Speller BCI Paradigm. *IEEE Transactions on Neural Systems and Rehabilitation Engineering, 20*(4), 584-594.

Pfurtscheller, G., Allison, B. Z., Bauernfeind, G., Brunner, C., Solis Escalante, T., Scherer, R., et al. (2010). The Hybrid BCI. *Frontiers in Neuroscience, 4*.

Pfurtscheller, G., Brunner, C., Schlögl, A., & Lopes da Silva, F. (2006). Mu Rhythm (de) Synchronization and EEG Single-Trial Classification of Different Motor Imagery Tasks. *Neuroimage, 31*(1), 153-159.

Philips, J., del R Millan, J., Vanacker, G., Lew, E., Galán, F., Ferrez, P. W., et al. (2007). *Adaptive shared control of a brain-actuated simulated wheelchair.* Paper presented at the Rehabilitation Robotics, 2007. ICORR 2007. IEEE 10th International Conference on.

Philips, J., del R.Millan, J., Vanacker, G., Lew, E., Galan, F., Ferrez, P. W., et al. (2007, 13-15 June 2007). *Adaptive Shared Control of a Brain-Actuated Simulated Wheelchair.* Paper presented at the Rehabilitation Robotics, 2007. ICORR 2007. IEEE 10th International Conference on.

Piccione, F., Giorgi, F., Tonin, P., Priftis, K., Giove, S., Silvoni, S., et al. (2006). P300-Based Brain Computer Interface: Reliability and Performance in Healthy and Paralysed Participants. *Clinical Neurophysiology, 117*(3), 531-537.

Pineda, J. A. (2005). The Functional Significance of Mu Rhythms: Translating "seeing" and "hearing" Into "doing". *Brain Research Reviews, 50*(1), 57-68.

Pires, G., Castelo-Branco, M., & Nunes, U. (2008). *Visual P300-based BCI to steer a wheelchair: A Bayesian approach.* Paper presented at the Engineering in Medicine and Biology Society, 2008. EMBS 2008. 30th Annual International Conference of the IEEE.

Polich, J., Ellerson, P. C., & Cohen, J. (1996). P300, Stimulus Intensity, Modality, and Probability. *International Journal of Psychophysiology, 23*(1-2), 55-62.

Postelnicu, C. C., Barbuceanu, F., Topoleanu, T., & Talaba, D. (2012). EOG-Based Interface for Manipulation Tasks. *Mechanisms, Mechanical Transmissions and Robotics, 162*, 537-542.

Postelnicu, C. C., Girbacia, F., & Talaba, D. (2012). EOG-based visual navigation interface development. *Expert Systems with Applications, 39*(12), 10857-10866.

Prasad, S., & Galetta, S. L. (2010). Eye Movement Abnormalities in Multiple Sclerosis. *Neurologic Clinics, 28*(3), 641.

Prueckl, R., & Guger, C. (2009). A brain-computer interface based on steady state visual evoked potentials for controlling a robot *Bio-Inspired Systems: Computational and Ambient Intelligence* (pp. 690-697): Springer.

Prueckl, R., & Guger, C. (2010). *Controlling a robot with a brain-computer interface based on steady state visual evoked potentials.* Paper presented at the Neural Networks (IJCNN), The 2010 International Joint Conference on.

Ramli, R., Mokhtar, N., Arof, H., Anwar, M. S. M., Hamzah, N. H. M., Ibrahim, F., et al. (2009). *Development of brain signal processing interface software for Trackit (TM)-LabVIEW.*

Rebsamen, B., Burdet, E., Guan, C., Teo, C. L., Zeng, Q., Ang, M., et al. (2007). Controlling a wheelchair using a BCI with low information transfer rate. *2007 IEEE 10th International Conference on Rehabilitation Robotics, Vols 1 and 2*, 1003-1008.

Rebsamen, B., Burdet, E., Guan, C., Zhang, H., Teo, C. L., Zeng, Q., et al. (2006). *A brain-controlled wheelchair based on P300 and path guidance.* Paper presented at the Biomedical Robotics and Biomechatronics, 2006. BioRob 2006. The First IEEE/RAS-EMBS International Conference on.

Rebsamen, B., Burdet, E., Guan, C. T., Zhang, H. H., Teo, C. L., Zeng, Q. A., et al. (2006). *A brain-controlled wheelchair based on P300 and path guidance*. Paper presented at the 2006 1st IEEE RAS-EMBS International Conference on Biomedical Robotics and Biomechatronics, Vols 1-3.

Rebsamen, B., Guan, C., Zhang, H., Wang, C., Teo, C., Ang, V., et al. (2010). A brain controlled wheelchair to navigate in familiar environments. *Neural Systems and Rehabilitation Engineering, IEEE Transactions on, 18*(6), 590-598.

Rebsamen, B., Guan, C. T., Zhang, H. H., Wang, C. C., Teo, C., Ang, M. H., et al. (2010). A Brain Controlled Wheelchair to Navigate in Familiar Environments. *IEEE Transactions on Neural Systems and Rehabilitation Engineering, 18*(6), 590-598.

Rebsamen, B., Teo, C. L., Zeng, Q., Ang, V., Burdet, E., Guan, C., et al. (2007). Controlling a wheelchair indoors using thought. *Intelligent Systems, IEEE, 22*(2), 18-24.

Ron-Angevin, R., Velasco-Alvarez, F., Sancha-Ros, S., & da Silva-Sauer, L. (2011). *A two-class self-paced BCI to control a robot in four directions*. Paper presented at the Rehabilitation Robotics (ICORR), 2011 IEEE International Conference on.

Sanchez, G., Diez, P. F., Avila, E., & Leber, E. L. (2011). Simple communication using a SSVEP-based BCI. *8th Argentinean Bioengineering Society Conference (Sabi 2011) and 7th Clinical Engineering Meeting, 332*.

Sanei, S., & Chambers, J. A. (2007). Introduction to EEG *EEG Signal Processing* (1st ed., pp. 1-31). West Sussex, England: Wiley.

Sanei, S., & Chambers, J. A. (2008). *EEG signal processing*: John Wiley & Sons.

Satti, A., Coyle, D., & Prasad, G. (2011). *Self-paced brain-controlled wheelchair methodology with shared and automated assistive control*. Paper presented at the Computational Intelligence, Cognitive Algorithms, Mind, and Brain (CCMB), 2011 IEEE Symposium on.

Satti, A. R., Coyle, D., & Prasad, G. (2011, 11-15 April 2011). *Self-paced brain-controlled wheelchair methodology with shared and automated assistive control*. Paper presented at the Computational Intelligence, Cognitive Algorithms, Mind, and Brain (CCMB), 2011 IEEE Symposium on.

Scherer, R., Lee, F., Schloegl, A., Leeb, R., Bischof, H., & Pfurtscheller, G. (2008). Toward self-paced brain-computer communication: Navigation through virtual worlds. *Ieee Transactions on Biomedical Engineering, 55*(2), 675-682.

Schlögl, A., Lugger, K., & Pfurtscheller, G. (1997). *Adaptive autoregressive parameters for a brain-computer-interface experiment.* Paper presented at the Proceedings of the 19th International Conference of the IEEE/EMBS.

Schutter, D. J. L. G., & Van Honk, J. (2005). Electrophysiological ratio markers for the balance between reward and punishment. *Cognitive Brain Research, 24*(3), 685-690.

Shin, B.-G., Kim, T., & Jo, S. (2010). *Non-invasive brain signal interface for a wheelchair navigation.* Paper presented at the Control Automation and Systems (ICCAS), 2010 International Conference on.

Speier, W., Arnold, C., Lu, J., Taira, R. K., & Pouratian, N. (2012). Natural Language Processing with Dynamic Classification Improves P300 Speller Accuracy and Bit Rate. *Journal of Neural Engineering, 9*(1).

Stamps, K., & Hamam, Y. (2010). Towards inexpensive BCI control for wheelchair navigation in the enabled environment–a hardware survey *Brain Informatics* (pp. 336-345): Springer.

Teymourian, A., Lüth, T., Graeser, A., Felzer, T., & Nordmann, R. (2008). *Brain-controlled finite state machine for wheelchair navigation.* Paper presented at the Proceedings of the 10th international ACM SIGACCESS conference on Computers and accessibility.

Thuraisingham, R. A., Tran, Y., Boord, P., & Craig, A. (2007). Analysis of Eyes Open, Eye Closed EEG Signals using Second-Order Difference Plot. *Medical & Biological Engineering & Computing, 45*(12), 1243-1249.

Townsend, G., LaPallo, B. K., Boulay, C. B., Krusienski, D. J., Frye, G. E., Hauser, C. K., et al. (2010). A Novel P300-Based Brain-Computer Interface Stimulus Presentation Paradigm: Moving Beyond Rows and Columns. *Clinical Neurophysiology, 121*(7), 1109-1120.

Trikha, M., Gandhi, T., Bhandari, A., & Khare, V. (2007). Multiple channel electrooculogram classification using automata. *MeMeA 2007: Second - IEEE International Workshop on Medical Measurement and Applications*, 35-39.

Tsui, C. S. L., & Gan, J. Q. (2007). Asynchronous BCI control of a robot simulator with supervised online training *Intelligent Data Engineering and Automated Learning-IDEAL 2007* (pp. 125-134): Springer.

Tsui, C. S. L., Gan, J. Q., & Hu, H. S. (2011). A Self-Paced Motor Imagery Based Brain-Computer Interface for Robotic Wheelchair Control. *Clinical Eeg and Neuroscience, 42*(4), 225-229.

Tsui, C. S. L., Gan, J. Q., & Roberts, S. J. (2009). A self-paced brain–computer interface for controlling a robot simulator: an online event labelling paradigm and an extended Kalman filter based algorithm for online training. *Medical & biological engineering & computing, 47*(3), 257-265.

Usakli, A. B., & Gurkan, S. (2010). Design of a Novel Efficient Human-Computer Interface: An Electrooculagram Based Virtual Keyboard. *IEEE Transactions on Instrumentation and Measurement, 59*(8), 2099-2108.

Vanacker, G., del R Millán, J., Lew, E., Ferrez, P. W., Moles, F. G., Philips, J., et al. (2007). Context-based filtering for assisted brain-actuated wheelchair driving. *Computational intelligence and neuroscience, 2007*, 3-3.

Velasco-Álvarez, F., Ron-Angevin, R., da Silva-Sauer, L., Sancha-Ros, S., & Blanca-Mena, M. J. (2011). Audio-cued SMR brain-computer interface to drive a virtual wheelchair *Advances in Computational Intelligence* (pp. 337-344): Springer.

Wang, H., Li, Y., Long, J., Yu, T., & Gu, Z. (2014). An Asynchronous Wheelchair Control by Hybrid EEG–EOG Brain–Computer Interface. *Cognitive Neurodynamics*, 1-11.

Waterink, W., & Van Boxtel, A. (1994). Facial and Jaw-Elevator EMG Activity in Relation to Changes in Performance Level During A Sustained Information Processing Task. *Biological Psychology, 37*(3), 183-198.

Wolpaw, J. R., Ramoser, H., McFarland, D. J., & Pfurtscheller, G. (1998). EEG-based communication: improved accuracy by response verification. *Rehabilitation Engineering, IEEE Transactions on, 6*(3), 326-333.

Woo, S. J., Ahn, J., Park, M. S., Lee, K. M., Gwon, D. K., Hwang, J.-M., et al. (2011). Ocular Findings in Cerebral Palsy Patients Undergoing Orthopedic Surgery. *Optometry & Vision Science, 88*(12), 1520-1523.

Xu, X., Zhang, Y., Luo, Y., & Chen, D. (2013). Robust Bio-Signal Based Control of an Intelligent Wheelchair. *Robotics, 2*(4), 187-197.

Yamawaki, N., Wilke, C., Liu, Z., & He, B. (2006). An enhanced time-frequency-spatial approach for motor imagery classification. *Neural Systems and Rehabilitation Engineering, IEEE Transactions on, 14*(2), 250-254.

Yong, X. Y., Fatourechi, M., Ward, R. K., & Birch, G. E. (2012). Automatic artefact removal in a self-paced hybrid brain-computer interface system. *Journal of Neuroengineering and Rehabilitation, 9*.

Yu, T. Y., Li, Y. Q., Long, J. Y., & Gu, Z. H. (2012). Surfing the Internet with a BCI Mouse. *Journal of Neural Engineering, 9*(3).

Yuanqing, L., Jiahui, P., Fei, W., & Zhuliang, Y. (2013). A Hybrid BCI System Combining P300 and SSVEP and Its Application to Wheelchair Control. *IEEE Transactions on Biomedical Engineering, 60*(11), 3156-3166.

Zander, T. O., Gaertner, M., Kothe, C., & Vilimek, R. (2010). Combining Eye Gaze Input with a Brain–Computer Interface for Touchless Human–Computer Interaction. *International Journal of Human-Computer Interaction, 27*(1), 38-51.

Zander, T. O., Gaertner, M., Kothe, C., & Vilimek, R. (2010). Combining eye gaze input with a brain–computer interface for touchless human–computer interaction. *Intl. Journal of Human–Computer Interaction, 27*(1), 38-51.

Zhang, H., Guan, C., & Wang, C. (2008). Asynchronous P300-based brain--computer interfaces: A computational approach with statistical models. *Biomedical Engineering, IEEE Transactions on, 55*(6), 1754-1763.

Zhijun, L., Shuangshuang, L., Chun Yi, S., & Guanglin, L. (2013). Hybrid Brain/Muscle-Actuated Control of an Intelligent Wheelchair. *2013 IEEE International Conference on Robotics and Biomimetics (ROBIO)*, 19-25.

Zhu, D., Bieger, J., Garcia Molina, G., & Aarts, R. M. (2010). A Survey of Stimulation Methods Used in SSVEP-Based BCIs. *Computational Intelligence and Neuroscience, 2010*.

APPENDIX A

CONSENT TO PARTICIPATE IN RESEARCH COLLECTING EEG DATA

Please answer the following questions by circling your choice:

a) Are you currently taking, or have you recently taken, any prescription or over-the-counter medicine?

   YES   NO

b) Have you ever suffered from epilepsy?

   YES   NO

c) Have you had surgery in which metal items have been placed in your head?

   YES   NO

d) Do you have a heart pacemaker fitted?

   YES   NO

e) Do you smoking?

   YES   NO

f) Do you suffer from nystagmus (fast, uncontrollable movements of the eyes called "dancing eyes")?

   YES   NO

g) Do you suffer from any chronic skin condition (e.g. dermatitis, eczema, psoriasis)?

   YES   NO

h) Have you consumed any alcohol or recreational drug over the last 24 hours?

   YES   NO

i) Do you suffer from any condition impairing blood clotting (e.g. haemophilia)?

   YES   NO

j) Do you currently have any cuts or abrasions on your head?

YES   NO

Participant's declaration

I give my informed consent to participate in the EEG Recording Session. I am aware that my participation is voluntary and that I may withdraw at any time without giving a reason. I am well aware of the fact that all information given by me or data recorded from me will be handled confidentially.

Participant signature   _____

Date   _____

Researcher's declaration

I believe the participant has been completely informed about the EEG recording procedure to the level necessary for the giving of informed consent. I have discussed all relevant aspects of the procedure with the participant, and answered all questions to their satisfaction.

Researcher signature   _____

Date   _____

Name   _____

APPENDIX B

2nd ORDER DIFFERENCE PLOT

The second-order difference plot displays the successive rates of variability against each other where $[x(n + 1) - x(n)]$ is plotted on x-axis versus $[x(n + 2) - x(n + 1)]$ on y-axis. Figure B.1 shows the signals of the open eye plotted in second-order difference plot at 5 EEG rhythms; delta, theta, alpha, beta and gamma. The distribution of samples is spread out with an increase in frequency while smaller and oblongated distribution can be found with a decrease in frequency.

Delta (<4Hz)   Theta (4-8Hz)   Alpha (8-13Hz)

Beta (13-30Hz)   Gamma (>30Hz)
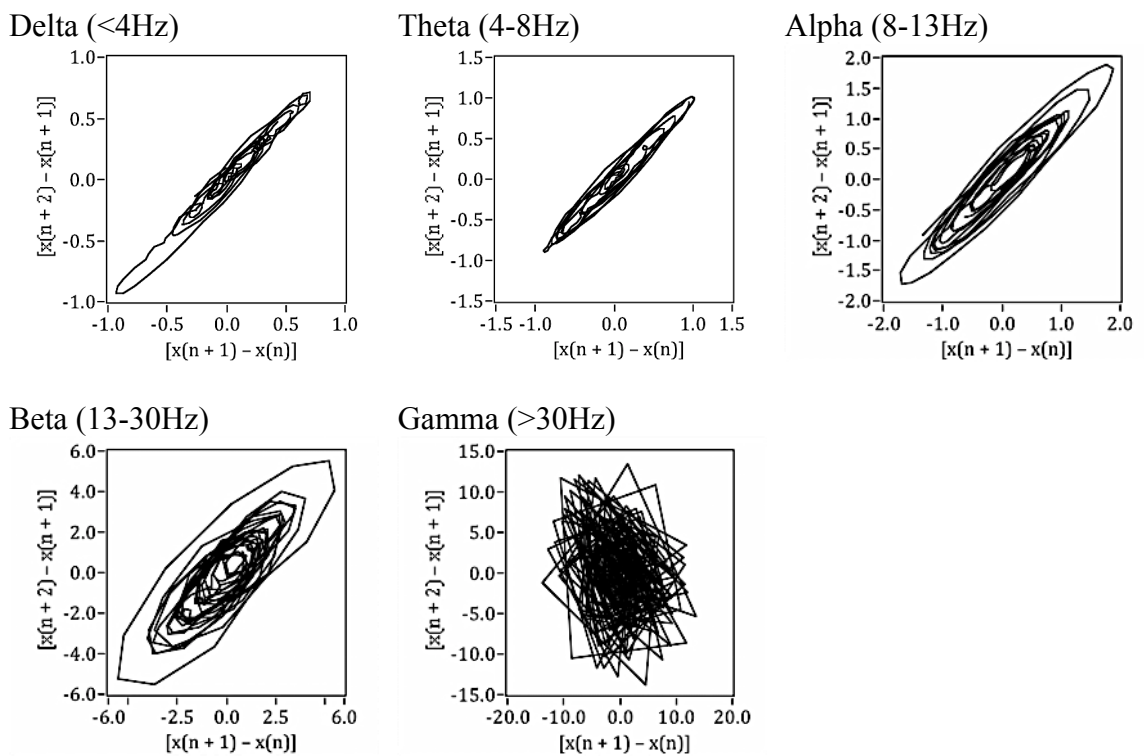
Figure B.1: The example of second-order difference plot for five EEG rhythms; delta, theta, alpha, beta and gamma during open eye.

APPENDIX C

LINEAR DISCRIMINANT ANALYSIS

The global mean (μ) is calculated by summing all the data in $X_{(x,y)}$ and divided by the total number of data ($n = 128$) from two predetermined groups as in equation (C.1).

$$\mu = \frac{1}{n} \sum_{i=1}^{n} X_{(x,y)i} \tag{C.1}$$

Then, group mean (μ_k) will be calculated from $X_{(x,y)}$ within the specific group, k:

$$\mu_k = \frac{1}{n_k} \sum_{i=1}^{n_k} X_{(x,y)i,k} \tag{C.2}$$

The covariance matrix of the group, c_k, and pooled covariance matrix, $C(r,s)$ are calculated from mean corrected data $(X_{(x,y)i,k} - \mu)$ as in equation (C.3) and (C.4).

$$c_k = \frac{\left(X_{(x,y)i,k} - \mu\right)^T \left(X_{(x,y)i,k} - \mu\right)}{n_k} \tag{C.3}$$

$$C(r,s) = \frac{1}{n} \sum_{i=1}^{k} n_i \cdot c_i(r,s) \tag{C.4}$$

The covariance matrix of group k was calculated for each row and column of the matrix denoted by r and s respectively. Then, prior probability of group (p_k) will calculate as total number of data of each group divided by the total number of data:

$$p_k = \frac{n_k}{n}$$

(C.5)

The prior probability vector in which each row represents the prior probability of group k can be described as follows:

$$P = \frac{p_{k-1}}{p_k}$$

(C.6)

Finally, discriminant function (f_k) will assign data to group k that has maximum f_k:

$$f_k = \mu_k C^{-1}(X_{(x,y)i})^T - \frac{1}{2}\mu_k C^{-1}\mu_k^T + \ln(p_i)$$

(C.7)

LDA will separate two groups linearly with dependable variable is the group, k and the independent variables are the data, $X_{(x,y)}$, that might describe the group.

APPENDIX D

K-MEANS

In the beginning, number of groups will be specified as center of the cluster. Then, follow by three steps repeatedly until convergence has been reached; centroid of data, distance data to centroids using Euclidean distance and grouping based on minimum distance to the group as Figure D.1.
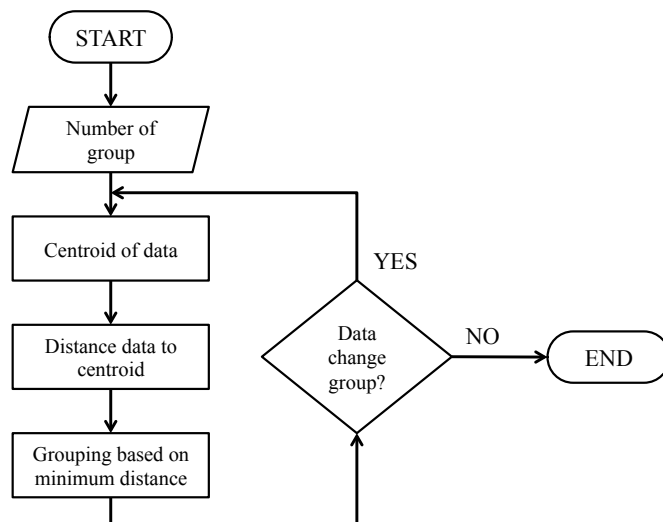
Figure D.1: Flow of the K-Means process to determine the group of the data and stability is reached once the data stop changing group.

The data are represented by X and the process of assigning data to the group is described as follows.

STEP 1 : Total number of groups (k) will be assigned as 2 ($k = 2$).

STEP 2 : The centroid (C) will be initialized associated with groups (j).

STEP 3 : The distance (d) between sample and centroid will be measured using

Euclidean distance as follow:

$$d = \sum_{j=1}^{k} \sum_{i=1}^{m} \|X_i - C_j\|^2$$

where, i = number of data, j = number of groups

STEP 4   The data will be assigned to the group with the minimum d to the respective centroid.

$$group_{ij} = \begin{cases} 1 \ if \ j = arg \ \min_{d}\|X_i - C_j\|^2 \\ 0 \ else \end{cases}$$

STEP 5 : A new centroid represented the new member of the group will be calculated.

$$C_j = \frac{1}{m_j} \sum_{i=1}^{m_j} X_i$$

where, m_j = number of data assign to group j

STEP 3 to STEP 5 will be repeated until convergence has been reached:

$$group_{ijr} = group_{ij(r-1)}$$

where, r = number of iterations

APPENDIX E

FEEDBACK FORM

1. We are interested in your experience during the Navigation Session. The results of this evaluation will be used to improve this study in the future.
2. Please rate the questions below between 0 to 5 from the least to the most.

| Questions | Attempts | | | | | |
| | Route 1 | | | Route 2 | | |
	1	2	3	1	2	3
Workload						
I found the task was difficult.						
I was able to complete the task quickly.						
Learnability						
I thought this system was easy to used.						
I needed a lot of training before get going with the system.						
Confidence						
I felt very confident using this system.						
I felt comfortable using this system.						

Participant signature _____

Date   _____

APPENDIX F

PUBLICATIONS

Conference:

1)   Ramli, R., Mokhtar, N., Arof, H., Anwar, M. M., Hamzah, N. M., & Ibrahim, F. (2009, December). Development of brain signal processing interface software for Trackit™-LabVIEW. In *Technical Postgraduates (TECHPOS), 2009 International Conference for* (pp. 1-5). IEEE.

Journal:

1)   Ramli, R., Arof, H., Ibrahim, F., Mokhtar, N., & Idris, M. Y. I. (2014). Using Finite State Machine and a Hybrid of EEG Signal and EOG Artifacts for an Asynchronous Wheelchair Navigation. *Expert Systems with Applications*.